Aerogeophysical constraints for the geodynamic evolution of Dronning Maud Land, East Antarctica

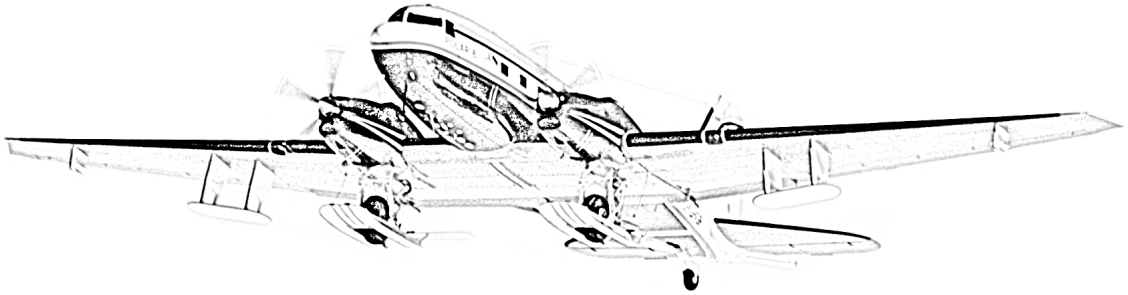

Dissertation

zur Erlangung des Grades Dr. rer. nat.
vorgelegt dem Fachbereich Geowissenschaften
der Universität Bremen
von

Matthias Mieth

February 17, 2014

Matthias Mieth
Alfred-Wegener-Institut
Helmholz-Zentrum für Polar- und Meeresforschung
Columbusstrasse
27568 Bremerhaven

Matthias.Mieth@awi.de

Gutachter:

Dr. Wilfried Jokat, Professor für Geophysik der Polargebiete
Universität Bremen und Alfred-Wegener-Institut

Dr. Cornelia Spiegel, Professorin für Geodynamik der Polargebiete
Universität Bremen

ALFRED-WEGENER-INSTITUT
HELMHOLTZ-ZENTRUM FÜR POLAR- UND MEERESFORSCHUNG

Universität Bremen

Erklärung

Hiermit versichere ich,

Matthias Mieth,
wohnhaft in Am Leher Tor 13, 27568 Bremerhaven,

dass ich

- die vorliegende Arbeit ohne unerlaubte fremde Hilfe angefertigt habe,
- keine anderen als die von mir angegebenen Quellen und Hilfsmittel benutzt habe und
- die den benutzten Werken wörtlich oder inhaltlich entnommenen Stellen als solche kenntlich gemacht habe.

Bremerhaven, 17. Februar 2014 _____

"We look forward to the next two years,
confident that they will be memorable years,
convinced that the interesting, absorbing work
we are doing is eminently worth-while, and humbly
grateful for having been given the opportunity of
being where we are and doing what we are."

- Ernest Frederick Roots, February 1950

(Member of the Norwegian-British-Swedish
Antarctic "Maudheim" Expedition 1949-52)

Zusammenfassung

Was sich unter dem Eis im Inneren der Antarktis verbirgt, ist die zentrale Frage dieser Arbeit. Wissen über den tektonischen Aufbau und die Entstehungsgeschichte der Antarktis zu erlangen, ist nicht nur von generellem geologischem Interesse. Kenntnisse über die Bildung und den Zerfall von Superkontinenten liefern auch wichtige Randbedingungen für die Erforschung der Entwicklung des Klimas und der Biosphäre in den vergangenen Erdzeitaltern. Darüberhinaus ist das Wissen über den tektonischen Aufbau der Antarktis eine wesentliche Grundlage für die Abschätzung des Erdwärmestromes, der benötigt wird um die Fließbewegungen und die zu erwartenden Veränderungen der antarktischen Eisbedeckung berechnen zu können. Nur an wenigen Stellen und zumeist am Rand des Kontinents ragen Bergspitzen aus der größtenteils kilometerdicken Eisschicht heraus und erlauben direkte geologische Untersuchungen. Daher erfordert die Erforschung des tektonischen Aufbaus des Kontinents eine flächendeckende geophysikalische Vermessung und eine Korrelation dieser Daten mit den geologischen Befunden. In den vergangenen Jahrzehnten konnte zwar die jurassische Aufbruchsgeschichte des Superkontinents Gondwana anhand des magnetischen Anomalienmusters der ozeanischen Kruste rekonstruiert werden und es zeigt sich, dass die Ostantarktis im Paläozoikum und frühen Mesozoikum zentral zwischen Afrika, Indien, Australien und Neuseeland positioniert war. Jedoch fehlen grundlegende Kenntnisse über den tektonischen Aufbau der Ostantarktis, um die Kollision von Gondwana am Ende des Proterozoikums und dem Beginn des Paläozoikums, sowie älterer Kollisions- und Aufbruchsprozesse genauer zu verstehen. Die vorliegende Arbeit beschäftigt sich mit der Frage, ob sich der innere Teil der Ostantarktis in verschiedene Krustensegmente gliedert. So wird nach den Verläufen von überregionalen tektonischen Störungszonen, der Lage einzelner krustaler Blöcke und deren Grenzen gesucht. Hierfür wurde die Region des Dronning Maud Landes (DML) und des Coats Landes in den vergangenen Jahren vom Alfred-Wegener-Institut Helmholtz-

Zentrum für Polar- und Meeresforschung (AWI) mittels flugzeuggestützter geophysikalischer Methoden systematisch erkundet. Dabei wurden die Strukturen des Eises und deren Mächtigkeit mit elektromagnetischen Wellen (Radar), sowie das von dem zum größten Teil unter dem Eis verborgenem Gestein verursachte magnetische und gravimetrische Anomalienfeld vermessen. Die Interpretation der magnetischen und gravimetrischen Daten und die daraus gezogenen Schlussfolgerungen stützen sich auf die geologischen Befunde im DML, sowie benachbarter Gebiete der Ostantarktis und des südlichen Afrikas. Eine für das Verständnis des tektonischen Aufbaus der Ostantarktis ganz wesentliche Erkenntnis dieser Arbeit ist die Identifizierung einer sich geophysikalisch deutlich abgrenzenden Provinz im südöstlichen DML und die Schlussfolgerung, dass diese ein eigenständiges Krustensegment darstellt. Es wird hier interpretiert, dass diese südöstliche DML Provinz während des pan-afrikanischen Zusammenschlusses von Gondwana mit dem südlichen Teil von Afrika kollidierte, wobei der grenvillsche Namaqua-Natal-Maud Gebirgsgürtel im Bereich des zentralen DML deformiert wurde. Die „Forster magnetische Anomalie“ stellt möglicherweise die bei dieser Kollision entstandene Sutur dar. Eine ostwärtige Fortsetzung der südöstlichen DML Provinz wird für den südlichen Bereich der Sør Rondane Region anhand der aeromagnetischen Daten des „Geodynamic Evolution of East Antarctica“ (GEA) Projektes aufgezeigt, während nördlich davon mehrere kleinräumige Terrane und Störungszonen kartiert werden. Die geophysikalischen Daten weisen darauf hin, dass der zentrale Sør Rondane Korridor ein tektonisch eigenständiges Gebiet ist, das vermutlich eine erhöhte Krustenmächtigkeit aufweist. Des Weiteren wird die Ostgrenze des im Coats Land liegenden BLM-Kratons kartiert und gezeigt, dass sein markantes magnetisches Anomalienmuster einzigartig für das gesamte DML und südliche Afrika ist, was die Vermutung bestätigt, dass dieses Krustensegment kein Teil der ursprünglichen ostantarktischen oder afrikanischen Kontinentalplatte war und auch nicht während der pan-afrikanischen Orogenese hochgradig überprägt wurde. Dahingegen wird das „Kohnen Lineament“ im südlichen DML als eine pan-afrikanisch Scherzone interpretiert und Vergleiche zur aufgeschlossenen Heimefront Scherzone gezogen. Zusätzlich wurden Detailuntersuchungen und Modellierungen über die „Giæver magnetische Anomalie“ durchgeführt und es wird abgeleitet, dass diese möglicherweise durch gebänderte Eisenerze verursacht wird. Mit der Vielzahl dieser Befunde, Erkenntnisse und Schlussfolgerungen liefert diese Arbeit neue und wichtige Beiträge zur Erforschung des tektonischen Aufbaus und der geodynamischen Entstehung der Ostantarktis.

Abstract

The central question of this thesis is: what is hidden under the ice sheet of Antarctica? To unravel the tectonic structure and to study the geodynamic evolution of Antarctica are not only of fundamental geological interest. Knowledge of the amalgamation and break-up of supercontinents provides basic information for studying the evolution of the climate and the biosphere during Earth's history. Furthermore, knowledge about the tectonic structure of Antarctica is essential for estimating its crustal heat flow, a key parameter when modeling ice flow and future changes of ice sheets. The Antarctic ice sheet is mostly several kilometers thick, and rocks crop out of it in only a few locations to allow direct geological sampling. None of these locations is in the innermost parts of the continent. Hence, regional geophysical reconnaissance and a correlation of its data with geological findings are required for unraveling the tectonic structure of Antarctica. In recent decades, the Jurassic break-up process of Gondwana has been reconstructed based on analyses of the magnetic striping pattern of the oceanic crust, making it apparent that East Antarctica was positioned centrally in this supercontinent between Africa, India, Australia, and New Zealand throughout Paleozoic and Early Mesozoic times. However, fundamental data about the tectonic structure of East Antarctica that would be needed to better understand the assembly of Gondwana in Late Proterozoic and Early Paleozoic times, as well as about earlier collision and break-up processes, are still missing. This study pursues the question of whether the interior of East Antarctica is composed of one or many crustal fragments. Its method objective is to search for the courses of supra-regional shear zones and the positions of crustal blocks and their boundaries. For this purpose, the Alfred-Wegener-Institut Helmholtz-Zentrum für Polar- und Meeresforschung (AWI) has undertaken systematic airborne geophysical surveying in the region of Dronning Maud Land (DML) and Coats Land over the last decades. The data set includes ice-penetrating radar, aeromagnetic and areogravity measurements. Interpretation of the

magnetic and gravity anomaly pattern caused by the rocks below the ice and the resulting conclusions are based on geological findings in DML and adjacent regions in East Antarctica and southern Africa. One substantial result of this thesis for understanding of the tectonic structure of East Antarctica is the discovery of a distinct aerogeophysical province in southeastern DML. It is concluded that the magnetic and gravity anomaly data of this province can be regarded as the signature of a discrete crustal fragment. This southeastern DML province is interpreted to have collided with southern Africa as part of the Pan-African amalgamation of Gondwana, during which the Grenvillian Namaqua-Natal-Maud belt was deformed within central DML. The prominent "Forster Magnetic Anomaly" might represent the suture zone of this collision. Aeromagnetic data of the "Geodynamic Evolution of East Antarctica" (GEA) project reveal an eastward extent of the southeastern DML province into the southern Sør Rondane region, while several smaller terranes, shear zones, and tectonic boundaries are mapped farther north. It is shown how the airborne geophysical data invite an interpretation of the central Sør Rondane region as a distinct tectonic unit with a presumably increased crustal thickness. Furthermore, the eastern boundary of the BLM craton in Coats Land is mapped and its prominent magnetic anomaly pattern is shown to be unique within DML and southern Africa, raising the question of the provenance of this crustal fragment, which appears not to have been high-grade reworked during the Pan-African orogeny. In contrast, the Kohnen lineament is interpreted as a Pan-African shear zone with similarities to the outcropping Heimfront shear zone. In addition, a detailed study and modeling of the "Giæver Magnetic Anomaly" show that it is likely to be the signal of a shallow subcrop of banded iron formation. With the multiplicity of these findings, results, and conclusions, this thesis contributes significant new knowledge and future prospects for unraveling the tectonic structure and the geodynamic evolution of East Antarctica.

Acknowledgments

First of all, I thank Wilfried Jokat and Cornelia Spiegel for reviewing my doctoral thesis and the involved expenditure of their time.

I wish to express my deepest gratitude to the Alfred-Wegener-Institut Helmholtz-Zentrum für Polar- und Meeresforschung (AWI) for giving me the opportunity to contribute to measuring the world in one of the most remote places of our planet.

I sincerly thank Wilfried Jokat for his supervision, discussions, constructive criticism, and assistance during my work at AWI in the last three years.

My work would not have been possible without Daniel Steinhage of the Glaciology section of AWI, who has been continuously preparing, managing, and leading aerogeophysical expeditions in Dronning Maud Land over the last two decades and is mainly responsible for the systematic acquisition and high quality of the aeromagnetic and aerogravity data presented here. During the course of two airborne campaigns in Antarctica, he taught and trained me to become an expedition leader myself.

I am much obliged to the researches around the world who have given their time to various discussions with me about aspects of the geodynamic evolution of East Antarctica; in particular: Joachim Jacobs, Fausto Ferraccioli, Michael K. Watkeys, Georg Kleinschmidt, and Andreas Läufer.

Many thanks go to all the editors and reviewers of the articles, manuscripts, and other chapters that make up this thesis, most of all to Graeme Eagles and Paul Lehmann, as well as to Aysel Sorensen, Jens Grützner, Tanja Fromm, and Gabriele Uentzelmann-Neben. I also thank all my colleagues at AWI and at the University of Bremen for their diverse support, the stimulating atmosphere, and a delightful time.

Last but not least, I thank my family, who solicitously followed the news from the expeditions and always believed in a successful completion of my doctorate.

Contents

List of Figures

List of Tables

Chapter 1

Introduction and Motivation

1.1 Dronning Maud Land

Dronning Maud Land (DML) is the sector of Antarctica around the Greenwich meridian, extending from Coats Land (20°W) to Enderby Land (44.6°E). It includes, from west to east, Kronprinsesse Märtha, Prinsesse Astrid, Prinsesse Ranghild, Prins Harald, and Kronprins Olav coasts, while no southern boundary is defined. Von Bellingshausen (1778-1852) first sighted the coast of DML in 1820. In the following decades whaling and sealing expeditions surveyed the coasts and offshore regions. The first inland reconnaissance surveys were conducted from aircraft under the leadership of Hjalmar Riiser-Larsen (1890-1965) in 1930/31, Viggo Widerøe (1904-2002) in 1936/37, and Alfred Ritscher (1879-1963) in 1938/39. The first land-based scientific expedition in DML, the Norwegian-British-Swedish Antarctic Expedition (*Maudheim Expedition*, 1949-52), was a milestone in international polar research, as it was the first international Antarctic research expedition to undertake geological, glaciological, geomorphological, and meteorological investigations and surveys (Giæver, 1954). Today, several nations maintain research stations in DML (Fig. 1.1), namely Princess Elisabeth (Belgium), Neumayer-III and Kohnen (Germany), Aboa (Finland), Maitri (India), Syowa and Dome Fuji (Japan), Troll and Tor (Norway), Novolazarevskaya (Russia), SANAE-IV (South Africa), and Wasa and Svea (Sweden). The British research station Halley is located near western DML on the Brunt ice shelf off the coast of Coats Land.

Most parts of DML are covered by a several kilometer thick ice-sheet, however, at a distance of approximately 150 to 250 km from the coast a line of mountain peaks crops

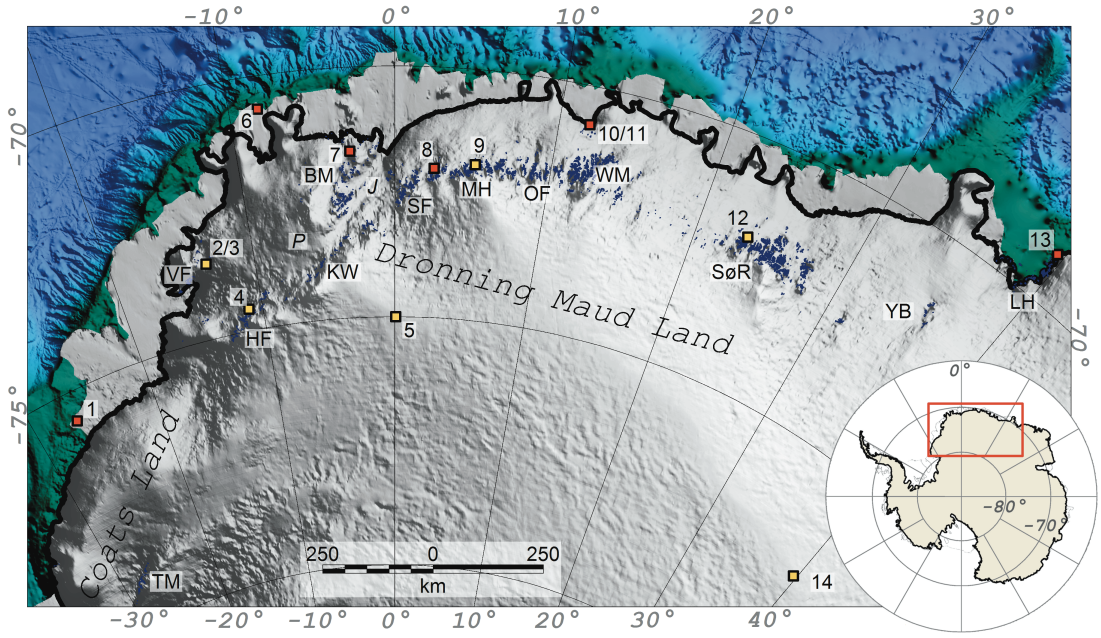

Figure 1.1: Research stations and mountain ranges in Dronning Maud Land and Coats Land. Ice surface is derived from satellite observations (Farr et al., 2007), while the bathymetry is taken from the International Bathymetric Chart of the Southern Ocean (Arndt et al., 2013). Permanently manned research station are marked by red squares and summer stations by yellow squares: 1 - Halley-VI (Coats Land), 2/3 - Aboa/Wasa, 4 - Svea, 5 - Kohnen, 6 - Neumayer-III, 7 - SANAE-IV, 8 - Troll, 9 - Tor, 10/11 - Novolarzarevskaya/Maitri, 12 - Princess Elisabeth, 13 - Syowa, 14 - Dome Fuji. Abbreviations: BM - Borgmassivet, HF - Heimefrontfjella, J - Jutulstraumen, KW - Kriwanveggen, LH - Lützow Holm Bay, MH - Mühlig-Hofmann Gebirge, OF Orvinfjella, P - Pencksøkket, SF - H.U. Sverdrupfjella, SøR - Sør Rondane, TM - Theron Mountains, VF - Vestfjella, WM - Wohlthatmassiv, YB - Yamato-Belgica Complex. Jutulstraumen and Pencksøkket are both major glacial streams in western Dronning Maud Land.

out of the ice. These outcrops are often called nunataks, from Inuit *nunataq*. Western DML comprises the mountain ranges of Vestfjella, Heimefrontfjella, Kirwanveggen, Borgmassivet, and H.U. Sverdrupfjella (Fig. 1.1, 'VF', 'HF', 'KW', 'BM', 'SF'). The Mühlig-Hofmann Gebirge, Orvinfjella, and Wohlthatmassiv are located in central DML (Fig. 1.1, 'MH', 'OF', 'WM'). The Sør Rondane mountains, the Queen Fabiola or Yamato mountains, and the nunataks of the Lützow Holm Bay region are found in eastern DML (Fig. 1.1, 'SøR', 'YB', 'LH'). Outcropping rocks of these mountain ranges provide only scattered glimpses of the subglacial tectonic framework of DML. Nonetheless, much detailed geological information has been gathered since the Maudheim expedition

60 years ago, and their compilation is improving the picture of the geodynamic evolution of East Antarctica (see chapters 4.3, 5.3, and 6.3). However, the tectonic terranes and boundaries interpreted from outcrop geology can only be mapped between the nunataks and into the completely ice-covered region south of them by the collection of regional geophysical measurements. Extensive reconnaissance surveys of such a large and remote region are only possible by aircraft, allowing for radar measurements of ice structures and thicknesses, as well as measurements of subglacial magnetic and gravity signals.

1.2 Rodinia, Gondwana, and Pangaea

Although the idea goes back as far as late medieval times, the first published map to show the complementary coastlines of South America and Africa lying close together based on the geometric aspects was generated by Antonio Snider-Pellegrini (1802–1885) in 1858. Alfred Wegener (1880-1930) formulated the theory of continental drift (Wegener, 1912a,b, 1929) based on the combination of observations in several scientific disciplines such as paleontology, paleoclimatology, geology, and geophysics. Although his theory offered elegant explanations for many observations in the different disciplines, it was not accepted for more than 50 years until the discovery of magnetic seafloor spreading anomalies by Vine and Matthews (1963). Based on the understanding of sea-floor formation and destruction, Wegener's theory was subsequently refined to form part of the plate tectonic paradigm. Today we know that the continents are in constant movement of a few centimeters per year as parts of immense tectonic plates, which also include the large areas of oceanic crust that is constantly formed along mid-oceanic ridges and vanishing into the mantle along subduction zones. Because of this destruction, oceanic crust is rarely preserved at the surface from more than ∼200 million years ago (Ma), except of relicts, which have been obducted onto the edge of continental plates forming ophiolites. The oldest preserved area of oceanic crust is thought to be ∼230 million years old (Myr), in the Ionian basin (Speranza et al., 2012). In contrast, the cratonic nuclei of the continental plates are several billion years old because continental crust is too buoyant in the mantle to undergo subduction. As a consequence of ongoing plate motions, the nuclei periodically collide and form continents and supercontinents, before breaking apart again. This cycle of collision and break-up is called Wilson-cycle after John Tuzo Wilson (1908-1993). Studies of a continent's tectonic structures aim to determine its

geodynamic evolution by interpreting the past kinematics of plates and microplates, and their interactions at their shared boundaries.

The outcrops of DML reveal evidence of two major continent collision phases, during Mesoproterozoic times (1200-1000 Ma) and during Neoproterozoic to Cambrian times (650-520 Ma). The first phase (1200-1000 Ma) is associated with the Grenvillian orogeny and the amalgamation of the supercontinent Rodinia, whose exact configuration is not known, but probably comprised all landmasses at that time. It is assumed that Rodinia broke apart in Neoproterozoic times (800-700 Ma). This phase of extension and rifting was soon followed by the second collision phase (650-520 Ma), which is associated with the Pan-African orogeny and the amalgamation of Gondwana. The collision of Gondwana and Laurussia, and Siberia happened at late Carboniferous / early Permian times (∼300 Ma) and formed the supercontinent Pangaea. The tectonic processes of this collision did not affect East Antarctica and, thus, it is not of importance for studying the tectonic structure of DML. In early Jurassic times, Gondwana started to break apart into the present-day plates of South America, Africa, Arabia, East Antarctica, India, Australia, and New Zealand. The timing of the individual rifting phases in this process can be determined from magnetic seafloor spreading anomaly patterns and the geochronological timescale of reversals of the geomagnetic field. Recently, Gondwana reconstruction models for the DML region have been refined by König and Jokat (2006) and Leinweber and Jokat (2012).

1.3 Aim of this thesis

In contrast to its break-up, the amalgamation of Gondwana remains to be understood in greater detail, because no oceanic crust remains to provide direct information about the plate motions that caused the assembly. Indirect constraints of tectonics processes before Jurassic times (>200 Ma) have to be derived from a combination of various geoscientific results of different disciplines, including structural geology and geophysics, geochronology, paleomagnetism, and paleontology. East Antarctica was the central part of Gondwana, with connections to continental Africa, Falkland Plateau, India, Sri Lanka, Australia, and New Zealand. Outcrop geological data are so sparse that it could only be assumed that the main parts of the interior of East Antarctica constitute a single large stable craton of Archaean age (Grunow et al., 1996; Jacobs et al., 1998; Moyes et al.,

1993; Shackleton, 1996; Shiraishi et al., 1994). However, results of intense geoscientific research within the last years are challenging this assumption (Boger, 2011 and references therein, Ferraccioli et al., 2011). Geological analysis and interpretation of the findings in the outcropping mountain ranges of DML raised the following guiding questions for this thesis: Which crustal segments collided during the formation of Gondwana? Where are their boundaries, major shear zones, and possible suture zones located? Can tectonic structures of southern Africa be traced into DML? Can the Sør Rondane region in eastern DML be associated with the completely ice-covered southern DML?

In order to answer these questions, airborne magnetic and gravity data were acquired by the Alfred-Wegener-Institut Helmoltz-Zentrum für Polar- und Meeresforschung (AWI) in widely unexplored regions of DML and Coats Land between 1994 and 2013. Data acquired between 2007 and 2013 have been processed within the scope of this thesis and compiled with existing published datasets (Jokat et al., 2003; König and Jokat, 2006; Leinweber and Jokat, 2012; Riedel, 2009; Riedel et al., 2012, 2013) and one previously unpublished dataset. They are supplemented by the airborne datasets in the Sør Rondane region, which were acquired during the "Geodynamic Evolution of East Antarctica" (GEA) campaign of the German Federal Institute of Geosciences and Natural Resources (BGR) and AWI in 2011-2012. By combining and interpreting these data alongside the results of geological investigations and ground-based geophysical measurements, this thesis contributes to unraveling the geodynamic evolution of East Antarctica and DML in particular.

Chapter 2

Methods

2.1 Positioning

Geophysical observation from aircraft has been carried out since the beginnings of civil aviation. The advantages of airborne geophysical surveying are its rapid acquisition speed and wide reach. In this way, over the last 20 years the AWI has been able to survey an area of more than 2.6 million square kilometers on- and offshore DML in East Antarctica. The main foci of these investigations were the region's ice structure and thickness, as well as its magnetic and gravity anomaly fields. One of the major challenges of airborne measurements has always been the accurate determination of the aircraft's position at all times during flight. Accuracy has improved greatly over recent decades with the use of global navigation satellite systems (GNSS) and the development of sophisticated navigation post-processing techniques. Since May 2000, the American Global Positioning System (GPS) has been free of selective availability, making positioning with optimal accuracy possible for civil users. Since then, positional inaccuracies have been limited only to those related to atmospheric distortion of the signal in the tropo- and ionosphere, poor satellite geometry, and receiver clock and orbital errors. The state of the art in high-accuracy positioning is achieved by differential GNSS post-processing, using position information simultaneously measured at both a moving object and a stationary base station. This technique requires knowledge of the exact location of the base station, which can be calculated from observations at the base station and stations of the International GNSS Service (IGS) network. The differential GNSS method takes advantage of the fact that the satellites are orbiting high enough above the Earth that the signals for the base

and moving receivers propagate through similar atmospheric conditions, from which the positioning errors can be calculated using the base-station's data set. This approach works well if the receivers are a few tens of kilometers apart or closer. However, in Antarctica, data are often collected at several hundred kilometers distance from the base station, because of the small number and wide spacing of bases and other landing and fuelling sites. Moreover, the base station itself may be located several hundred kilometers away from the nearest IGS network station. Hence, the high accuracy of the differential GNSS post-processing method cannot always be achieved and may vary along flight paths. Because of these drawbacks, the less accurate precise point position (PPP) post-processing technique was tested and applied successfully during this study. This method, which has been extensively investigated during the last two decades, differs substantially from the differential GNSS method as it uses the signal of a single receiver only in combination with precise orbit ephemerides and satellite clock information. It has been demonstrated that a sub-decimeter accuracy level is achievable with the PPP method (e.g. Zumberge et al., 1997; Gao and Chen, 2004; Choy, 2009).

2.1.1 Processing and QC

Four independent GNSS receiver antennas for scientific use are mounted on each of AWI's Basler BT-67 polar aircraft *Polar 5* and *Polar 6*. Their positions are illustrated in Fig. 2.1 together with the positions of the front and rear magnetic sensors and the air/sea gravimeter (s56). Tab. 2.1 lists the local coordinates. Note that the positions of the wing-mounted antennas are estimated for flight conditions and will differ from any ground-based measurements, because the wings flex upwards during flight and sag whilst the aircraft is on ground. Position post-processing was carried out using the Waypoint GPS software package. Position information from each antenna is processed individually as the software does not include a direct solution for a receiver network installed on a moving object. Such a simultaneous solution for all receivers would substantially improve accuracy and reduce operator effort. On the other hand, the current workflow makes it possible to check the quality of the individual receiver positions by calculating their relative distances after the processing, and compare the result to the actual distances (Fig. 2.2). In this way, simple errors can be identified promptly (e.g. wrongly labeled files) and it is possible to compare the quality of different processing techniques. For the latter, calculation of the antennas' height differences has proven to be very suitable. The

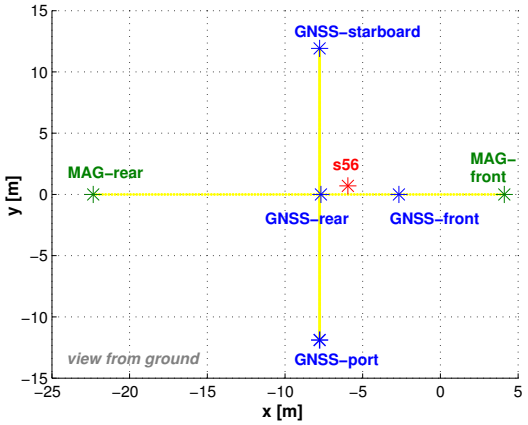

Figure 2.1

	x [m]	y [m]	z [m]
cabin door	-1.94	0.00	0.00
GNSS front	-2.67	0.00	-2.01
GNSS rear	-7.69	0.00	-2.04
GNSS port	-7.77	-11.89	-0.83
GNSS starboard	-7.77	11.92	-0.83
gravimeter (s56)	-5.95	0.70	-0.35
magnetic front	4.11	0.00	0.69
magnetic rear	-22.34	0.00	-2.04
(inertial navigation)	-1.75	0.40	-0.75

Table 2.1

***Polar 5* sensor and GNSS-antenna positions during flight. Local coordinates are defined with: $x = 0$ at cockpit instrument board and positive in flight direction, $y = 0$ at aircraft center line and positive to starboard, $z = 0$ at cabin floor and positive downwards.**

height difference between front or rear antenna and the midpoint of the wing antennas is preferably used for this quality check, as thus the influence of aircraft roll is minimized. The influence of the pitch angle is much less for the height difference between the rear antenna and wing-antennae mid-point; a pitch angle of 5° leads to a height difference of 1.5 cm, whilst for the front antenna it leads to a difference of 45 cm.
The following GNSS post processing options have been tested and the results of height differences are shown in Fig. 2.3:

a) None (raw position)

b) Precise point processing (PPP)

c) Differential GNSS with averaging the raw position for the base station (DGNSS-avg)

d) Differential GNSS with PPP processing for the base station position (DGNSS-ppp)

e) Differential GNSS with IGS network processing for the base station position (DGNSS-net)

f) Differential GNSS combined with tight coupled inertial navigation information and PPP processing for the base station position (IMUTC-ppp)

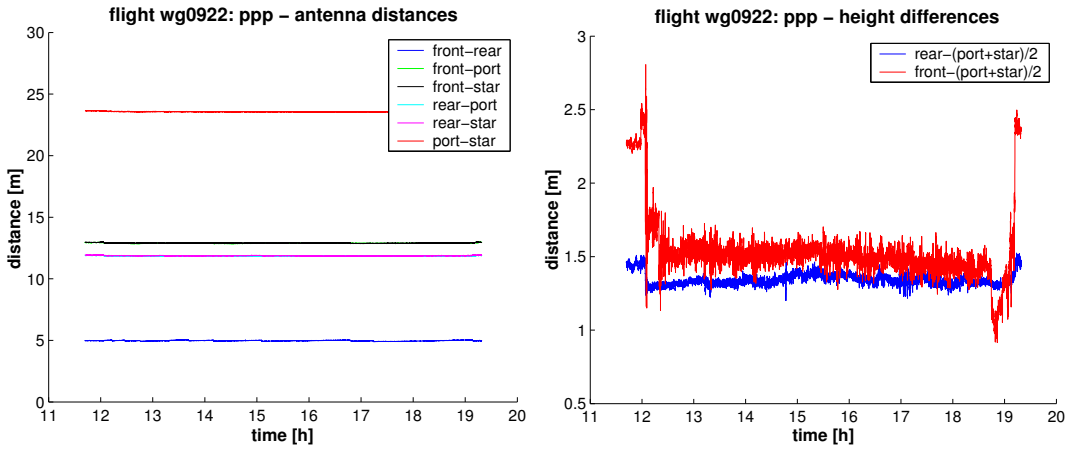

Figure 2.2: GNSS antenna distances for *Polar 5* during a typical flight. Left: absolute distances between antennas. Right: height difference between front/rear and midpoint of port and starboard antennas.

2.1.2 Impact on gravity processing

The height difference analysis for the different position post-processing options (Fig. 2.3) shows that the accuracies for all options lead to a similar range of improvements on the unprocessed raw position, although small differences are detected. Notably, the IMUTC-ppp option uses a smoothing filter on the along-track positions, leading to smoother results in the height analysis. However, the essential question is whether the observed small position differences lead to significantly different results in gravity processing. Vertical accelerations due to aircraft movements are usually much greater in magnitude than the targeted gravitational acceleration anomalies that arise from density heterogeneities in the crust and upper mantle. Hence, it is essential to correct precisely for aircraft accelerations, and these are determined from the post-processed navigation information. Fig. 2.4 shows free-air anomalies calculated for the same flight line using the different position post-processing options listed above. Of course, the raw-positions give unacceptable results, but with the exception of minor differences the free-air anomalies are identical for

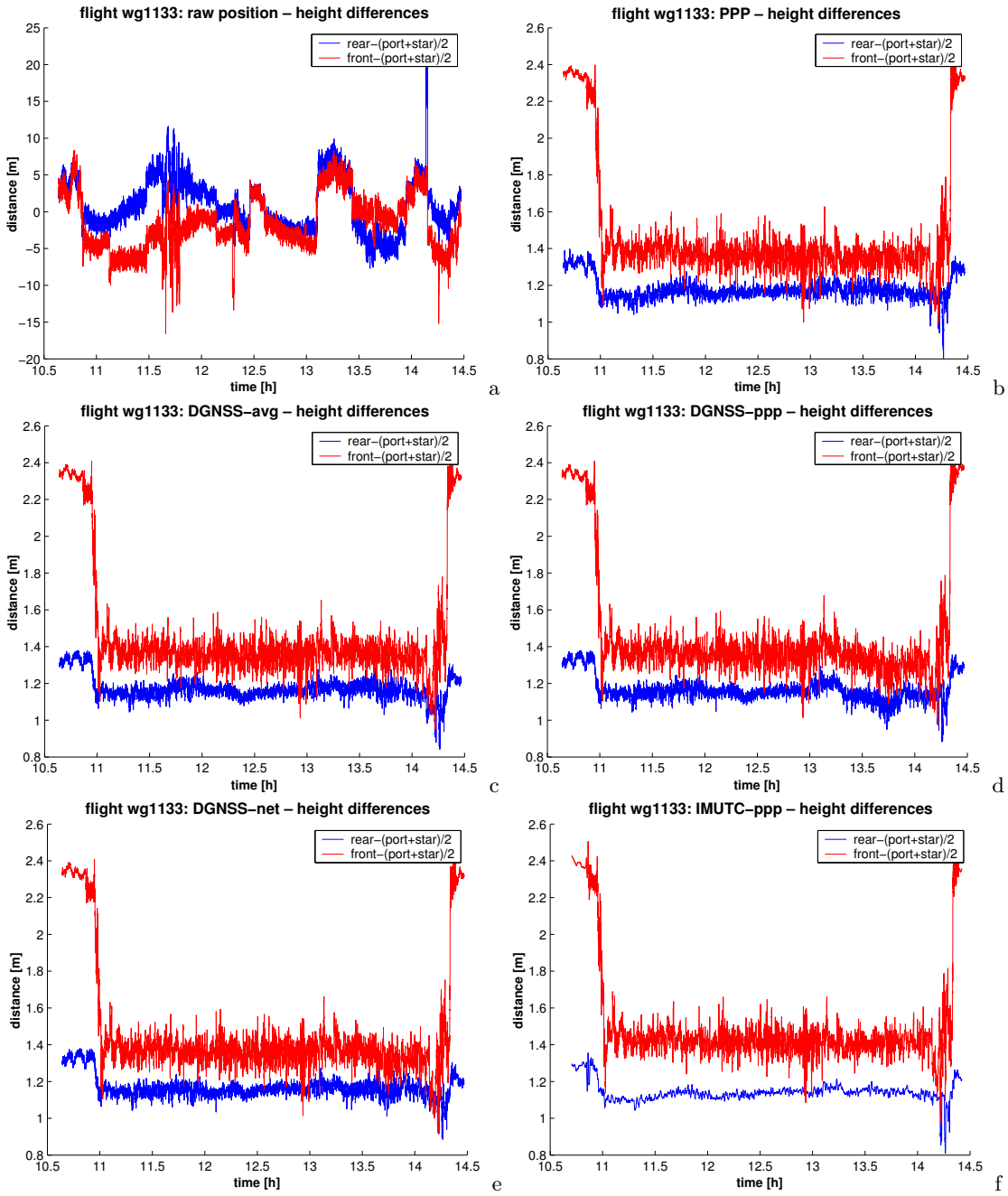

Figure 2.3: Different GNSS post-processing methods tested based on height difference quality check.

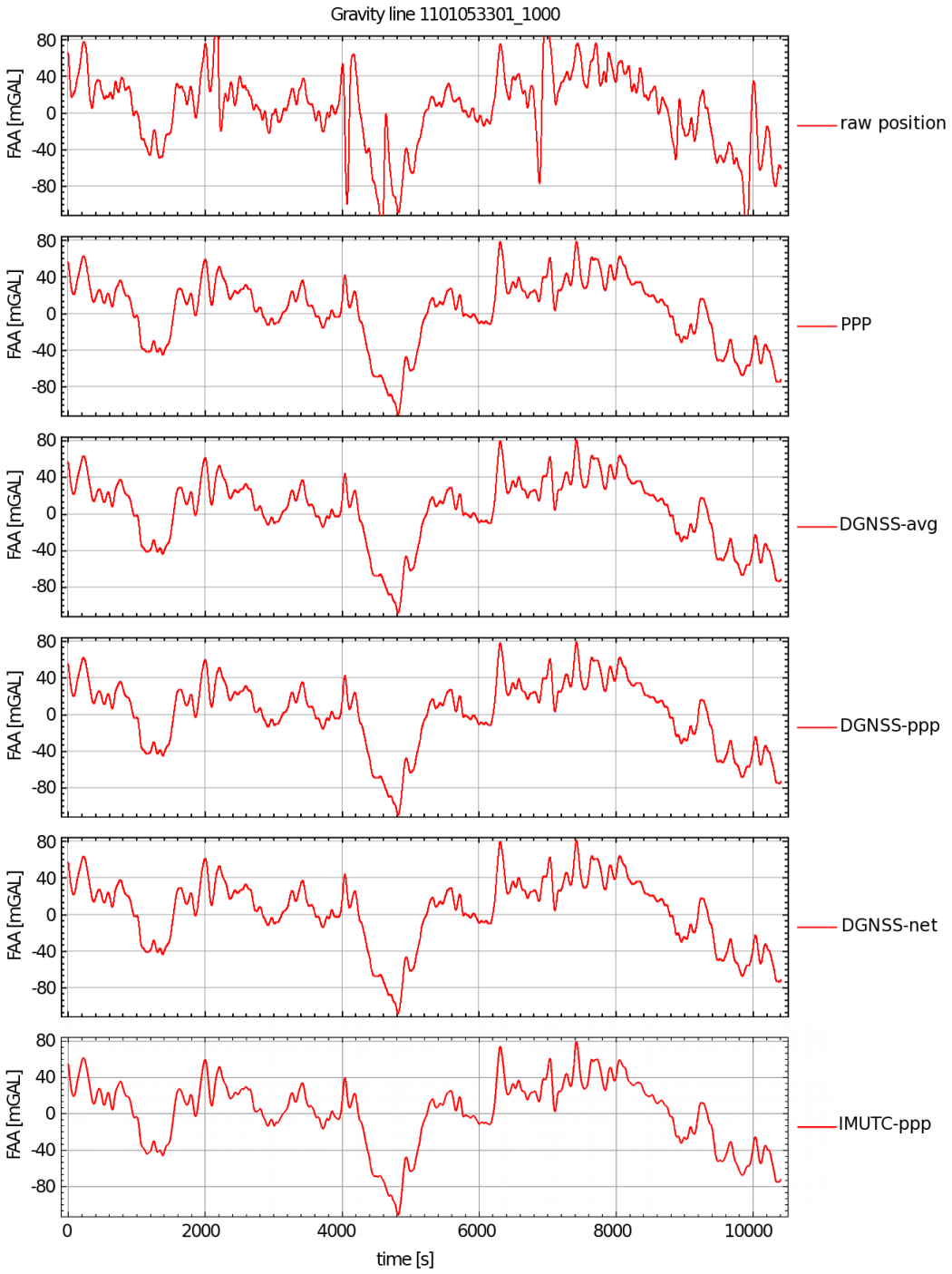

Figure 2.4: Gravity results for different GNSS post-processing methods for a typical aerogravity flight section. Same raw gravity values, but different GNSS post-processing methods applied.

all other options. Subsequently, it is here concluded that the much faster and less data-intensive PPP-method can be used instead of the laborious differential GNSS techniques, without quality impairment when using the LaCoste&Romberg sea-/air-gravimeter s56 and the AWI / Optimare gravity processing software 'airgrav'.

2.2 Aeromagnetics

The total magnetic intensity was measured using Cesium vapor magnetometers. Two Scintrex Cs-2 magnetometers were installed in the wing tips of *Polar 2* and *Polar 4* (both Dornier DO-228) aircraft, whereas on *Polar 5* and *Polar 6* (both Basler BT-67 aircraft) total field sensors were mounted at the end of nose and tail booms (Fig. 2.5). Scintrex Cs-3 magnetometers have been in use since 2011. On all aircraft, a fluxgate magnetometer (Billingsley TFM 100) was installed and used for magnetic compensation. Data processing was carried out using Fugro-LCT and Geosoft Oasis Montaj software. The processing flow included de-spiking, core-field and diurnal variation correction, upward continuation, and leveling.

Figure 2.5: Scintrex Cs-3 magnetic total field sensors are mounted in the ends of nose and tail booms on *Polar 6* (Basler BT-67 aircraft).

2.2.1 Diurnal variations

The Earth's magnetic (or geomagnetic) field is composed of three main components: the core-field, the field due to magnetization of rocks in the upper crust, and the external field. The major portion is the core-field that accounts for 98 % of the entire geomagnetic field. The core-field displays long-period variations measurable over a timescale of years, and random polarity reversals every few hundred thousand to several millions of years. At present, the total intensity is decreasing at 0.1 to 0.2 % per year in DML, and both the core field's inclination and declination are changing by a few arc minutes per year. These long-period variations of the core-field are well monitored by a global network of surface and orbiting magnetic observatories. A prediction of the near future variation is published as the International Global Reference Field (IGRF) every 5 years (International Association of Geomagnetism and Aeronomy, Working Group V-MOD. Participating members: Finlay et al., 2010).

The external magnetic field is caused by the flow of electromagnetic cosmic particles from the sun and movement of the electrically-conducting ionosphere. By its interactions with the core field the external component varies diurnally in the same range as the anomaly field caused by the magnetization of rocks. Each of these smaller components contributes ∼1 % to the entire geomagnetic field near the surface. Diurnal variations of the geomagnetic field range from a few nT to rarely thousands of nT during magnetic storms. Measurements made with a moving total magnetic field sensor include components from both these smaller fields. In order to estimate and to account for the influence of the external field component it is essentially to measure the diurnal variation of the geomagnetic field at a stationary base during the survey period. Fig. 2.6 shows (a) the diurnal variation over 13 consecutive days and (b) the same measurements in a 24-hour plot. It can be seen that the diurnal variations follow a periodic pattern with an optimum quiet window from the morning hours to the afternoon. It is important to consider the actual local time for planning flight activities and to note that often the station time in Antarctica or on research vessels differs from the true local time.

The recorded base-station data were de-spiked and subtracted by the IGRF value for the station location before low-pass filtering with a filter length of 1800 s. Fig. 2.7 demonstrates the magnitude of the diurnal variation during an airborne survey in relation to the magnetic anomaly data.

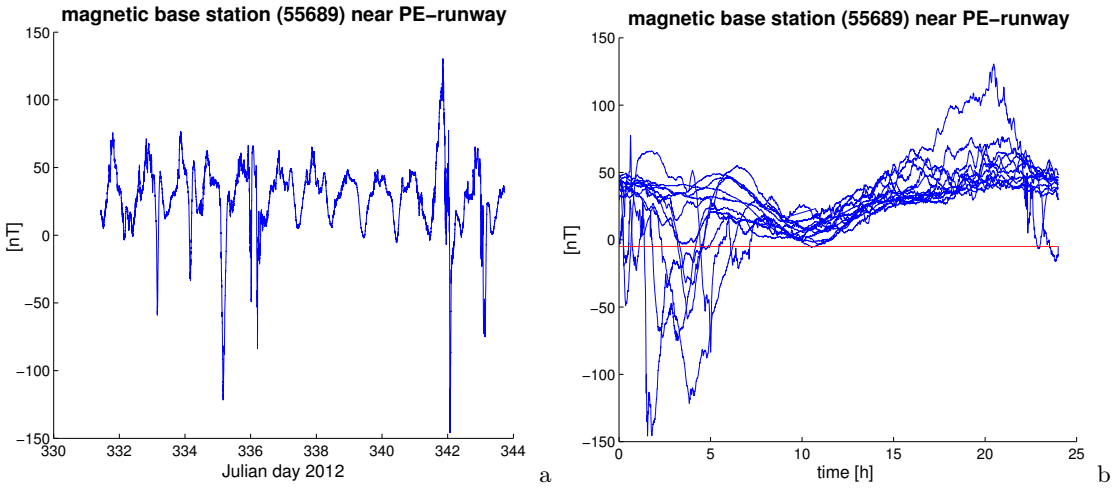

Figure 2.6: Magnetic base station measurements over 13 consecutive days in November/December 2012 near the runway of Princess Elisabeth station (PE). (a) continuous plot, (b) 24-hour plot, red line represents the quiet-level of -5 nT.

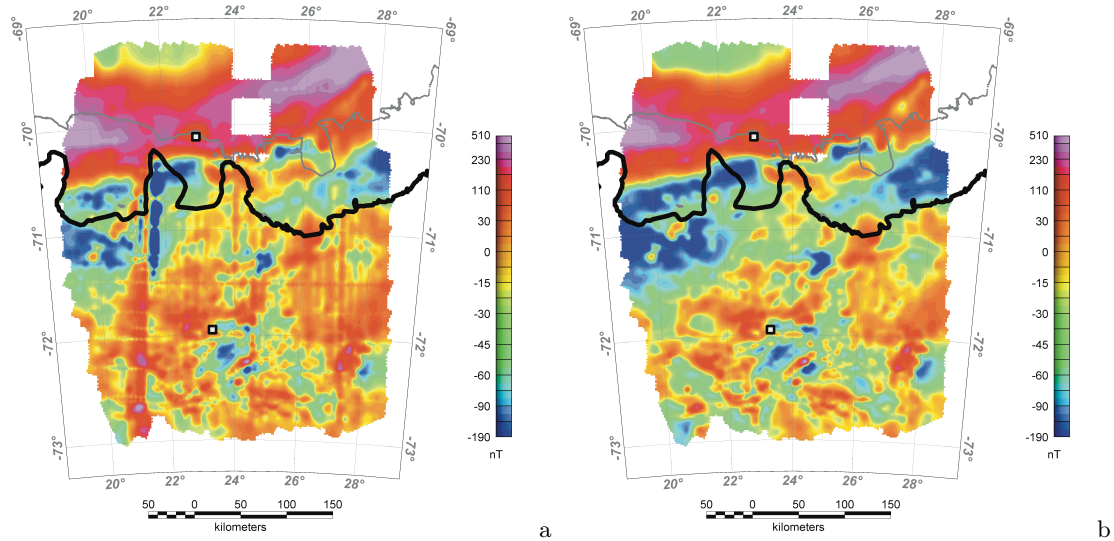

Figure 2.7: Magnetic anomaly map without (a) and with (b) diurnal variation correction. Data were collected during the "Geodynamic Evolution of East Antarctica" (GEA) campaign (see chapter 6).

2.2.2 Compensation

The effects of the aircraft's own permanent magnetization and the magnetization induced as it moves through the geomagnetic field cannot be neglected for the acquisition and processing of aeromagnetic data (e.g. Luyendyk, 1997). AWI uses an AADC-II control unit from RMS-Electronics Limited for recording aeromagnetic data. This system implements a scheme for online compensation for such magnetic aircraft effects, which is based on the equations of Leliak (1961). A set of aircraft maneuvers needs to be flown for the calculation of the compensation parameters at the beginning of a survey. A full set involves subsets of five rolls (±10°), five pitches (±5°), and five yaws (±5°), each subset lasting ∼30 s, to be repeated in each cardinal magnetic heading, beginning with northward. The bank angle between legs is best to be ∼25°. The flown figure is called a compensation box and is illustrated in figure 2.8. It takes about 8 to 10 minutes to fly an complete compensation box. Afterwards, the internal software of the AADC-II system needs less than 60 s to calculate the compensation solution parameters. Thus, it is possible to immediately check the quality of a solution by flying a second compensation box and comparing in real time the uncompensated and the compensated data from the total field sensors. For a successful determination of compensation parameters, it is required that the magnetic field does not change rapidly or by more than 200 nT within the compensation box (the smaller the changes the better the solution). To make this more likely, it is usually aimed to fly the compensation box high above the surface far from any outcrops or shallow bedrock. Near the coast of DML, relatively strong magnetic anomalies are observed that could lead to unsuccessful compensation trials, which needs to be considered when planning the outline of the compensation flight.

Another effect that leads to incomplete compensation determinations are the insensitive 'dead zones' of Cesium vapor magnetometers. Cs-2/3 magnetometers are only sensitive to magnetic fields aligned at angles in the range of 10° to 85° to the optical axis of the sensor. Measurement fails if the sensor is aligned at less than 10° or more than 85° to the inclination of the geomagnetic field. Cs-2/3 sensors are usually installed in a vertical position, in order to avoid the effects of changing instrument sensitivity with changing flight direction. This installation setup fails near the magnetic poles, where the sensors are best mounted in a 45° angle to the horizontal plane. However, depending on the local orientation of the geomagnetic field, the measurement can fail and result in spikes in the recorded data if the aircraft rolls or pitches in a certain flight direction, such that the

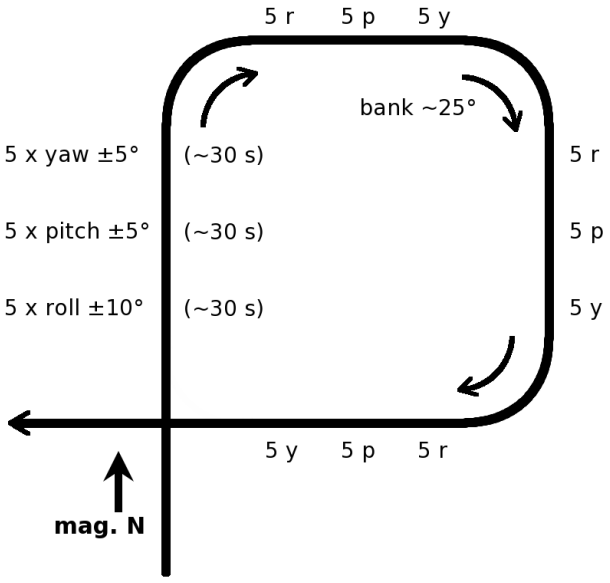

Figure 2.8: Sketch of compensation box with subsets of aircraft maneuvers in each cardinal magnetic heading.

sensor orientation enters its dead zone. Since the compensation is calculated in real time, such spikes in the data cannot be edited before calculating the solution and the entire compensation box needs to be repeated. This is uncomfortable for the crew, expensive, and preventable. Therefore, it is suggested here to calculate the angle between sensor and the inclination for all headings, depending on roll, pitch, inclination, declination, and sensor positioning beforehand (e.g. using the Matlab script given in appendix C) and in addition, as the bank angle in flight turn maneuvers is the most critical factor, to fly a full circle with the desired bank angle (less than the estimated maximum roll) directly before the magnetic compensation, ensuring that no spike occurs in the data between 0° and 270° magnetic heading. Note that the flight turn maneuver from magnetic west to north is not part of the compensation box (Fig. 2.8).

2.2.3 Random line leveling

Despite the inclusion of magnetic compensation and corrections for diurnal variations in the processing flow, cross-point differences can still reach several nT and it is necessary to subject the pre-processed data to a leveling procedure. Cross-point errors occur due to a mixture of inaccuracy, simplifications, and other residual errors (e.g. in compensation,

in upward continuation, due to positioning errors, due to large distances to the magnetic base station, and the height difference between base station and flight elevation). Without applying any leveling, the flight lines are usually apparent at first glance in a magnetic anomaly map. The leveling procedure seeks to remove short-period magnetic artefacts from the anomaly data by minimizing the cross-point errors. Hence, leveling is more successful with a larger amount of cross-points. A full automatic leveling method as offered by Geosoft Oasis montaj software can be applied if the cross-points are evenly distributed over the survey area and if the ratio between measurement lines and tie lines is between 1:5 and 1:10. Doing so requires the processor to distinguish between measurement lines and tie lines. However, in Antarctica, where resources of time and fuel are at a premium and force surveys to aim for maximum coverage, it is difficult to obtain an optimal quantity or distribution of cross-points (e.g. Riedel et al., 2013). A major contribution of this thesis to the scientific community studying the geodynamic evolution of East Antarctica was the compilation of aeromagnetic data systematically measured by AWI in DML from 1994 to 2012 (see chapter 4). The benefit of compiling these data was, besides the large area covered, a significant improvement in the quantity and distribution of cross-points, as the different surveys were flown in different directions and partly overlapping each other (Fig. 4.3-inset). The disadvantage of such a compilation is that it is not possible to distinguish between measurement lines and tie lines. A line of a particular survey might be a tie line for another survey and vice versa. The total number of lines (1091) made it necessary to develop a partially automatic leveling procedure, named here 'random line leveling'. This random line leveling procedure is an adaption of the median leveling technique (Mauring et al., 2002) for practicable usage in Geosoft Oasis montaj. It includes the following steps:

1. Calculation of all cross-point errors.
2. Division of the cross-point errors by two (each cross-point error is captured twice, as positive and negative value on each crossing line respectively).
3. Calculating and applying static line shifts for all lines.
4. Repeating step 1 to 3 until satisfaction (∼2 to 4 times).
5. Repeating step 1 to 2 and calculating tensioned splines for all lines.

6. Low pass filtering of the tensional splines and subsequent application.

7. Repeat steps 1 to 2 and 5 to 6 until satisfaction by reducing smoothness, tension, and filter length.

The advantage of using filtered tensioned splines is that it handles lines with only a few, with many, and with unevenly distributed cross-points without introducing large artificial anomalies, as demonstrated in Fig. 2.9.

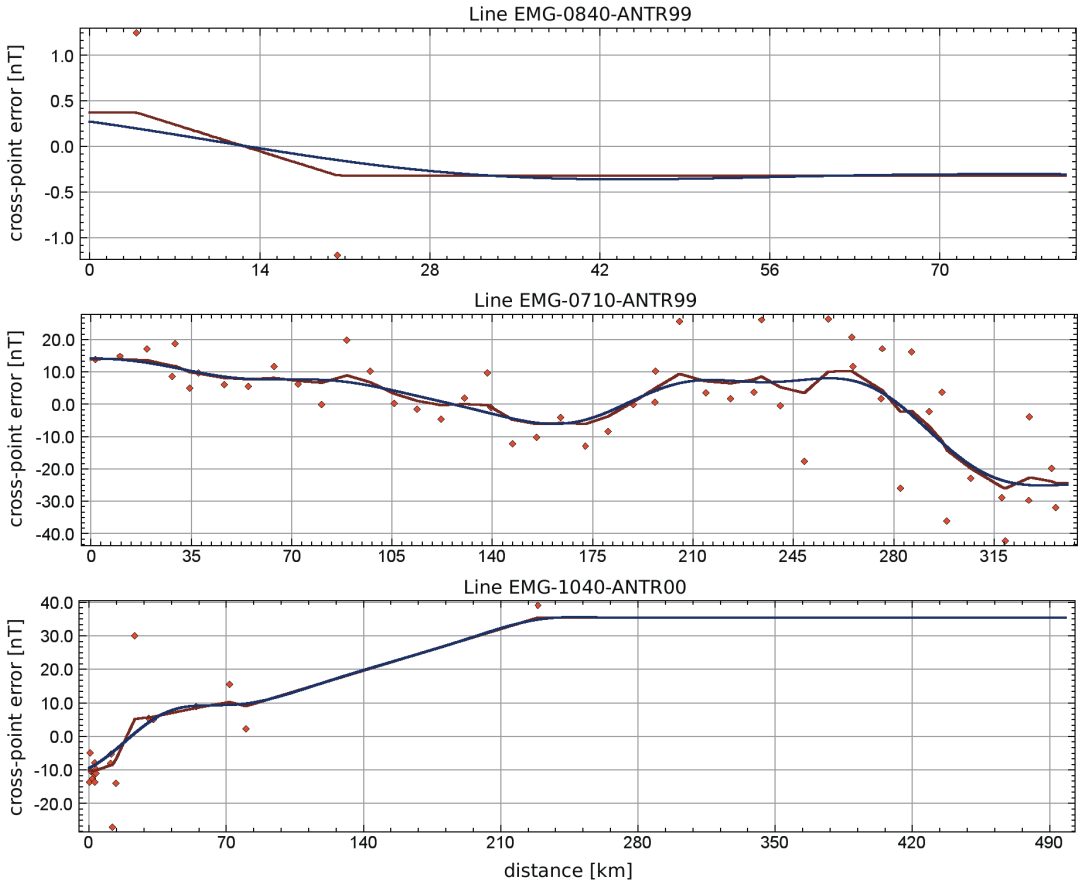

Figure 2.9: Examples of filtered tensioned spline correction for lines with only a few, many, and unevenly distributed cross-points; red dots - cross-point errors, brown line - tensioned spline, blue line - low pass filtered tensioned spline.

Due to the fact that the mean filter had to be substituted by low pass filtering in Geosoft Oasis montaj, the method is not as robust in removing the influence of singular outliers as the mean leveling technique. Because of this, problematic lines with obvious

extreme cross-point errors have to be treated separately before applying the random line leveling technique. Like all leveling methods, the random line leveling workflow is empirical and, therefore, it is necessary to visually check the quality of the data after each leveling iteration. Fig. 2.10 shows a comparison of the compiled AWI-DML magnetic data set before and after leveling. The interpretation of this data set, and its implication for the understanding of the geodynamic evolution of the DML and adjacent regions, are discussed in chapter 4.

2.2.4 Analysis of magnetic anomaly maps

The readiness, of which rocks produce a magnetic field of their own by induction due to the presence of the main geomagnetic field, depends on their mineral composition. Some minerals possess an additional permanent remanent magnetic field, e.g. magnetite (Fe_3O_4) or pyrrhotite (FeS). This remanent magnetization disappears completely at temperatures greater than the mineral-dependent Curie temperature, while the induced magnetization decreases with T^{-1} as the temperature increases. Curie temperatures of common rock-forming minerals range from 500 to 700 °C, corresponding to a depth of ∼20 km in the continental crust. Hence, the lithospheric magnetic anomaly field is mostly caused by heterogeneities of rocks in the oceanic and upper continental crust. The Königsberger ratio, Q, is defined as the ratio between remanent and induced magnetization. Induced magnetization is predominant ($Q<1$) in the rocks of most geological settings, including those of old (up to 4000 Myr) mainly granitic continental crust. Therefore, the inclination and declination of the geomagnetic field needs to be taken into account when interpreting magnetic anomalies of the continental crust. In DML, the usual inclination is about -63° and isolated magnetic anomalies clearly show a bipolar character with a strong high to the north and a weak low to the south of the source body. The reduction-to-the-pole technique takes into account local inclination and declination of the geomagnetic field and transforms magnetic anomaly data so that they appear as if they had been induced within a vertically-inclined field, like that at the magnetic pole. This technique eases interpretation because it changes anomaly characteristics from bipolar to monopolar and shifts the center of the anomaly above the center of the source body.

Derivative maps can be calculated from either the magnetic anomaly map or the reduced-to-the-pole map for further analysis and interpretation. The analytical signal (square

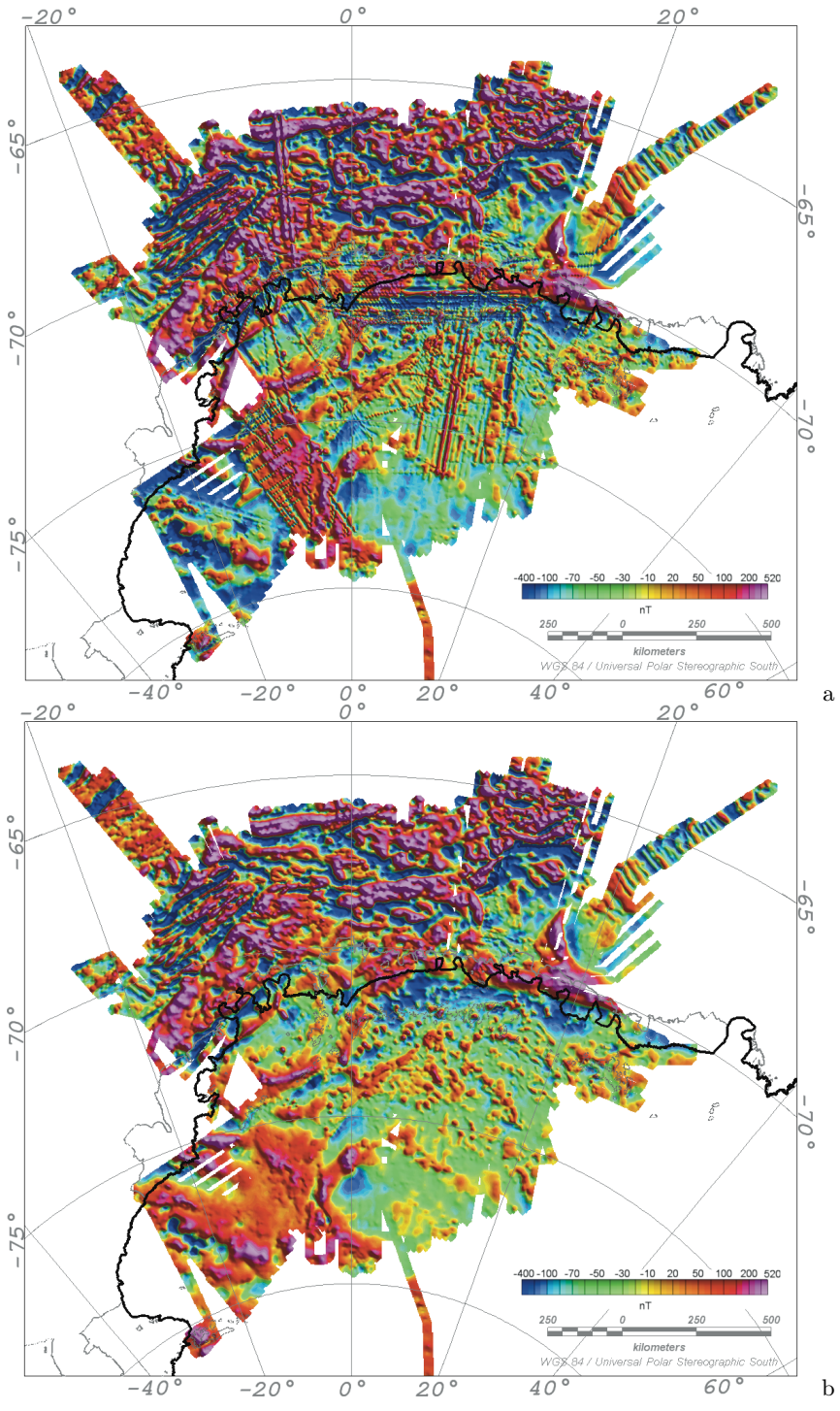

Figure 2.10: Comparison of the compiled DML magnetic data set of the AWI before (a) and after (b) partial automatic random line leveling. The interpretation and its implication for our understanding of the geodynamic evolution of this region are discussed in detail in chapter 4.

root of the sum of squares of derivatives in all three dimensions) and enhanced horizontal derivative maps (Fedi and Florio, 2001) helps to analyze the shape, extent and size of source bodies, while the tilt derivative (arc tangent of ratio between horizontal and vertical derivative) can be used to identify and map the strike of magnetic anomalies (Fig. 4.6 and Fig. 6.2).
The detailed investigation of a remarkable local magnetic high at Giæverryggen in western DML (chapter 5) using measurements made on two profiles at two different flight levels permitted a depth calculation for a spherical source body and subsequently an estimation of the minimum magnetic susceptibility. The following equation for a profile above a spherical source body as given in Lindner and Scheibe (1978) was used in this slightly modified version:

$$M_{sphere} = R^3 \kappa \cdot \frac{T_0 \cos^2 I}{3\sqrt{x^2 + (h-t)^2}^5} \cdot ...$$
$$... \cdot (2(h-t)^2 - x^2) \tan^2 I + 3x^2 \sin^2 L - 6x(h-t) \sin L \tan I - x^2 - (h-t)^2,$$

where R is radius, κ is magnetic susceptibility, t is midpoint depth, T_0 total intensity of the geomagnetic field, I is inclination, L is declination plus line orientation, h is vertical distance (flight elevation), and x is horizontal distance. Because the cubed radius and the magnetic susceptibilities are prefactors, they can take on many pairs of plausible values that produce identical anomalies, demonstrating the non-unique nature of potential field data. However, often the source geometry can be constrained by additional information (e.g. bedrock topography and gravity data). A spherical source with a mid-point depth of 5.6 km, a radius of 4.7 km, and a magnetic susceptibility of 0.3 SI reproduces the measured values at the elevations of both flights crossing the Giæver Magnetic Anomaly (chapter 5). The theoretical anomaly profile at two flight elevations and the vertical decay of the anomaly at a horizontal distance of -2 km from the center of a spherical source body are shown in Fig. 2.11.

2.3 Aerogravity

During aerogeophysical surveys in DML, relative airborne gravity data were acquired with a ZLS modified LaCoste & Romberg Air/Sea gravimeter (s56) mounted on a platform stabilized with gimbals. The platform (Fig. 2.12a) has an oscillation period of four

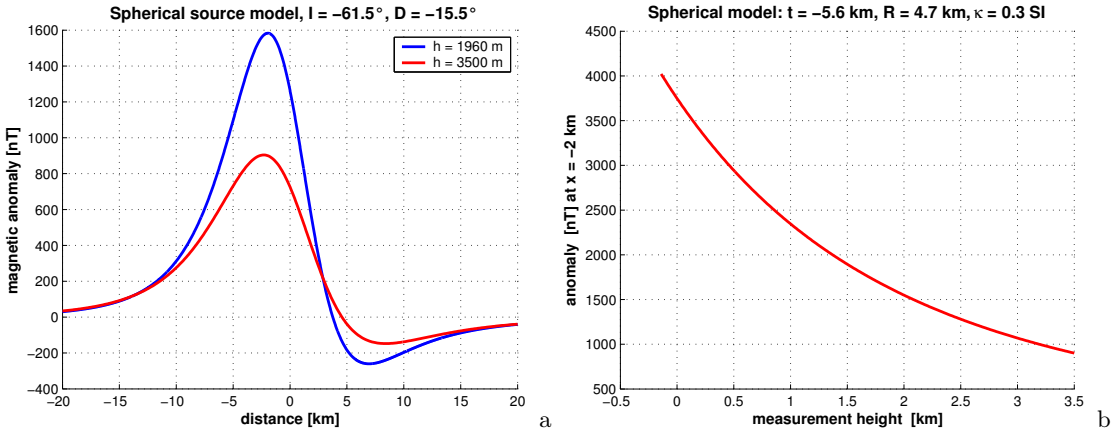

Figure 2.11: Calculated magnetic anomaly of a spherical source model with a mid-point depth of -5.6 km, a radius of 4.7 km, and a magnetic susceptibility of 0.3 SI: (a) anomaly pattern at two flight elevations on a NNW-SSE line, (b) vertical decay of the anomaly at a horizontal distance of -2 km. The model corresponds to a detailed investigation of a conspicuous magnetic high at Giæverryggen in western DML (chapter 5).

minutes. Gravity values were recorded with a sample rate of 1Hz. Before and after each flight, base readings were taken simultaneously with the air/sea gravimeter in the aircraft and with a LaCoste & Romberg portable land gravimeter below the aircraft (Fig. 2.12a). Readings with the land gravimeter were also taken several times during the campaigns at points of known absolute gravity at the Antarctic research stations Princess Elisabeth (O. Francis, pers. comm.) and Novolazarevskaya (J. Mäkinen, pers. comm.), as well as at the International Gravity Standard Network (IGSN-71) station at the University of Cape Town at the beginning and end of each field season. A detailed overview of the ZLS Ultrasys airborne gravity system of the AWI is given by Boebel (2000) and Riedel (2009). It is important to emphasize that vertical accelerations during a flight usually exceed the range of gravity anomalies caused by density contrasts in the crust. Although gimbal mounting and platform stabilization correct for a certain amount of turbulence and tilt, the system is not designed to compensate for larger vertical accelerations and subsequently, a constant barometric flight level needs to be maintained during airborne gravity measurements.

Processing of airborne gravity data includes corrections for latitude, height, vertical aircraft acceleration, tilt, and for motion on the spinning Earth (Eötvös correction), and a 90 s low pass filter – all carried out with the AWI / Optimare program 'airgrav'. This

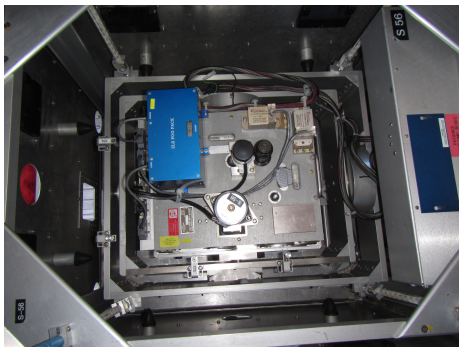

a

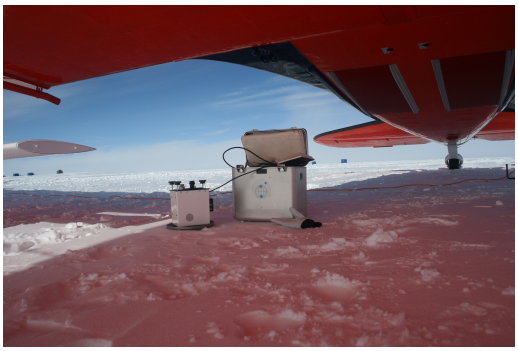
b

Figure 2.12: Relative air/sea and land gravimeters: (a) ZLS modified LaCoste & Romberg Air/Sea gravimeter (s56) mounted on a stabilized platform near the gravity center of the aircraft, (b) land gravimeter used for tying base readings to measurements at points of known absolute gravity.

C-code program was originally a Windows-based application and during this study it was adopted for command line use in the Unix / Linux environment so it could be implemented it in a repeatable batch processing sequence. The low pass filter corresponds to a spatial resolution of ∼7 km, assuming an average speed of 75 m/s over ground during aerogeophysical data acquisition with the Basler BT-67 *Polar 5* or *Polar 6*. The resulting free-air anomaly data after pre-processing needs to be investigated thoroughly as external perturbations might cause artificial anomalies and require additional splitting of lines. Thereafter, the free-air anomaly line data can be subjected to careful leveling as described in chapter 2.2.3 depending on the number of tie lines. Additionally micro-leveling methods (e.g. Ferraccioli et al., 1998) can be applied to the gridded data afterwards.

Chapter 3

Contributions to Scientific Journals

This chapter summarizes the titles, submission histories, main topics, and the contributions of the author and co-authors of the scientific articles, which are presented in chapters 4, 5, and 6.

New aeromagnetic view of the geological fabric of southern Dronning Maud Land and Coats Land, East Antarctica

Matthias Mieth and Wilfried Jokat

Alfred-Wegener-Institut Helmholtz-Zentrum für Polar- und Meeresforschung (AWI)
Columbusstrasse, D-27568 Bremerhaven, Germany

Gondwana Research 25 (2014), pp. 358-367
DOI: 10.1016/j.gr.2013.04.003

Submitted 03 November 2012
Accepted 04 April 2013
Available online 19 April 2013
Published in print January 2014

In this article, we present a compilation of onshore aeromagnetic data in the Dronning Maud Land (DML) and eastern Coats Land that have been systematically acquired by the Alfred-Wegener-Institut Helmholtz-Zentrum für Polar- und Meeresforschung (AWI) between 1994 and 2012. We discuss several aspects of the geodynamic evolution of

this part of East Antarctica and adjacent regions constrained by the new aeromagnetic data. Major new discoveries are made in southern DML, including the southeastern DML province and the Kohnen lineament. The eastern boundary of the BLM craton (or Coats Land block) is mapped based on the aeromagnetic data and two magnetic highs are indicated to represent a probable continuation of the South African Beattie Magnetic Anomaly into East Antarctica. I processed all data acquired between 2007 and 2012, compiled new and already existing magnetic data and developed an adaptive leveling technique for numerous random lines (described in chapter 2.2.3). I developed the interpretational model, and wrote the manuscript, while Wilfried Jokat (AWI project leader) contributed to the results in several discussions.

Banded iron deposits (?) at Grunehogna Craton, East Antarctica - constraints from aeromagnetic data

Matthias Mieth and Wilfried Jokat

Alfred-Wegener-Institut Helmholtz-Zentrum für Polar- und Meeresforschung (AWI)
Columbusstrasse, D-27568 Bremerhaven, Germany

Precambrian Research

Submitted 15 August 2013
Still in review 17 February 2014

We investigated a localized and very strong magnetic high at Giæverryggen within the Grunehogna craton in East Antarctica, measured in detail during the field campaign 2012/13. By comparison with other magnetic highs in western Dronning Maud Land and southern Africa, and by estimating the minimum magnetization based on two level measurements and forward modeling, we infer that the most likely source of the anomaly is a subcrop of banded iron formation. I aquired and processed new aeromagnetic data, and subsequently compiled them with existing data. I estimated the minimum magnetization based on two-level measurements, developed a 2.75-D forward model, and wrote the manuscript, while Wilfried Jokat (AWI project leader) contributed to the results in discussions.

New detailed aeromagnetic and geological data of eastern Dronning Maud Land: Implications for refining the tectonic and structural framework of Sør Rondane, East Antarctica

Matthias Mieth[1], Joachim Jacobs[2], Antonia Ruppel[3], Detlef Damaske[3], Andreas Läufer[3], and Wilfried Jokat[1]

[1] *Alfred-Wegener-Institut Helmholtz-Zentrum für Polar- und Meeresforschung (AWI)*

Columbusstrasse, D-27568 Bremerhaven, Germany

[2] *University of Bergen, P.O.Box 7800, 5020 Bergen, Norway*

[3] *Federal Institute for Geosciences and Natural Resources (BGR)*

Stilleweg 2, 30655 Hannover, Germany

Precambrian Research

Submitted 11 November 2013
Reviewed 24 January 2014
Revision submitted 11 February 2014

We present initial results of the geological-geophysical expedition "Geodynamic Evolution of East Antarctica" (GEA), a collaborative research programme of the German Federal Institute of Geosciences and Natural Resources (BGR) and the Alfred-Wegener-Institut Helmholz-Zentrum für Polar- und Meeresforschung (AWI) and, in cooperation with the Universities of Bergen (Norway), Bremen (Germany), and Ghent (Belgium). Aeromagnetic data, acquired in 2011 and 2012, are correlated with magnetic susceptibility measurements and geological findings in the Sør Rondane Mountains and allow a projection of tectonic terranes into ice-covered areas. In large parts of the mountain range, the geological and geophysical data agree reasonably well. The new data allow mapping and in part refinement of several tectonic boundaries, and reveal that the central part of the SRM is of important significance for understanding the geodynamic evolution of the region. Furthermore, the discovered continuation of the in chapter 4 described southeastern DML province into the southern Sør Rondane region allows a scattered glimps of its rock composition at a few outcrops.

I contributed to the aerogeophysical data acquisition as member of the scientific flight crew in January 2012 and as expedition leader in November/December 2012. I processed

the aeromagnetic data, compiled them with already existing data, and derived a 2.75-D forward model for a strong magnetic anomaly within the survey area. I generated all figures and wrote the manuscript. Joachim Jacobs was leader of the geological field party in 2010/2011 and a member of the party in 2011/2012. He supported me in the geological interpretation of the magnetic data, contributed to the results in several discussions, wrote the section “Geological overview of Sør Rondane”, and greatly enhanced the manuscript. Antonia Ruppel was member of the geological field party in 2011/2012 and of the scientific flight crew in November/December 2012. She processed and summarized the magnetic susceptibility measurements, wrote the subsection "Magnetic susceptibility measurements" and contributed to the results in discussions. Detlef Damaske (member of the geological field party in 2010/2011 and 2011/2012), Andreas Läufer (leader of the geological field party in 2011/2012), and Wilfried Jokat (AWI project leader) contributed to the results in discussions.

Chapter 4

New aeromagnetic view of the geological fabric of southern Dronning Maud Land and Coats Land, East Antarctica

Matthias Mieth and Wilfried Jokat

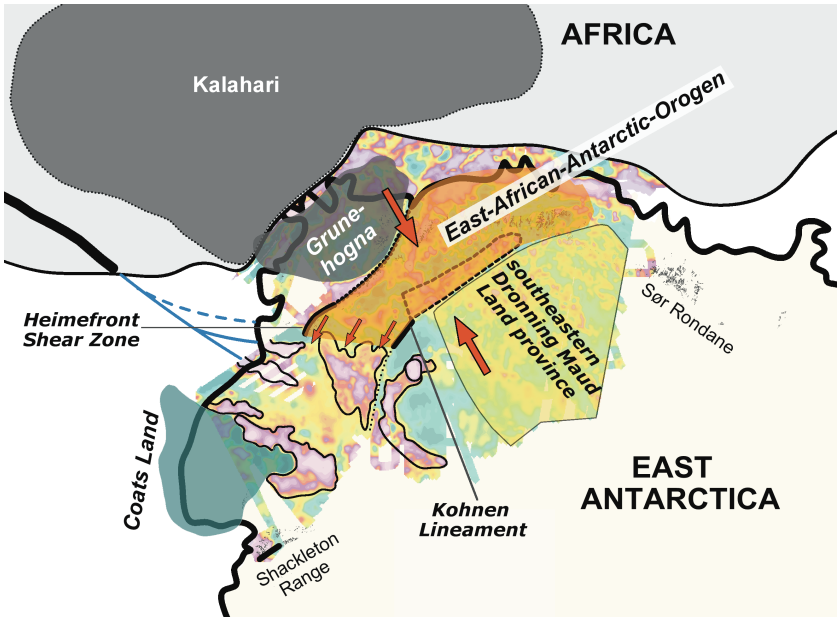

Figure 4.1: Graphical abstract

4.1 Abstract

The ice shield of Antarctica, which measures several kilometers in thickness, presents a challenge when attempting to unravel the subglacial geology. Here, we report about systematic airborne magnetic surveys conducted over the last decade, which investigated a significant part of Dronning Maud Land (DML), imaging for the first time the crustal architecture of the interior of this sector of East Antarctica. High-resolution data reveal parallel, elongated magnetic anomalies in southeastern DML. These NW-SE trending anomalies can be traced farther east into sparser Russian magnetic data sets. Several high amplitude magnetic anomalies with values above 400 nT have been observed in southwestern DML and Coats Land. They differ clearly in wavelength and amplitudes from the magnetic pattern found in the east and do not show any evidence of a Pan-African orogenic belt or suture zone connecting the Shackleton Range with eastern DML, as hypothesized in several studies. This leads to the assumption of the existence of a hitherto unrecognized large tectonic province in southeastern DML. Whereas an over 100 km long magnetic lineament in the interior of the Dronning Maud Land may reflect a major shear zone akin to the Pan-African age Heimefrontfjella shear zone. Both findings bring new evidences to the still open question about the amalgamation of East and West Gondwana. In addition, the magnetic data allow mapping the eastern extent of the presumable cratonic province of Coats Land, a region considered as a key piercing point for reconstructions of Rodinia. Furthermore, the Beattie Magnetic Anomaly in southern Africa is assumed to continue into East Antarctica. Two magnetic highs in western DML are identified as possible eastward continuation of this prominent anomaly.

KEY WORDS: Aeromagnetic, Dronning Maud Land, Coats Land, East Antarctica, Gondwana Suture, Rodinia

4.2 Introduction

East Antarctica represents the central puzzle piece in the attempt to reconstruct Gondwana, containing continental fragments of both East- and West-Gondwana, and our study area Dronning Maud Land (DML) is somehow located in between. The exposed rocks of DML show a Pan African (∼650-490 Ma) metamorphic reworking, except for the most western part, which consist of Archaean (>2.5 Ga) and undeformed Grenvillian (∼1.1

Ga) basement rocks (see review by Boger (2011) and references therein).

Therefore, the Antarctic part of the suture zone between East- and West-Gondwana is supposed to be located somewhere in DML (Fig. 4.2, blue dashed lines), either as an extension of the Mozambique belt (Moyes et al., 1993; Shiraishi et al., 1994; Grunow et al., 1996; Shackleton, 1996) forming a continuous East African-Antarctic orogen (Jacobs et al., 1998), as a curvilinear continuation of the Kuunga suture (Boger and Miller, 2004), or as a combination of both (Kleinschmidt and Boger, 2009). The variety of models exists because most of the geology is not accessible to direct sampling due to the extensive ice coverage. Hence, aero-geophysical data play a key role in extrapolating the sparse geological information into the interior of East Antarctica for purposes of developing a reliable tectonic model. Several onshore aeromagnetic surveys (Golynsky et al., 1996; Golynsky et al., 2002; Damaske et al., 2005; Ferraccioli et al., 2005a,b; Shepherd et al., 2006; Riedel et al., 2013) were conducted in DML to better constrain and understand the Gondwana pre-breakup geology (older than ∼180 Myr). In this context, an important discovery by Riedel et al. (2013) identified, among other magnetic anomalies, a linear NE-SW trending anomaly in central DML (Fig. 4.2, gray area (6): Forster Magnetic Anomaly), which might represent the suture zone of the East African-Antarctic orogen in Antarctica (Riedel et al., 2013). Since 2008 subsequent surveys constantly densified the magnetic data set in the unexplored southern DML (Fig. 4.3-inset, red lines). The latest compilation of this larger data set is subject of this contribution, including a hitherto unpublished data set over eastern Coats Land, providing new insights about the tectonic fabric of southern DML. The analysis of our data supports not only the conclusion of Riedel et al. (2013) about the location of the E-W Gondwana suture zone in DML and identifies its possible continuation, but also indicating that the interior of East Antarctica is not comprised of one stable craton but rather of a mosaic of different crustal fragments. The latter will be of interest for studies of both the Gondwana and the Rodinia assembly.

4.3 Geological setting

Very little is known about the geology of the ice-covered interior of DML since all outcrops are located at the northern rim of the area of interest. The prominent Archaean Grunehogna province is located in the NW of DML (Fig. 4.2, G). Prior to the Gondwana break-up (∼180 Ma), this craton was juxtaposed to the Kaapvaal craton in southern

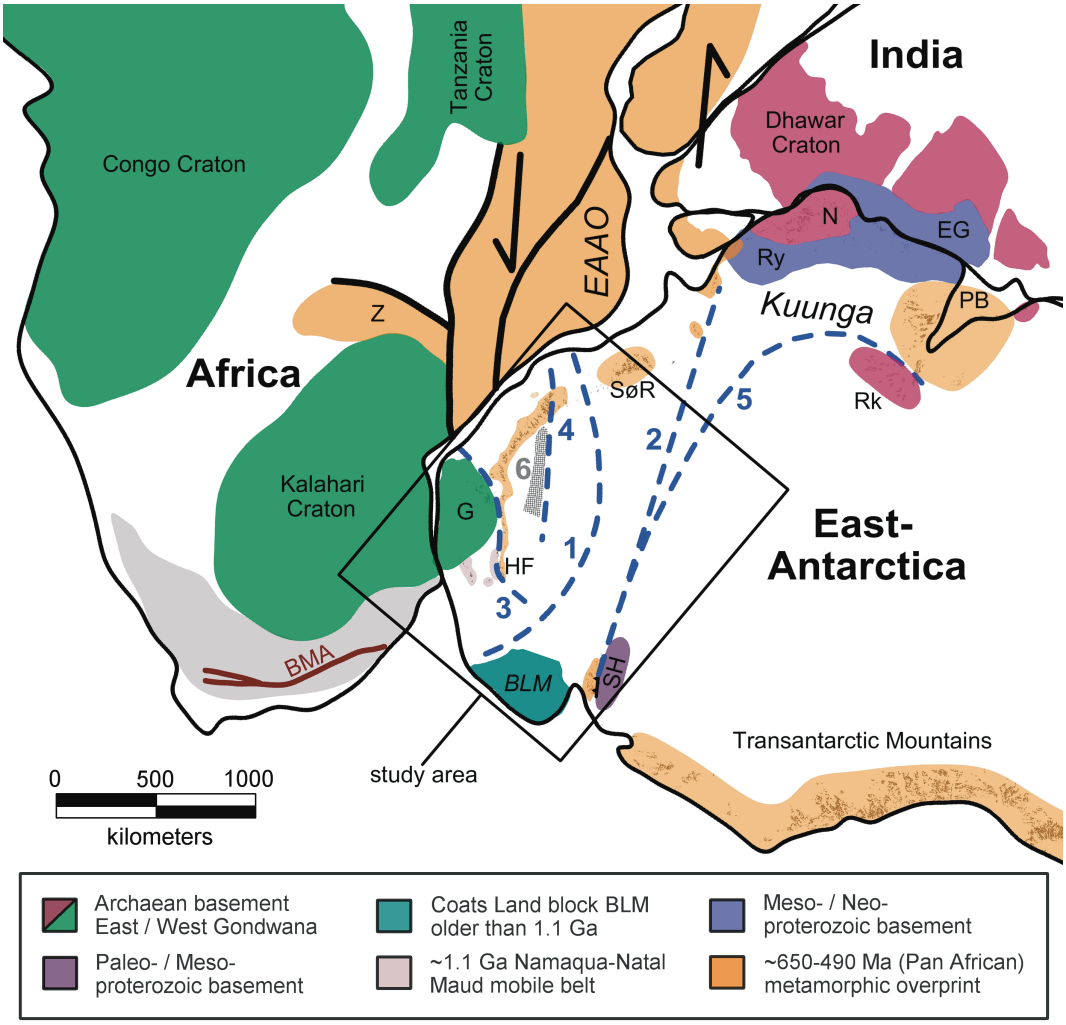

Figure 4.2: Geological setting of the study area within Gondwana at ~500 Ma. The simplified sketch is adapted from Jacobs and Thomas (2004) and Helferich et al. (2004). Blue dashed lines showing hypothesized traces of the E-W Gondwana suture: 1 – Moyes et al. (1993), 2 – Grunow et al. (1996), 3 – Shackleton (1996), 4 – Jacobs et al. (1998), and between East Antarctica and West-Gondwana: 5 – Kleinschmidt and Boger (2009). The gray area (6) marks the Forster Magnetic Anomaly interpreted as suture by Riedel et al. (2013). The East African orogen is assumed to continue into Antarctica forming one orogen (EAAO), while the term Kuunga is used for collision of India and East Antarctica. Abbreviations: BLM – Betrab-Littlewood-Molke province (Coats Land block), BMA – Beattie Magnetic Anomaly, EAAO – East African Antarctic orogen, EG – Eastern Ghats, G – Grunehogna craton, HF - Heimefrontfjella, N – Napier, PB – Prydzbay, Rk – Ruker craton, Ry - Rayner, SH – Shackleton Range, SøR – Sør Rondane, Z – Zambezi belt.

Africa (e.g., Martin and Hartnady, 1986; Leinweber and Jokat, 2012). The low-grade sedimentary and volcanogenic rocks of the Ritscherflya Supergroup overlay the Archaean basement in the eastern part of the Grunehogna province. These Mesoproterozoic rocks are intruded by tholeiitic sills and dykes (Wolmarans and Kent, 1982), interpreted as part of the Umkondo large igneous province (LIP) and are linked to coeval LIPs in Laurentia (Hanson et al., 1998, 2004), supporting the SWEAT hypothesis (Moores, 1991). The area of Borgmassivet is associated with magnetic high frequency anomalies of medium amplitudes up to 150 nT Ferraccioli et al. (2005a).

A Grenvillian (∼1.1 Ga) collision belt named Namaqua-Natal-Maud fringes around the Kaapvaal-Grunehogna craton (e.g. Jacobs et al., 1998). It is commonly interpreted to be formed by an juvenile island arc, but Grosch et al. (2007) concluded from isotopic data and geochemical characteristics that at least the Maud belt in Antarctica was once an active continental volcanic arc, thereby neglecting the existence of a major Grenvillian crustal suture between both provinces. The eastern part of the Maud belt underwent a metamorphic overprint of Pan-African ages (∼560-490 Ma). The main shear zone at Heimefrontfjella (Fig. 4.2, HF), separating the metamorphic overprinted rocks in the east from non-overprinted rocks in the west, represents a major tectonic feature, as the entire Grenvillian basement of central DML shows Pan-African metamorphic reworking and, hence, is regarded as the western front of the East African-Antarctic orogen (Golynsky and Jacobs, 2001). Perritt and Watkeys (2003) suggested that an unknown block east of western DML moved NNW with respect to the Grunehogna craton, leading to shearing and escape tectonics in a compressional regime in western DML. Jacobs and Thomas (2004) presented a lateral-escape tectonic model for the southern termination of the East African-Antarctic orogen, thus explaining the origin of the microplates Falkland Island, Ellsworth-Haag and Filchner blocks (not shown in Fig. 4.2), and suggesting that the exposed Heimefront shear zone is just one of several shear zones in western DML. Pan African events in central DML can be differentiated into two stages, an early compressional phase (560-550 Ma) and a subsequent dilational phase (530-490 Ma), whereas the latter phase is associated with voluminous intrusions of post tectonic granotoids and interpreted as a time of orogenic collapse (Jacobs et al., 2003).

The deep Jutul-Penck graben system (up to 1000 m b.s.l.) is located at the eastern rim of the Grunehogna Province and continues westward as well as southward through the Maud belt (Fig. 4.5, JP). This graben system is most likely a failed rift system of

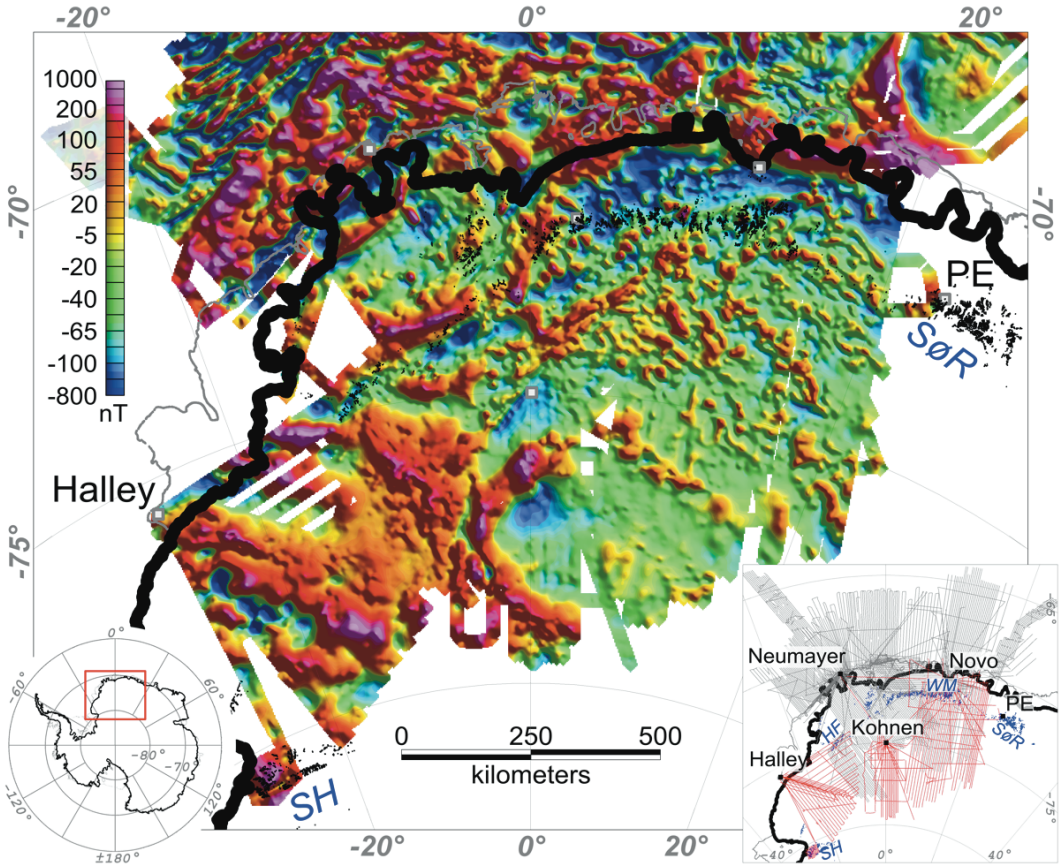

Figure 4.3: Aeromagnetic anomaly map of Dronning Maud Land and Coats Land. Inset shows AWI-survey lines (1994-2012). Abbreviations: HF – Heimefrontfjella, PE – Princess Elisabeth, SH – Shackleton Range, SøR – Sør Rondane, WM – Wohlthatmassiv

Jurassic age (Grantham and Hunter, 1991). Both flanks of the graben contain Jurassic dolerite dikes and basalts, which erupted some ∼183 Ma as part of the Karoo LIP (e.g. Harris et al., 1990) as well as Jurassic alkaline intrusions, which can be associated with a number of complex magnetic positive anomalies, while a prominent magnetic low over the Jutul graben indicate either an amagmatic rift or thick subglacial sediments (Ferraccioli et al., 2005a; Riedel et al., 2013). Our dataset covers some poor studied outcrops like the Steingarden nunataks between the Wohlthatmassiv in central DML and Sør Rondane in eastern DML, yet not the Sør Rondane region itself. The geological structure of Sør Rondane is quite similar to that of central DML, with a Proterozoic basement, medium- to high-grade metamorphic reworking during Pan-African times and intrusions of plutonic rocks and minor mafic dykes (Shiraishi et al., 1994). Several Pan

African aged events have been identified, an early granulite facies metamorphism in the northeastern terrane (600-650 Ma) and an amphibolite facies metamorphism (∼570 Ma) in the southwestern terrane, which was followed by granotoid intrusions and contact metamorphism (560-500 Ma), (Shiraishi et al., 2008). Important to note is the existence of an ENE-WSW trending main shear zone in the southwestern terrane. The terrane south of this main shear zone is dominated by partly undeformed granodiorites (Ruppel, 2012). Hence, the grade of metamorphism is decreasing from N to S. Dark graphite- and pyrite-bearing schists have recently been discovered at moraines near the Steingarden nunataks (72.3°S/16.1°E). Similar metamorphosed black-shale-type sediments have not been reported from anywhere else in central DML, but higher grade metamorphosed equivalents have been found in SøR (Schlüter et al., 2011).

The Shackleton Range is situated in the westernmost part of the investigated area at 80°-81°S and 19-31°W (Fig. 4.2, SH). It is a key area for studying the geological architecture of Antarctica and reconstructing the Gondwana assembly. A prominent E-W striking and southward directed thrust fault caused by nappe tectonics (Kleinschmidt et al., 2001) separates the southern terrane, regarded to be part of the East Antarctic craton, and the northern terrane which underwent Pan-African high-grade deformation between 530 and 500 Ma, while in both terranes Paleoproterozoic ortho- and paragneises show a high-grade metamorphism at ∼1.7 Ga (e.g. Clarkson et al., 1995; Tessensohn et al., 1999; Zeh et al., 2004 and references herein). The latter distinguishes the Shackleton Range basement from the Grenvillian (∼1.1 Ga) basement of the Maud belt in western and central DML, whereas orientation and collisional-related Pan African orogenic processes can be correlated to similar processes in DML, rather than to the coeval, yet orthogonal oriented subduction-related Ross-orogeny processes of the Transantarctic Mountains (Kleinschmidt et al., 2001).

The exposure of an ophiolitic complex at Herbert Mountains in the northern terrane is of high relevance for Gondwana reconstructions. It is a relict of oceanic crust younger than 1 Ga and older than 500 Ma, presumably a part of the Mozambique Ocean (Talarico et al., 1999). Thus, the Shackleton Range is part of the E-W Gondwana collision. It has been proposed in several studies that the Shackleton Range suture zone continues underneath the ice-covered southern part of DML to Lützow Holm Bay region in eastern DML (e.g. Grunow et al., 1996) or further to the Prydz Bay region (Boger and Miller, 2004; Kleinschmidt and Boger, 2009), however, these models are challenged by our data.

North of the Shackleton Range, only the few nunataks of Touchdown Hills (Bertrab, Littlewood, and Moltke) at Vahsel Bay (77.9°S/34.3-35.5°W) provide an insight into the subglacial geological basement of Coats Land. The exposed rhyolites and granophyres at Bertrab and Littlewood nunataks, emplaced ∼1.1 Ga, show no significant Pan-African metamorphic overprint (Gose et al., 1997). The ages of meta-sediments at Moltke nunatak are unknown, but they are interpreted to be older than 1.1 Ga, thus, this area may represent an independent cratonic province named Coats Land block or BLM after the nunataks Bertrab, Littlewood, and Moltke (Kleinschmidt, 2002) – separated from the Grunehogna province by the Maud belt (Fig. 4.2). The emplacement of the igneous rocks is coeval with the Umkondo LIP, but paleomagnetic data showed a separation of ∼30° of latitude at 1.1 Ga (Gose et al., 1997). Pb isotopic data of the igneous rocks of Coats Land showed both a strong correlation with Keweenawan-LIP of Laurentia and no overlap with Umkondo LIP – implying that the BLM province is possibly a fragment of Laurentia (Loewy et al., 2011) and an important tracer for Rodinia reconstruction models. The western extent of the BLM province was identified by Russian aeromagnetic and gravity data (Studinger and Miller, 1999; Golynsky and Aleshkova, 2000), while the eastern extent remained undefined until this study. Figure 1 shows a simplified sketch of the tectonic features of DML and Coats Land, as briefly reviewed herein, and their linkage to adjacent regions. For a broader picture of the geology of East Antarctica, we refer to the overview paper of Meert (2003), Satish-Kumar et al. (2008), Talarico and Kleinschmidt (2008), and Boger (2011).

4.4 Data acquisition and processing

Over 260 000 km of magnetic survey lines have been acquired in DML by AWI from 1994 to 2012. An area of about 2.3 million km^2 was covered with a general line spacing of 10 km (Fig. 4.3-inset). Scintrex Cs-2 Caesium magnetometers were installed in the wing tips of *Polar 2* and *Polar 4* (both Dornier DO-228), in nose and tail booms of *Polar 5* (Basler BT-67), or towed ∼35 m below the helicopter on offshore campaigns (operated from *RV-Polarstern*). Scintrex Cs-3 Caesium magnetometers have been used in nose and tail booms of *Polar 6* (Basler BT-67) since 2011. On all fixed-wing aircraft, a fluxgate magnetometer was installed and used for magnetic compensation.
Data processing was carried out using Fugro-LCT and Geosoft Oasis Montaj software.

The processing flow included de-spiking, core-field and diurnal variation correction, upward continuation to 4600 m for onshore and 350 m for offshore data, as well as leveling. Static shift corrections were applied between the different survey areas – notably, the survey over Coats Land from 1994/95 was shifted by +109 nT, reducing the cross-point errors from 54.1 ± 64.1 nT to 21.7 ± 25.2 nT, followed by low pass filtered tensional spline correction, reducing the cross-point error to 4.0 ± 5.3 nT.
The offshore data have been previously used to refine kinematic models for the early Gondwana break-up (Jokat et al., 2003; König and Jokat, 2006; Leinweber and Jokat, 2012) and are not shown here. The onshore data cover a large area of 1.5 million km^2 – nearly half the size of India. The magnetic anomaly maps in Figures 4.4 and 4.5 are superimposed on data from the Antarctic Digital Magnetic Anomaly Project (ADMAP, Golynsky et al., 2007). Data sets have been reduced to the pole with a mean inclination (I) and declination (D) for each region (I_{fig3} = -63°, D_{fig3} = -31°, I_{fig4a} = -64°, D_{fig4a} = -6°, I_{fig4b} = -67°, D_{fig4b} = 1°, and I_{fig5} = -64°, D_{fig5} = -19°), as we assume that induced magnetization is dominant in the onshore region. Derivative maps (analytical signal, positive tilt derivative, and enhanced horizontal derivative) have been calculated for the area of the Kohnen lineament (Fig. 4.6) in order to enhance the source boundaries. Calculation of the enhanced horizontal derivative map was based on the method of (Fedi and Florio, 2001), with first order vertical derivative of the reduced to the pole field as start signal.

4.5 Results

4.5.1 Magnetic anomaly pattern of southeastern Dronning Maud Land

A very large area (600 km x 900 km) of a rather weak magnetic anomaly field (Fig. 4.4, A) dominates the magnetic pattern of southeastern DML. This area contains narrow (10-20 km) and elongated (100-200 km) positive, small amplitudes anomalies (50-100 nT) (Fig. 4.4, white lines). These anomalies are parallel oriented and strike NW-SE. They are truncated by the Forster Magnetic Anomaly (Fig. 4.4, FMA) in the NW and confined by the Wohlthatmassiv (Fig. 4.4, WM) in the north, but they can be traced farther east (Fig. 4.4, blue dashed lines) where ADMAP data are available. However, the actual extent of this anomaly pattern remains unknown due to the sparse line spacing and data gaps of existing ADMAP-data in the east. The magnetic anomaly field in area A is, in

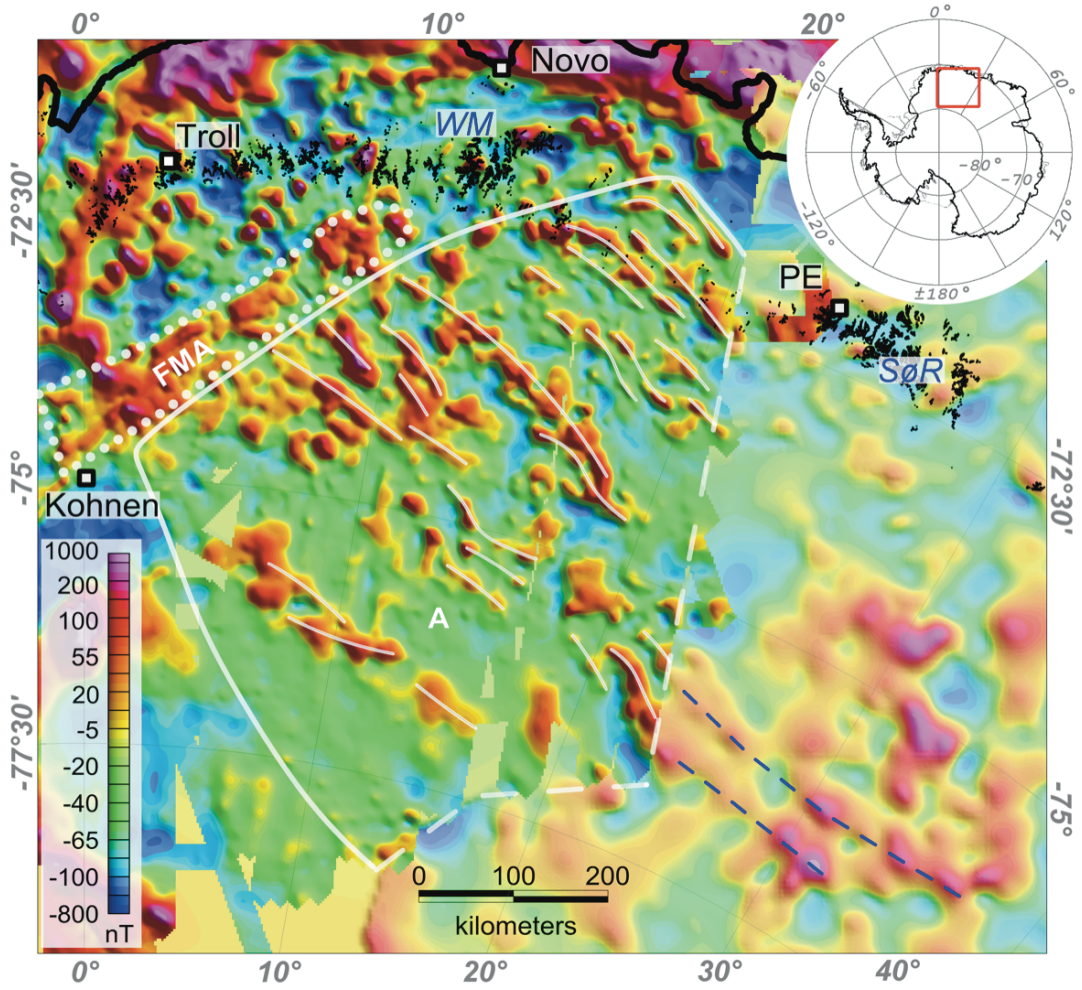

Figure 4.4: Aeromagnetic anomaly map of southeastern Dronning Maud Land. Data are superimposed on ADMAP data (Golynsky et al., 2007) in pale colors (no grid-knitting applied), both maps are reduced to the pole (inclination = -63°, declination = -31°). Anomaly area A characterizes the southeastern Dronning Maud Land province by a weak magnetic amplitude level with parallel elongated positive anomalies of 50-100 nT (white lines). Abbreviations: FMA – Forster Magnetic Anomaly, PE - Princess Elisabeth, SøR – Sør Rondane, WM – Wohlthatmassiv.

general, so smooth that a correction of diurnal variation as well as leveling techniques can introduce artificial anomalies along survey lines, but fortunately the trend direction significantly deviates by ∼55° from the main flight direction, ensuring the reliability of the presence of the elongated anomalies.

The Forster Magnetic Anomaly south of the central DML mountain range is one of the most interesting findings of Riedel et al. (2013). This nearly 400 km long and 65 km wide feature consists of a system of segmented linear SW-NE trending anomalies with moderate positive values up to 200 nT, truncating the elongated anomalies of area A by an angle of ∼80°. Notably, the data SE of the Forster Magnetic Anomaly presented here differ from Riedel et al. (2013), since two additional surveys have densified the line spacing to 10 km in the meantime, and significantly increased the number of tie lines.

4.5.2 Magnetic anomaly pattern of southwestern Dronning Maud Land and Coats Land

Our data revealed a weak but linear local maximum SW of Kohnen Station (Fig. 4.5, B), striking NE-SW. The anomaly, here named Kohnen lineament, is about 100 km long and less than 10 km wide and is characterized by a sharp gradient toward negative values in the SE. A 30 km wide and 240 km long trough characterized by small magnetic anomalies (Fig. 4.5, dashed white line) follows in SW-projection of the Kohnen lineament. This trough separates the magnetic highs C1/C2 and D.

Figure 5 shows the derivative maps for a subsection including the Kohnen lineament and the Heimefrontfjella, together with the actual survey lines. The analytical signal and the positive tilt derivative enhance the linearity of the Kohnen lineament and show its similarity to magnetic anomaly of the Heimefront shear zone. We derived the location of the Kohnen lineament between 74.995° S / 0.684°W and 75.667°S / 2.742°W from the enhanced horizontal derivate map. The derivative maps also enhance three small circular anomalies close to the western flank of the Kohnen lineament, with a diameter of 8-10 km and peak values of 110 nT, 120 nT, and 180 nT.

A strong positive (>400 nT) anomaly with a radius of 100 km is located directly 200 km south of the Kohnen station (Fig. 4.5, C1). It is part of an arch-shaped, high amplitude feature (100-400 nT) (Fig. 4.5, C2), which is ∼500 km long and ∼70 km wide, most likely continuing beyond the southern extent of our survey area. Broad negative anomalies (up to -150 nT) have been found north and south of the positive anomaly C1.

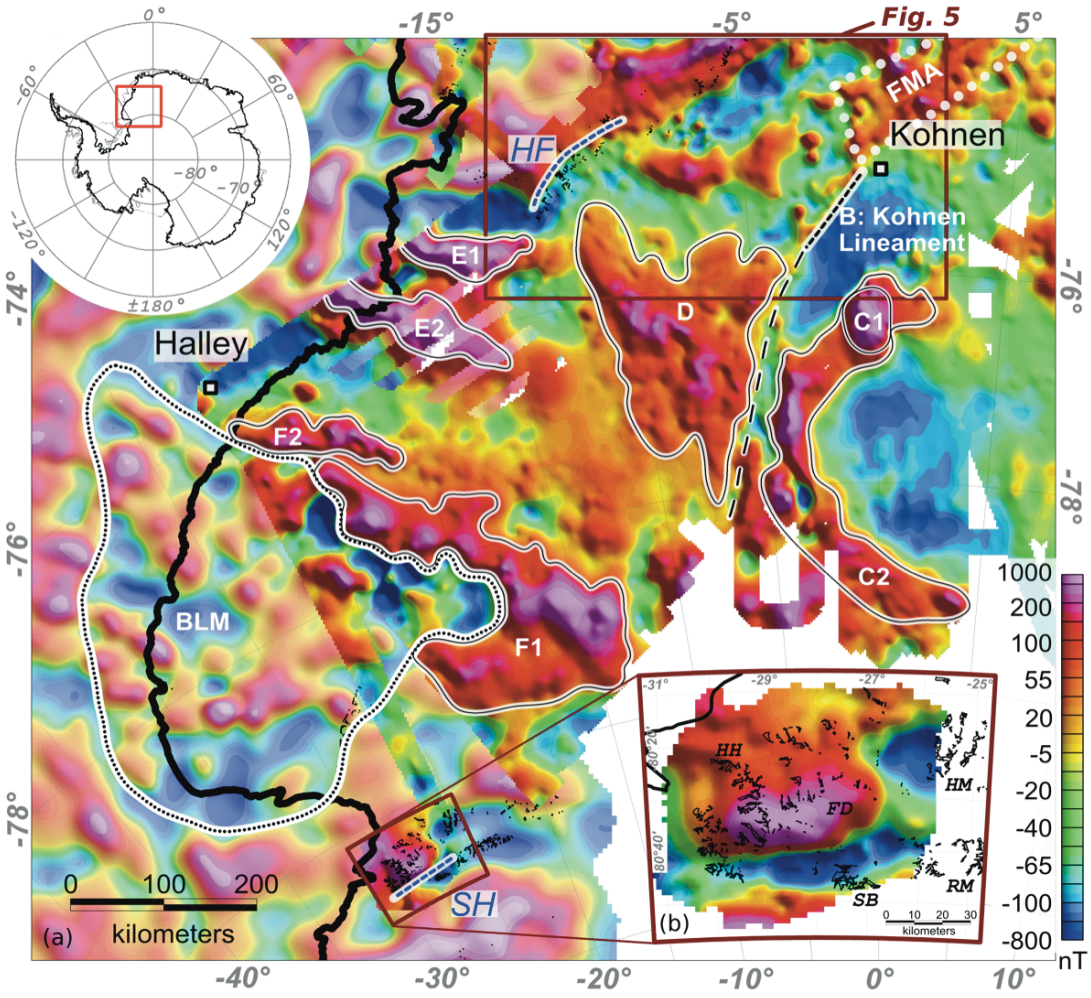

Figure 4.5: (a) Aeromagnetic anomaly map of southwestern Dronning Maud Land and Coats Land. Data are superimposed on ADMAP data (Golynsky et al., 2007) in pale colors (no grid-knitting applied), both maps are reduced to the pole (inclination = -64°, declination = -6°). In this study, anomaly B is named Kohnen lineament. C – F are other discussed magnetic anomalies. Abbreviations: BLM – Bertrab-Littlewood-Moltke province (Coats Land block), FMA – Forster Magnetic Anomaly, HF – Heimefrontfjella, SH – Shackleton Range. (b) Aeromagnetic anomaly map over western Shackleton Range. Same color scale is used for both figures. Survey lines are 6 km separated. Mean flight level was 2400 m (a.s.l.). Data are not upward continued, but reduced to the pole (inclination = -67°, declination = 1°). Abbreviations: FD – Fuchs Dome, HH – Haskard Highlands, HM – Herbert Mountains, RM – Read Mountains, SB – Stephenson Bastion.

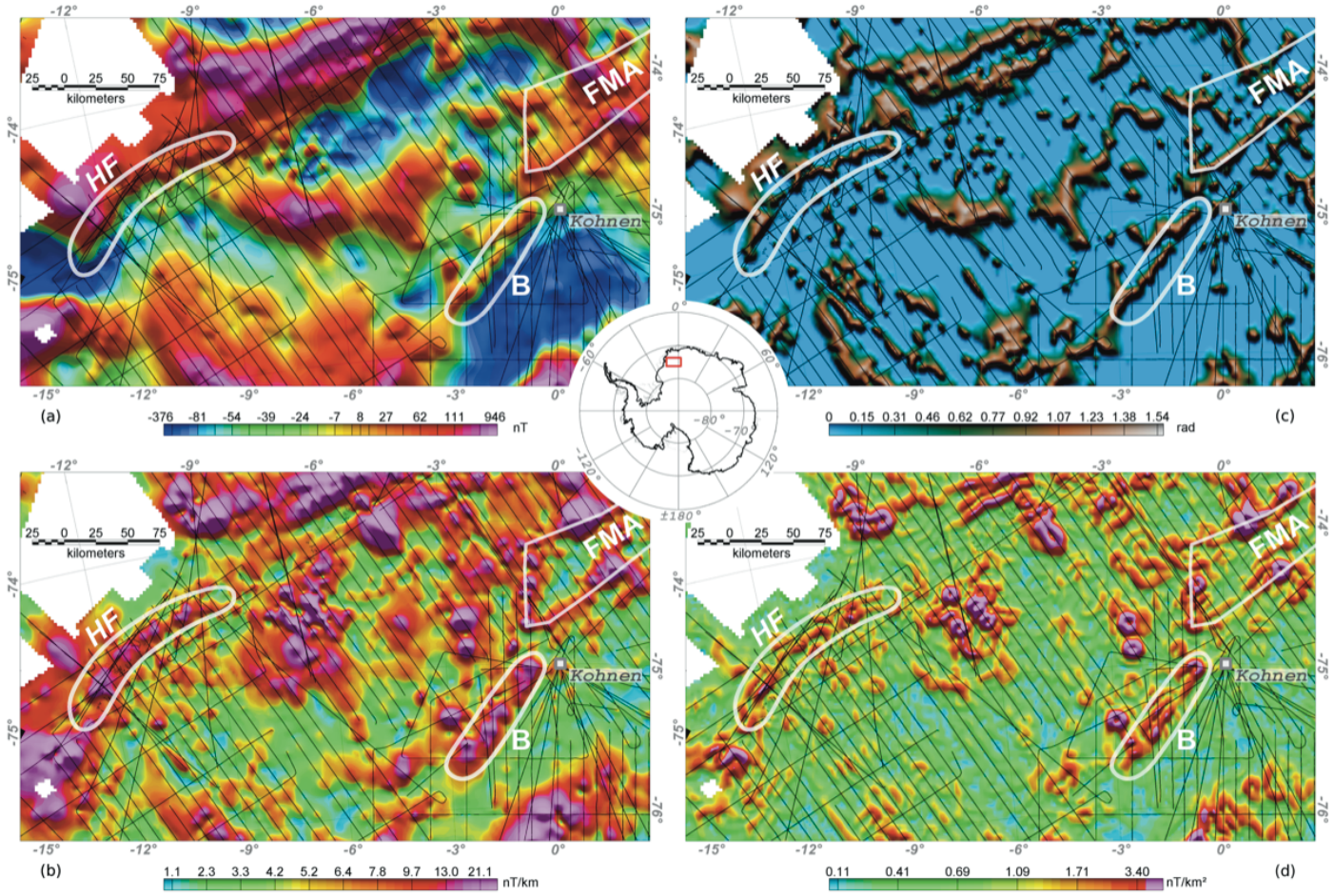

Figure 4.6: Derivative aeromagnetic anomaly maps of Kohnen lineament and Heimefront shear zone: (a) reduced to the pole (inclination = -64°, declination = -19°), (b) analytical signal, (c) positive tilt derivative, and (d) enhanced horizontal derivative. Survey lines (black) are not along strike direction of the Kohnen lineament. Abbreviations: B – Kohnen lineament, FMA – Forster Magnetic Anomaly, HF – Heimefrontfjella.

The nearly triangle shaped area (Fig. 4.5, D) of moderate to high anomalies (50-250 nT) has an areal extent of about 80 000 km^2. In the NW, it reaches almost to the Heimefront shear zone, and is bounded by the extension of the Kohnen lineament in the E. The joint leveling with data from 1994/95 and 2011 significantly improved the regional magnetic anomaly pattern in this region. In contrast to Riedel et al. (2013), this more complete data set shows a more diffuse anomaly pattern and no dominating NW-SE strike direction for area D. Farther west two high amplitude anomalies (Fig. 4.5, E1 & E2) are located SW of HF. Both anomalies are ∼40 km wide and have amplitudes of up to 500 nT.

After superimposing our data set on top of ADMAP data, a unique magnetic anomaly pattern became recognizable in Coats Land (Fig. 4.5, BLM). Golynsky and Aleshkova (2000) described the BLM pattern as intricate or broken and composed of irregular high anomalies (± 300 nT) of short wavelength (20-50 km). Our data confirm this unique pattern and allow us to constrain its eastern extent. The BLM area is surrounded by anomalies of moderate to small amplitudes (-100 to 150 nT) and two large anomalies of high amplitudes (400 nT) of wavelengths above 100 km (Fig. 4.5, F1 & F2). Notably, the southern extent is not well constrained by our data and is therefore based on the interpretation of Golynsky and Aleshkova (2000).

The western Shakleton Range (Fig. 4.5, SH) was investigated with a local pattern of 6 km line spacing across the exposed mountain range, using a barometric flight altitude of only 2400 m. The content of information was clearly reduced by the upward continuation to 4600 m. Therefore, a separated anomaly map of magnetic data that was not upward continued and not statically shifted over western Shackleton Range is shown in Figure 4.5b. The data show a magnetic high (up to 570 nT) over Fuchs Dome (Fig. 4.5b, FD) and Haskard Highlands (Fig 4b, HH), both part of the northern terrane, and a narrow (8 km wide) linear E-W oriented magnetic low (up to -220 nT) over the Stephenson Bastion (Fig. 4.5b, SB), also extending easterly towards the Read Mountains (Fig. 4.5b, RM), both part of the southern terrane. The ADMAP data show negative magnetic anomaly values for the entire Read Mountains. Negative magnetic anomaly values (up to -190 nT) are measured as well near the Herbert Mountains (Fig. 4.5b, HM). Another magnetic high is indicated at the southern edge of our data and south of the exposed mountains, which is in accordance with the ADMAP data (Fig. 4.5).

4.6 Interpretations and discussion

4.6.1 Southeastern Dronning Maud Land province

The discovery of the elongated, small amplitude magnetic anomalies between Sør Rondane and Kohnen Station (Fig. 4.7, A) sheds new light on pre-break-up tectonic evolution of Gondwana in East Antarctica. We assume that these elongated anomalies are real and represent a predominant structural strike direction of a major geological unit, here named southeastern DML province. This pattern is observed currently in an area of at least 270 000 km^2. The Steingarden nunataks (72.3°S/16.1°E) might provide a clue for interpreting the magnetic anomalies, since the Nunataks are located at the northern edge of the southeastern DML province between Wohlthatmassiv and Sør Rondane, and were visited for the first time by scientists searching for meteorites in 2007/2008 (Schlüter et al., 2011) and by geologist in 2011/2012 (Jacobs et al., 2012). Unfortunately, no information on the magnetic susceptibilities as well as age constraints are available for the dark graphite- and pyrite-bearing schists found on moraines south of the Nunataks, but they indicate that the geological evolution of the southeastern DML province differs from that of the central DML mountain range. The weak amplitude level of this region differs clearly from the high amplitude anomalies in southwestern DML. Hence, we interpret the southeastern DML province to be a distinct geological terrane, separated from the southwestern DML (Fig. 4.7). In the same manner, this region differs from the magnetic Ruker province west of the Prydz Bay region (Fig 6, gray dotted line, around Mellor Anomaly), which is dominated by negative magnetic amplitudes of -300nT (Golynsky, 2007) and lacks any indication for elongated positive anomalies.

We speculate that the southeastern DML province underwent a metamorphic deformation under compressional forces perpendicular to the strike direction of the anomaly pattern. Considering the possible continuation of this magnetic pattern in the east (Fig. 4.4 and 4.7, blue dashed lines), the anomaly pattern might represent the NW part of an orogenic belt of unknown age, but some indications about the timing can be argued as follows.

First, the truncation of the elongated anomalies in the NW by the Forster Magnetic Anomaly (Fig. 4.4 and 4.7) strongly supports the hypothesis of Riedel et al. (2013) that the Forster Magnetic Anomaly represents a major fault or even suture zone, which is, in absence of direct geological measurement, interpreted as a Pan African (650-490 Ma)

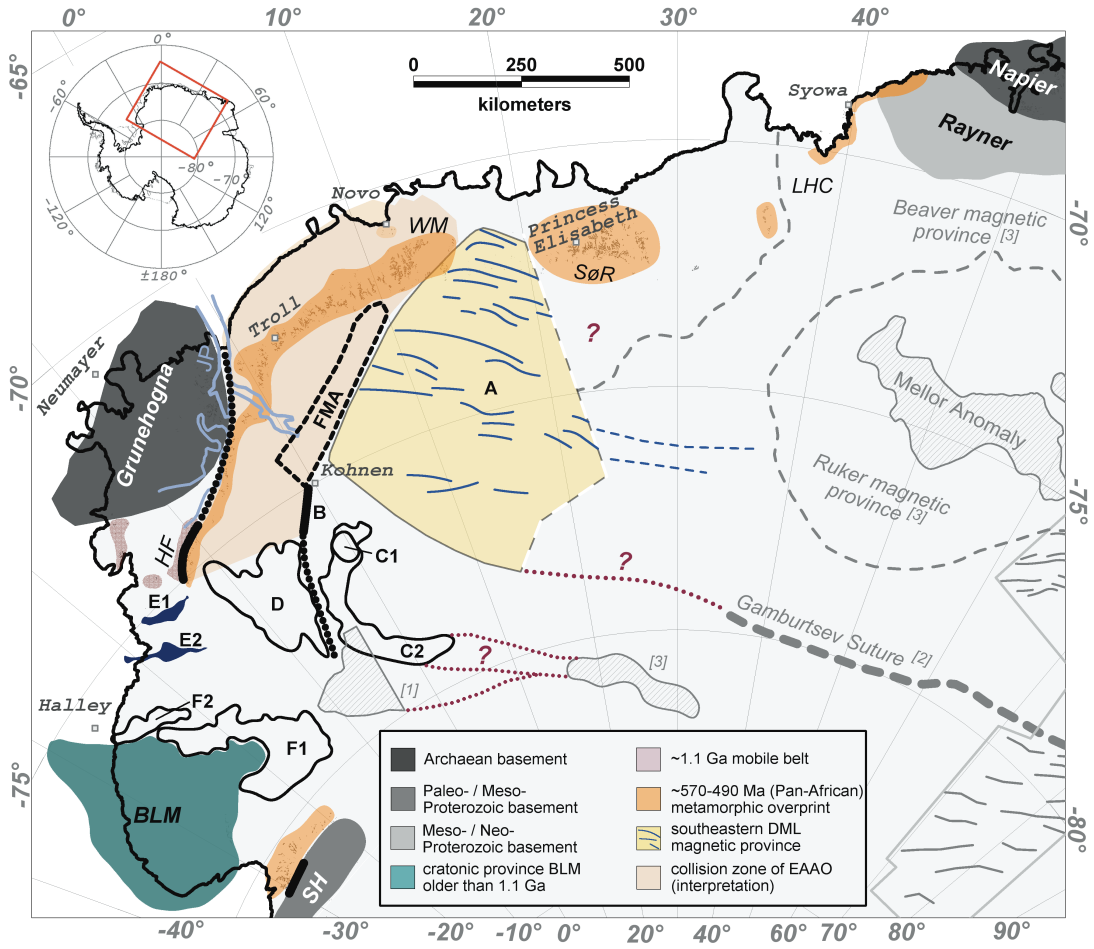

Figure 4.7: Interpretive sketch of magnetic anomalies (A-F, BLM), geological information, and presumed continuations of magnetic anomalies (dark-red dotted lines). Magnetic information from other studies are included: [1] Shepherd et al. (2006), [2] Ferraccioli et al. (2011), and [3] Golynsky (2007) - magnetic high (gray dashed area), elongated anomalies (gray lines), and province boundaries (gray dashed lines). Abbreviations: BLM – Bertrab-Littlewood-Moltke province (Coats Land block), FMA-Forster Magnetic Anomaly, HF – Heimefrontfjella, LHC – Lützow Holm Complex, SH – Shackleton Range, SøR – Sør Rondane, WM – Wohlthatmassiv.

structure (Riedel et al., 2013). We conclude that the formation of the elongated magnetic anomalies predates the formation of the Forster Magnetic Anomaly.
Second, Sør Rondane Mountains are located at the NW edge of our data. At the moment, it is unclear if it is part of the southwestern DML province or not. The mountain range show Pan-African deformation with a decreasing grade of metamorphism from N to S, and the Pan-African aged main shear zone could mark the boundary of the southeastern DML province, which would indicate that the elongated anomalies represent an older structure.
Third, based on aeromagnetic data, Golynsky (2007) interpreted the region east of the southwestern DML province as a continuous crustal province (Rayner-Beaver province) around the Archean Ruker province, extending to the Prydz Bay region as well as to the northern Gamburtsev Mountains. How far the elongated anomalies extend into this region is unclear due to the sparser line spacing there, but high-resolution aeromagnetic data show anomalies with a similar wavelength and orientation at Prydz Bay (Golynsky et al., 2006) and southern Prince Charles Mountains (Damaske and McLean, 2005). McLean et al. (2009) showed that these anomalies in the western Prydz Bay region correlates with orthogneisses of the Porthos series and intrusive charnockites, which both have much higher magnetic susceptibilities (1-100 $\cdot$ 10^{-3} SI units) compared to the surrounding paragneisses of the Athos series ($\sim$0.5 $\cdot$ 10^{-3} SI units). The emplacement age of the Porthos orthogneisses is interpreted as late Mesoproterozoic - early Neoproterozoic ($\sim$1020 Ma) by 207Pb/206Pb ratios (Boger et al., 2000). If the southern DML Province and Prydz Bay region, separated by $\sim$1500 km, form actually one geological unit, both time constrain and rock information can be deduced from the findings in the Prydz Bay region. Moreover, the Gamburtsev suture (Ferraccioli et al., 2011) lines up with the western extent of the southeastern DML province (Fig. 4.7), and it could be speculated that the Gamburtsev suture follows this line, but that is not supported by the existing, but sparse ADMAP data. It is necessary to close the high-resolution data gap to provide better constraints on its origin. Notably, similar magnetic trends (Fig 6, gray lines) exist in southern Gamburtsev Mountains (Ferraccioli et al., 2011).

4.6.2 Kohnen lineament

The Kohnen lineament (Fig. 4.5, 4.6, and 4.7, B) SW of the Kohnen Station is the most important new finding in the southwestern part of our study area. Similarities to

the magnetic anomaly pattern of the Heimfront shear zone are shown in figure 5. Both anomalies striking NW-SE and are separated by ∼300 km. The Heimefront shear zone is regarded to represent the western front of the East African-Antarctic orogen (Golynsky and Jacobs, 2001). Subsequently, we interpret the Kohnen lineament as a major shear zone, possibly representing the eastern front of this orogen in this region. The Forster Magnetic Anomaly adjoins the Kohnen lineament in the NE accompanied by a change in orientation by ∼20°. We follow the presumption of Riedel et al. (2013) that the Forster Magnetic Anomaly represents a collision zone, namely of the southeastern DML province with W-Gondwana, and speculate that the formation of the Kohnen lineament was caused mainly by shearing, which is in alignment with the escape tectonic model of Jacobs and Thomas (2004).

The magnetic trough SW of the Kohnen lineament (Fig. 4.5, black dotted line) could be a continuation of this eastern front, though its magnetic signature is different. It separates the magnetic highs C1/C2 in the east from the nearly triangularly shaped anomaly D of moderate positive values in the west (Fig. 4.5). The interpretation of anomaly D is of yet unclear. It could very well represent a collision fragment of the East African-Antarctic orogen as well as an independent geological terrane. Our new data set shows that it is not a continuation of the Forster Magnetic Anomaly, which differs from the presumption of Riedel et al. (2013) based on a less complete data set.

4.6.3 Possible continuation of the Beattie Magnetic Anomaly

In the westernmost part of our research area, two ∼40 km wide magnetic highs (Fig. 4.5 and 4.8, E1 and E2) allow the interpretation that both features are the eastward continuation of the Beattie Magnetic Anomaly in southern Africa into East Antarctica (Fig. 4.8, BMA), based on the latest tight fit in the Gondwana reconstruction of this region by Leinweber and Jokat (2012). This interpretation differs from Corner (1989) and the concretized location of Riedel et al. (2013), who suggested a continuation of the Beattie Magnetic Anomaly into DML farther north. It is feasible that both interpretations are valid and that the anomaly splits into three branches, similar to the bifurcation at its westerly extent in southern Africa. The Beattie Magnetic Anomaly has no gravity expression and its interpretation is speculative. Corner (1989) suggested magnetite enrichment in granitic basement as a source, while Lindeque et al. (2011) interpreted the origin as a partly mineralized massive sulfide-magnetite ore deposit at a depth of ∼7 to

15 km. The new magnetic data provide no additional information on the composition of the magnetic source bodies of the Beattie Magnetic Anomaly, as there are no outcrops located at anomalies E1 and E2, but the interpretation might help to reconstruct a tight fit for microplates (e.g. Falkland Islands) between East Antarctica and Africa.

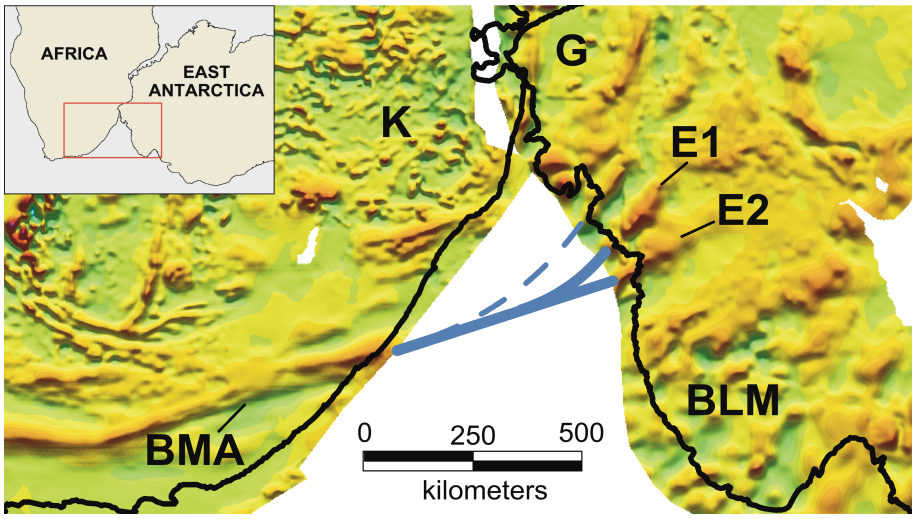

Figure 4.8: Supposed continuation of Beattie Magnetic Anomaly. Magnetic anomaly map of Antarctica is a compilation of AWI-data (this paper) and ADMAP data (Golynsky et al., 2007), for Africa data from (Maus et al., 2007) are used. Reconstruction of Africa and Antarctica carried out after Leinweber and Jokat (2012) with tight fit 189 Ma. A linear color scale is used, blue and green representing negative values, orange and red positive values. Abbreviations: BLM – Betrab-Littlewood-Molke province (Coats Land block), BMA – Beattie Magnetic Anomaly, E1/E1 magnetic highs, G – Grunehogna Craton, K – Kaapvaal Craton. Continuous blue lines proposed continuation in this this study, dashed blue line indicated by Riedel et al. (2013).

4.6.4 BLM province (Coats Land block)

Another area for which our magnetic data set provides new information is the BLM province in Coats Land (Fig. 4.7, BLM). The outline of this province is well defined by its irregular positive and negative short wavelength (40-60 km) anomalies (Fig. 4.5, BLM). Golynsky and Aleshkova (2000) discussed a possible relation of the magnetic anomalies to the few outcrops at Touch Down Hills and Theron Mountains, but due to the line spacing, a direct correlation was not possible. What is new here is the mapping of the eastern extent and that its unique anomaly pattern is not found elsewhere in Coats Land, DML, and southern Africa, supporting the hypothesis that the BLM province was neither a part

of Kalahari nor of the southern DML before amalgamation of Rodinia. Comparisons with magnetic anomaly maps worldwide (Maus et al., 2007) reveal similarities with anomaly patterns in Baltica and Laurentia. This is in accordance with the findings of Loewy et al. (2011), who showed strong Pb isotopic correlation of rhyolites and granophyres of the BLM province and Keweenawan igneous rocks of Laurentia, as well as with the paleomagnetic indication of a separation of Kalahari and the BLM province by 30° in latitude (Gose et al., 1997). Moreover, Kleinschmidt (2002) discussed that the rocks of the Touch Down Hills nunataks differ petrologically, lithologically and structurally from those found in western Dronning Maud Land, and that they match neither the low- to high-grade metamorphic basement rocks nor the Pan-African reworking of the of the northern terrane of the Shackleton Range.

4.6.5 Southwestern Dronning Maud Land and Shackleton Range

Rather speculative and not geologically constrained are the interpretations of magnetic highs C1/2, D, and F1/F2. Similarities to the magnetic anomaly pattern of the NW Shackleton Range terrane can be drawn by appearance and amplitude level. Although this very weak similarity does not allow any conclusions, it shows that an interpretation of the Precambrian basement is potentially feasible. This interpretation is also provided by Shepherd et al. (2006), for a magnetic high that partly overlaps with anomaly C2 (Fig. 4.7).

Another, yet very unlikely, hypothesis would be the presumption of massive Jurassic magmatic rocks as a source. Dykes and sills of Jurassic dolorities are found in our study area along the Jutul-Penck graben, at Theron Mountains and at the northern Shackleton Range terrane, but they correlated with much higher frequency magnetic anomalies (Golynsky and Aleshkova, 2000; Ferraccioli et al., 2005a; Shepherd et al., 2006). The circular shape of anomaly C1 suggests an intrusive source body. The similar, yet in extension much smaller, magnetic anomalies of Straumsvola and Tvora at the eastern flank of the Jutul-Penck graben have been correlated with mid-Jurassic alkaline intrusions Ferraccioli et al. (2005a).

However, we prefer the interpretation of exposed Pre-Cambrian basement for the largely extended magnetic highs. It is not unlikely that anomalies F1/F2 represent the collision zone between the BLM province and the Namaqua-Natal-Maud belt. From Shepherd et al. (2006) we know that anomalies F1 and C2 are disconnected (Fig. 4.7), and we

assume that C2 continues SE, where it might connect to a magnetic high at 80-82°S/30-55°E, forming a continuous S-shaped 1000 km long anomaly (Fig. 4.7). Notably, only data of the end of one survey line contributed to the circular magnetic low within C2. Therefore, we do not interpret this small-scale anomaly, as it cannot be determined if the data had been corrupted during measuring or pre-processing.
Regardless of the interpretation of the magnetic highs in southwestern DML, we note that the overall pattern of this area, with its high and diversified amplitudes, differs clearly from the coherent weak amplitude pattern in the southeastern DML province, supporting our assumption of a separated tectonic terrane SE of the Forster Magnetic Anomaly and, at the same time, opposing the hypothesis of a structural link between Shackleton Range and Lützow Holm Bay region in eastern DML.

4.7 Conclusion

We have presented a compilation of new reconnaissance aeromagnetic data in the southern part of Dronning Maud Land and eastern Coats Land, and mapped provinces and boundaries for the first time in this mostly ice-covered part of East Antarctica, and discussed some indications of their geological meaning and importance for studying the tectonic evolution of East Antarctica, which appears to be a mosaic of several distinct crustal provinces. The main conclusions are:

- A hitherto unrecognized southeastern Dronning Maud Land province is characterized by parallel and NW-SE trending elongated positive (50-100nT) magnetic anomalies and a weak background amplitude level. An eastward continuation into the Beaver-Rayner province is indicated, and a hypothesis can vaguely be formulated that the elongated anomalies may be caused by charnockitic felsic gneiss of Meso- to Neoproterozoic age as part of a continuous mobile belt extending out into the Prydz Bay region, but it needs to be pointed out that the reliability of this hypothesis is very weak, as it is based only on the similarities in grain of magnetic patterns.

- The Kohnen magnetic lineament may reflect a major shear zone in the interior of East Antarctica akin to the Pan-African aged Heimefront shear zone. It adjoins the Forster Magnetic Anomaly, which we interpret to represent the collision zone of the southeastern Dronning Maud Land province with West-Gondwana.

- The magnetic anomaly maps provide no evidence of a previously hypothesized continuous Pan-African orogenic belt or suture zone connecting the Shackleton Range and the Lützow Holm Bay region in eastern Dronning Maud Land.
- The easterly extent of the possible cratonic BLM province (Coats Land block) is mapped and it is pointed out that its magnetic amplitude pattern is unique for Dronning Maud Land and southern Africa, yet showing similarities to those of Laurentia and Baltica.
- Two anomalies in western Dronning Maud Land have been identified as possible continuations of the Beattie Magnetic Anomaly, in addition to a previously assumed continuation in this region.

4.8 Acknowledgments

We thank the flight and science crews of AWI-Polar aircraft for data acquisition, the visited research station in Dronning Maud Land for logistic support, J. Jacobs and G. Kleinschmidt for inspiring discussions, the anonymous reviewer for constructive comments that significantly enhanced the manuscript, and A. Sorensen for stylistic help and improvement of the English language.

Chapter 5

Banded iron deposits (?) at Grunehogna Craton, East Antarctica - constraints from aeromagnetic data

Matthias Mieth and Wilfried Jokat

5.1 Abstract

We report a strong magnetic high over the Giæverryggen at the Grunehogna craton in western Dronning Maud Land, East Antarctica. The anomaly was coarsely mapped by previous surveys. Recently acquired magnetic data (2012/13) better constrain its spatial extent and permit the estimate of a theoretical amplitude value of +4000 to 4200 nT at the bedrock surface. From the magnetic data, we estimated a minimum magnetic susceptibility in a spherical source body with a midpoint depth of ∼5.6 km to be greater than 193×10^{-3} SI, in the absence of relevant remanent magnetization. 2.75-D forward modeling and comparisons with neighboring magnetic highs in a plate tectonic reconstruction of western Dronning Maud Land and southern Africa reveal similarities to Paleoproterozoic banded iron formations.

KEY WORDS: Aeromagnetics, Giæver Magnetic Anomaly, Banded Iron Formation, Grunehogna Craton, Dronning Maud Land, East Antarctica

5.2 Introduction

East Antarctica, especially Dronning Maud Land (DML), has experienced a quite complex geological and tectonic evolution since the Archaean. However, the few outcrops penetrating the thick ice sheet provide only scattered insights into the subglacial tectonic domains. Thus, most of the current tectonic models are based on aerogeophysical data, in particular aeromagnetic data, combined with geological sampling of the sparse outcrops in DML. The combination of these data sets has allowed several large-scale crustal domains to be distinguished in DML (Golynsky and Aleshkova, 2000; Mieth and Jokat, 2014; Riedel et al., 2012, 2013). Despite ongoing survey activities, however, little is known about the detailed subglacial geology within the domains. Here, we focus on a localized but remarkable magnetic anomaly in DML at Giæverryggen south of Halvarryggen, which we name the Giæver Magnetic Anomaly. This strong magnetic anomaly (∼900 nT at 3500 m measurement altitude) was detected during a regional aerogeophysical campaign in 2001-2005 (Riedel et al., 2013). At that time, the existence and spatial extent of the anomaly was debatable; 2001-2005 data reveal the anomaly on just one flight in a survey of measurement lines at 10 km spacing (Fig. 5.1a), although Golynsky and Aleshkova (2000) reported of two circular magnetic highs (800 and 1700 nT) in the same region based on Russian reconnaissance data acquired in 1977—1989 (Golynsky et al., 2000). In 2012/13, new magnetic data were acquired during ferry flights perpendicular to those of 2001-2005 (Fig. 5.1b), confirming the presence of the anomaly and allowing its shape to be mapped more clearly. The Giæver Magnetic Anomaly is located in a trough-shaped valley (∼140 m b.s.l.; Fig. 5.1c) at the northern edge of a subglacial mountain range, which reaches up to 1900 m a.s.l. The trough is covered by ∼1170 m thick ice and, hence, the bedrock is not accessible for direct geological sampling.
A compilation of all aeromagnetic data in the study area acquired by the Alfred-Wegener-Institut Helmholtz-Zentrum für Polar- und Meeresforschung (AWI) is presented and analyzed here for estimates of source depth, minimum magnetic susceptibility, and geometry. Furthermore, 2.75-D forward magnetic modeling is carried out. The results are discussed in view of other magnetic highs in western DML and southern Africa.

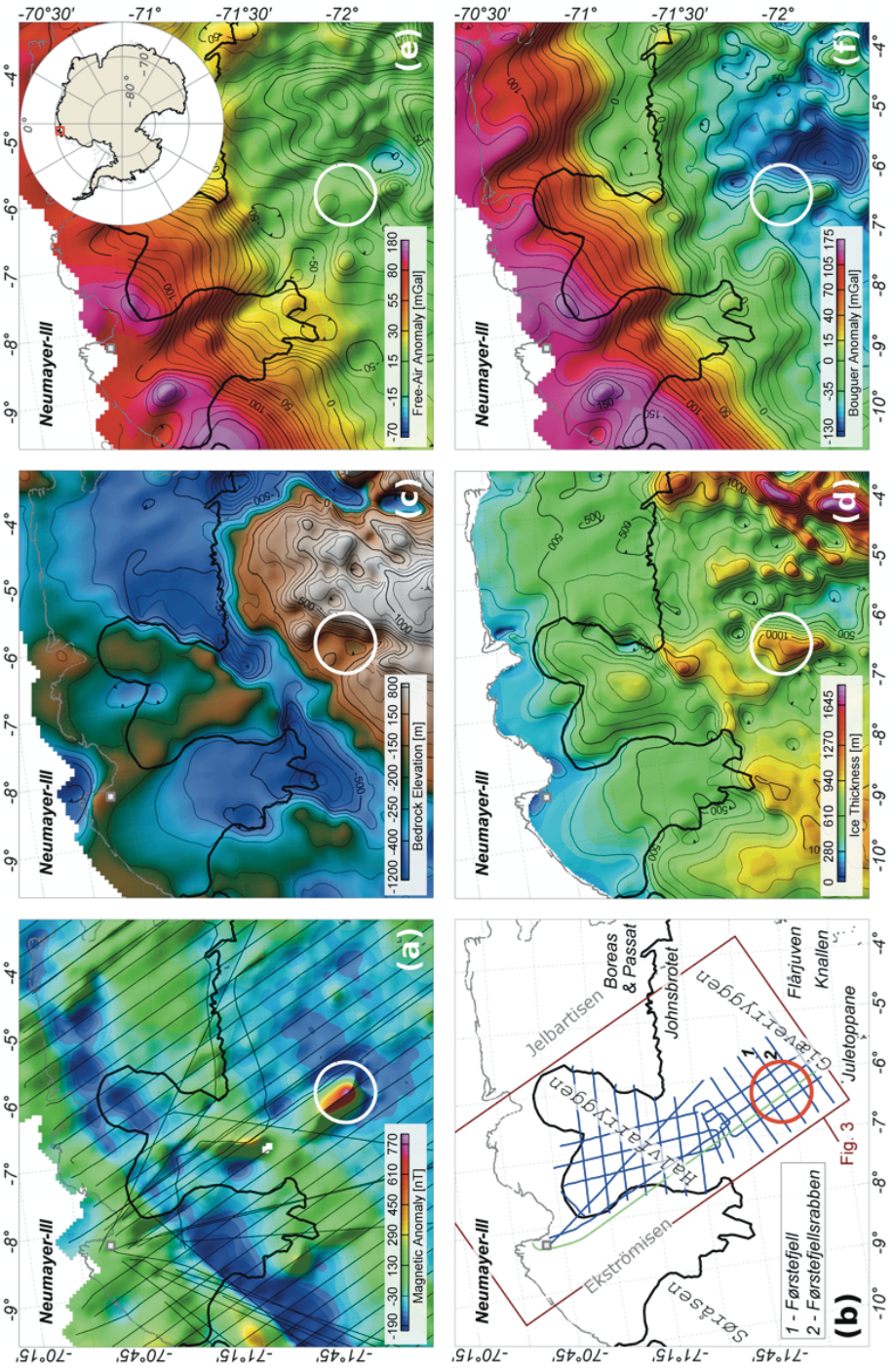

Figure 5.1: Detailed map of aerogeophysical data in study area of the flight campaigns 2001-2005 (Riedel et al., 2012, 2013): (a) magnetic anomaly map and flight tracks of 2001-2005; (b) geographic overview and flight paths of magnetic measurements (green: 2011/12 blue: 2012/13); (c) subglacial topography; (d) ice thickness; (e) free-air gravity map; (f) complete Bouguer gravity map. The white/red circle marks the area of the Gæver Magnetic Anomaly.

5.3 Geological setting

The Giæver Magnetic Anomaly is located within the Grunehogna craton (Fig. 5.2), which was juxtaposed with the Kaapvaal craton in southern Africa prior to Gondwana break-up ~200 Ma (König and Jokat, 2006; Leinweber and Jokat, 2012; Martin and Hartnady, 1986). The Archaean granite basement crops out in the southwest at the

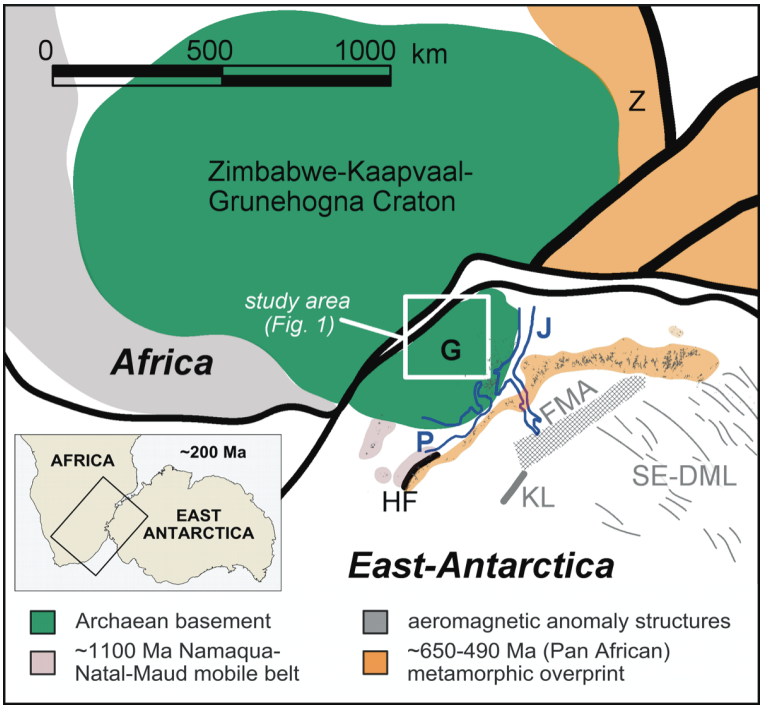

Figure 5.2: Geological setting of the study area in a Gondwana framework. Reconstruction of East Antarctica relative to Africa after Leinweber and Jokat (2012) with tight-fit 189 Ma. The simplified sketch is adapted from Mieth and Jokat (2014) and Jacobs and Thomas (2004). The study area (white box) is located entirely within the Archaean Grunehogna craton. Abbreviations: FMA - Forster Magnetic Anomaly, G - Grunehogna craton, HF - Heimefrontfjella, J - Jutulstraumen graben, KL - Kohnen lineament, P - Pencksøkket graben, SE-DML - southeastern Dronning Maud Land province, Z - Zambezi belt.

Annandagstoppane nunataks and is dated to be older than 3 billon years (Halpern, 1970; Marschall et al., 2010). The northeastern Annandagstoppane and Juletoppane (Fig. 5.1b) consist of Paleoproterozoic magmatic-layered dolerite (Krynauw et al., 1984). At Ahlmannryggen and Borgmassivet the basement is overlain by relatively undeformed Mesoproterozoic sedimentary and volcanogenic rocks of the Ritscherflya Supergroup, intruded by tholeiitic sills and dikes (Wolmarans and Kent, 1982). The Ritscherflya Su-

pergroup is interpreted as a molasse-type deposit in a shallow marine to braided river system associated with the late Kibaran orogeny 1.2-1.1 Ga (Moyes et al., 1995). High frequency magnetic anomalies with medium amplitudes of up to +150 nT are associated with the Borgmassivet intrusions (Ferraccioli et al., 2005a). These intrusions into mainly unconsolidated sediments have been interpreted as part of the ∼1.1 Ga Umkondo large igneous province of southern Africa based on their age, geochemistry, and paleomagnetism (Grosch et al., 2007; Hanson et al., 1998, 2004; Jones et al., 2003; Powell et al., 2001). The closest outcrops to the Giæver Magnetic Anomaly are the isolated nunataks Førstefjellsrabben (19 km away) and Førstefjell (26 km away; Fig. 5.1b). Members of the Norwegian-British-Swedish Antarctic Expedition discovered them in 1950 (Giæver, 1954), but only Førstefjell was described geologically. It consists of sedimentary rocks of the Ritscherflya Supergroup and Borgmassivet intrusions (Krynauw, 1989). However, none of these published geological findings offers an explanation for the nature of the Giæver Magnetic Anomaly.

5.4 Data acquisition and processing

Magnetic data from different flight campaigns of AWI have been used and compiled for this study. Magnetic data from 1996, 1998, 2002, 2003, 2004, 2012 and 2013, totaling up to 5300 km line length and cover an area of 20˙000 km^2 across Giæver- and Halvfarryggen. The magnetic data were acquired using Scintrex Cs-2 Caesium magnetometers installed at the wing tips of *Polar 2* (Dornier DO-228) through 2004, and Scintrex Cs-3 Caesium magnetometers in nose and tail booms on *Polar 6* (Basler BT-67) in 2012 and 2013. On both aircraft, a fluxgate magnetometer was operated and used for magnetic compensation. Data processing was carried out using Fugro-LCT and Geosoft Oasis montaj software. The processing flow included de-spiking, core-field and diurnal variation corrections, upward continuation to 3900 m, and leveling. The leveling process included two steps; a set of static shifts reduced cross-point errors from 79.3 ± 57.2 nT to 19.6 ± 19.8 nT, and was followed by low pass filtered tensional spline corrections to further reduce the cross-point errors to 3.2 ± 4.1 nT. Reduction-to-the-pole was performed with mean inclination of -61.5° and mean declination of -15.5°, while the analytical signal was calculated directly from the magnetic anomaly field.

Depth estimation for spherical source geometry was calculated from measurements at

two different flight altitudes, using the equations given by Lindner and Scheibe (1978). Furthermore, we applied the grid-based method of Euler deconvolution (Reid et al., 1990) and the grid-based AN-EUL method (Salem and Ravat, 2003) to investigate the depth and the structural index of the geological body. The structural index defines the attenuation rate of the magnetic field with distance depending on the source geometry: 3 – center of sphere/dipole, 2 – center horizontal/vertical cylinder, 1- top of dike/ edge of sill, 0 – contact (Thompson, 1982). 2.75-D forward modeling was conducted using the GM-SYS tool of the Geosoft Oasis montaj software.

5.5 Results

5.5.1 Line data

The Giæver Magnetic Anomaly was detected on a single flight in January 2002, on which it measured a maximum value of 903 nT at an altitude of 3500 m (Fig. 5.1a, white circle). The line was almost re-flown (∼800 m separation) at the same flight altitude 10 years later (Fig. 5.1b, green line), revealing a maximum value of 858 nT and a second local maximum of 435 nT, 51 km farther to the NNW (Figs. 3a and 5). Several lines were acquired perpendicular to these during the austral summer 2012/13 (Fig.5.1b, blue lines), flown at a barometric flight altitude of 1960 m across Giæverryggen and at a constant altitude of 1500 m above surface across Halvfarryggen. A maximum value of 1572 nT (Fig. 5.4a) was measured for the Giæver Magnetic Anomaly at a horizontal distance of 370 m from its cross point with the 2002 line. Here, the ice surface lies ∼1030 m a.s.l. The ice thickness, calculated from radar measurements along the flights, is ∼1170 m across the anomaly and, thus, the subglacial surface topography is at ∼140 m b.s.l. Using the measurements at two different levels (1960 m and 3500 m), we estimated a theoretical magnetic anomaly value of +4191 nT at bedrock surface for an assumed spherical source body. Furthermore, we calculated a midpoint depth of 5487 m below bedrock surface for the same source and a minimum magnetic susceptibility of 193 $\times$ 10^{-3} SI, assuming no remanent magnetization and a maximum radius equal to the midpoint depth.

5.5.2 Gridded data

The gridded magnetic anomaly data, upward continued to a common altitude of 3900 m, show that the Giæver Magnetic Anomaly (+840 nT) is associated with a smaller but

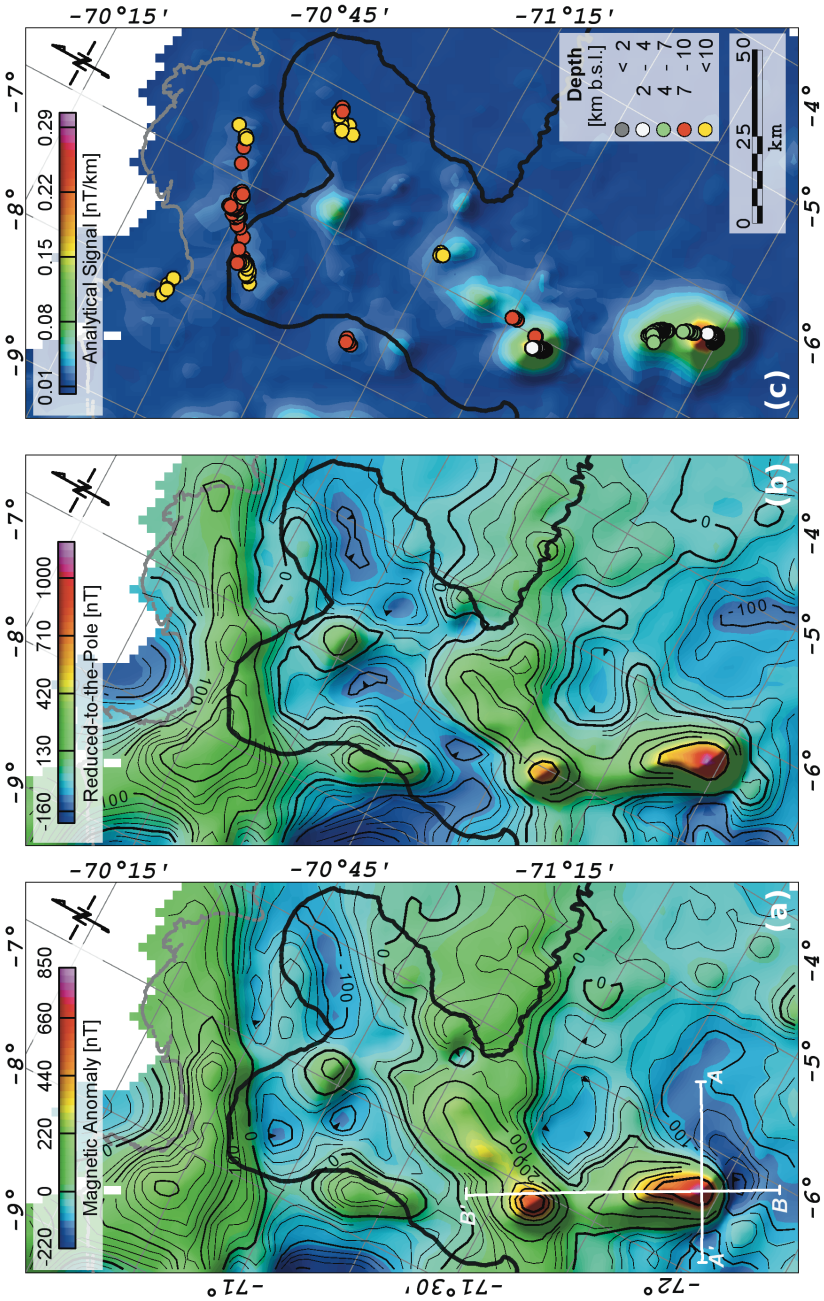

Figure 5.3: New compilation of all AWI - aeromagnetic data in the study area over Halvfar- and Gæverryggen, derivatives, and depth estimation: (a) magnetic anomaly map at 3900 m reference altitude, white lines are showing location of profiles used for modeling (Fig. 5.4); (b) reduction-to-the-pole with inclination of -61.5° and declination of -15.5°; (c) analytical signal and depth estimation by Euler deconvolution below sea level. Outline of the figure area is given in Fig. 5.1b.

distinct negative anomaly (-220 nT) in the SE (Fig. 5.3a), which is most likely a result of induced magnetization by the geomagnetic field and its inclination and declination in this region. Reduction-to the-pole should relocate the maximum anomaly amplitude above the center of the source body, assuming its magnetization is entirely induced magnetization or its remanent magnetization is aligned with the present-day geomagnetic field. In the absence of additional information, we can only assume here that induced magnetization is dominant. This assumption is supported by the fact that the maximum of the reduced-to-the-pole field (Fig. 5.3b) coincides with the maximum of the analytical signal (Fig. 5.3c), which is calculated independently of the inclination and declination of the geomagnetic field. The reduced-to-the-pole map shows the Giæver Magnetic Anomaly to extend for 28 km NNW-SSE with a WSW-ENE width of 12 km, and reveals a circular secondary anomaly of slightly lower amplitude to lie 48 km farther NNW. This secondary anomaly, with a radius of 6 km, is located on a NNE-SSW trending ridge of moderately positive amplitudes that is 45 km long and 13 km wide. The amplitude of the surrounding anomaly field varies between -100 and +50 nT.

Depth estimates from 3D grid-based Euler deconvolution for a cylindrical source geometry range between 2540 and 3560 m b.s.l. for the main anomaly and between 2820 and 3930 m b.s.l. for the secondary anomaly (Fig. 5.3c). Tab. 5.1 summarizes depth estimates for both anomaly sources, using a range of source geometries and different methods. Notably, the AN-EUL method is very sensitive to noise because it uses the third derivative of the magnetic anomaly field. Pre-smoothing of the gridded data for this technique means that it tends to represent the anomalies as more circular features and, hence, leads to higher structural indices and deeper depth estimations. We tested gentle smoothing with Gaussian low pass filters and Hanning convolution filters. Compared to the results from 3D grid-based Euler deconvolution, the estimated depth values are in a wider range of 1.7 to 5.5 km b.s.l., with a range of structural indices of 1.7 to 2.7.

5.5.3 Forward modeling

Results of 2.75-D forward modeling along the 2011/12 flight line and the 2012/13 line perpendicular to it are shown in Fig. 5.4. A natural aspect of potential field data is that an infinite number of geological bodies can cause the same anomaly pattern. In the absence of additional geophysical and geological constraints on the source body for the Giæver Magnetic Anomaly, our best guide is to aim for geometrical simplicity in

	main anomaly		secondary anomaly	
	structural index	*depth estimate*	*structural index*	*depth estimate*
2 level measurements	3	5627	-	-
3D Euler deconvolution	3	5120-8100	3	6450-7790
	2	2540-3560	2	2820-3930
	1	(-620-1060)	1	(-620-910)
3D located Euler deconvolution	3	5567	3	5333
	2	2873	2	2987
	1	(-178)	1	(-640)
AN-EUL method	1.94	2675	(3.0)	(7226)
AN-EUL with smoothing	1.7-2.7	1720-5530	-	-

Table 5.1: Depth estimates for the main and secondary magnetic anomaly (mid-point depth below sea level). The structural index depends on the source geometry: 3 –sphere/dipole, 2 –horizontal/vertical cylinder, 1- dike/ sill (Thompson, 1982). Results for structural index 1 are partly above bedrock surface and, thus, unrealistic.

our modeling. To do this, we applied the following simplifying assumptions: a) a high magnetic susceptibility of 300×10^{-3} SI, as indicated by the spherical model calculations that constrain the least possible magnetic susceptibility to be 193×10^{-3} SI, b) negligible magnetic susceptibility in the host rock, and c) no remanent magnetization effects, either owing to a Königsberger ratio much smaller than 1 or to a remanent magnetization aligned parallel to the present-day geomagnetic field. In the latter case, the assumed magnetic susceptibility for the anomaly body would be reduced by the Königsberger Ratio.
The anomaly bodies of the 2.75-D models have a finite constant cross-profile extent. We chose widths of 19 km for profile A and 14 km for the main and 9 km for the secondary anomaly body at profile B. For self-consistency, the top and bottom depths of the source bodies are equal on both profiles.

5.5.4 Magnetic anomaly map of the reconstructed Kaapvaal-Grunehogna craton

In order to study similarities between magnetic anomalies in western DML and in southern Africa, we reconstructed East Antarctica and Africa according to the rotation poles given by Leinweber and Jokat (2012) with tight-fit 189 Ma (Fig. 5.5). For southern Africa, we show the World Digital Magnetic Anomaly Map (WDMAM) at 5 km reference altitude (Korhonen et al., 2007). In Antarctica, our own data set is shown at 4.6

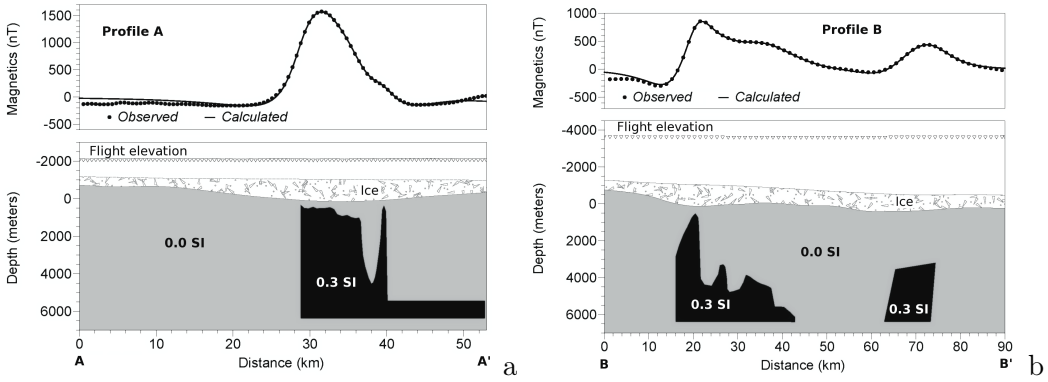

Figure 5.4: 2.75-D magnetic forward models: a) Profile A: magnetic line data and 2.75-D depth model, with anomaly body expansion of 19 km perpendicular to profile line. b) Profile B: magnetic line data and 2.75-D depth model, with anomaly body expansion of 14 km perpendicular to profile line for the main body and 9 km for the secondary body. No remanent magnetization is assumed and magnetic susceptibility in the host rock is neglected for both profiles. Location of the profiles is displayed in Fig. 5.3a (white line: A-A' and B-B').

km reference altitude (Mieth and Jokat, 2014), merged in some parts with data from the Antarctic Digital Magnetic Anomaly Project (ADMAP; Golynsky, 2007). In the reconstruction, an anomaly similar in amplitude range, wavelength and orientation is located ∼400 km to the west of the Giæver Magnetic Anomaly. The anomaly is ∼55 km long and ∼14 km wide, and located at the Mhlapitsi fold belt SW of Polokwane (formerly Pietersburg) in South Africa. Other magnetic anomalies of similar amplitudes in western DML (Fig. 5.5, 'c', 'd', 'e', and 'f") are located along the Jutulstraumen-Pencksøkket graben system (Fig. 5.5, 'J' and 'P'), which is interpreted as a failed Jurassic amagmatic rift associated with early Gondwana break-up (Golynsky and Aleshkova, 2000; Grantham and Hunter, 1991; Ferraccioli et al., 2005a). The maximum values of these anomalies, locations, and outcropping sources are summarized in Tab. 5.2.

5.6 Discussion

The magnetic data acquired during the field seasons 2012/13 perpendicular to those of 2001-2005 confirm the existence and constrain the extent of a strong magnetic anomaly at Giæverryggen and reveal a secondary anomaly 48 km farther to the NNW (Figs. 5.1 and 5.3). The associated negative anomaly SSE of the Giæver Magnetic Anomaly can be explained by the inclination of the geomagnetic field in this region and, thus, we assume

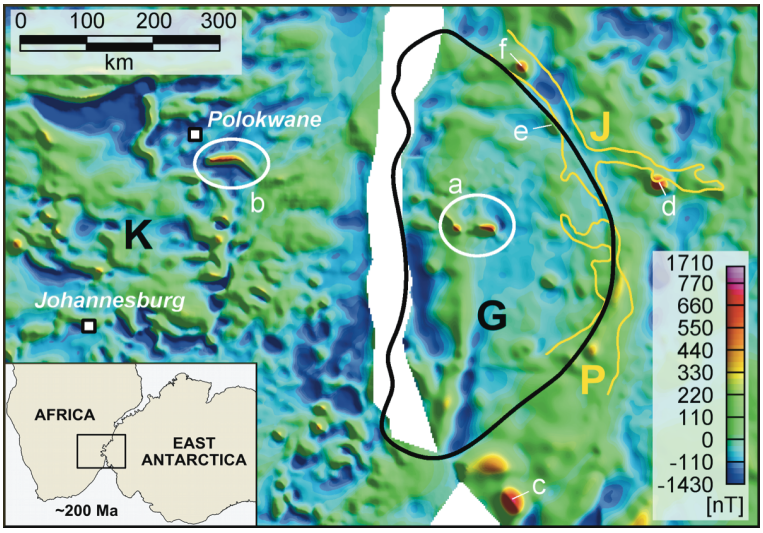

Figure 5.5: Magnetic highs within western Dronning Maud Land and southern Africa. Reconstruction of East Antarctica relative to Africa after Leinweber and Jokat (2012) with tight-fit 189 Ma. Continents are overlain by magnetic anomaly maps: WDMAM data at 5 km reference altitude (Korhonen et al., 2007) in southern Africa and our own data sets at 4.6 km reference altitude (Mieth and Jokat, 2014) merged in some parts with ADMAP data (Golynsky, 2007) for East Antarctica. The white circle marked with 'b' near Polokwane (former Pietersburg) marks the magnetic anomaly of the Mhlapitsi fold belt, which shows similarity in amplitudes, wavelength and after reconstruction in strike direction to the magnetic high at Giæverryggen marked with 'a' (Giæver Magnetic Anomaly). Other magnetic highs in western Dronning Maud Land are marked with 'c', 'd', 'e', and 'f'. Abbreviations: G - Grunehogna craton, J - Jutulstraumen graben, K - Kalahari craton, P - Pencksøkket graben.

label	*region*	*max. value**	*outcropping source*
'a'	Giæverryggen	630 nT	-
'b'	Mhlapitsi fold belt	620 nT	banded iron formation (2500 Ma)[1]
'c'	Vestfjella	790 nT	olivine-gabbro (<170 Ma)[2]
'd'	Sistefjella	860 nT	syenite intrusion (173 Ma)[3]
'e'	Straumsnutane	270 nT**	(covered)[4]
'f'	Fimbulisen	620 nT	-

*reference altitude 4.6 km for anomalies 'a' and 'c'-'f', 5 km for anomaly 'b'
** not overflown at its maximum

Table 5.2: Intensities of magnetic highs labeled in Fig. 5.5. Source rock information after: 1 – Beukes (1983) and references therein, 2 – Luttinen et al. (1994), 3 – Harris (1995); Harris et al. (2002), and Knoper et al. (1997), 4 – outcropping Jurassic andesites are not interpreted as the magnetic source (Ferraccioli et al., 2005a).

that the source body has either no or a vertical dip. From our data, we calculate a theoretical anomaly value of +4000 to +4200 nT would be measured at bedrock surface. Similarly strong values were reported from the Ruker Mountains, west of Prydz Bay in East Antarctica. There, the high magnetic anomaly values correlate with an outcropping Paleoproterozoic banded iron formation of the lower Ruker group (Damaske and McLean, 2005; Golynsky et al., 2002; McLean et al., 2008).

The spherical model we used for estimating minimum magnetic susceptibility under the assumption of no relevant remanent magnetization is rather simple, but it allows us to easily calculate the midpoint depth and subsequently the minimum magnetic susceptibility of 193 $\times$ 10^{-3} SI, which would have to be exceeded in any other-shaped source. Both the Euler deconvolution and the AN-EUL method return structural indices in the range 1.7-3.0, meaning that the geometry of the source body cannot be a narrow dike or sill, but must be of cylindrical or spherical shape. Depending on the source geometry, the depth estimations for the center of the source body range between 3 and 8 km (Tab. 5.1). We prefer a cylindrical source model with a midpoint depth of 3 km b.s.l., as indicated by the AN-EUL method. Our 2.75-D models are based on such a model (Fig. 5.4). Notably, a deeper horizontal layer is included in the magnetic source body on profile-A towards A' (Fig. 5.4a) in order to reproduce the level of the regional field near A'. Alternatively, the details of the regional field may relate to remanent magnetization in the anomaly body and/or magnetization of the host rock that we did not consider for our modeling.

We do not observe a pronounced gravity anomaly across the magnetic Giæver Magnetic Anomaly. Instead, the complete Bouguer anomaly (Riedel et al., 2012) for this area (Fig. 5.1f) correlates conspicuously well with the subglacial topography (Fig. 5.1c), and thus, we assume here is a residual topography and terrain effect. However, such a remarkable high magnetic anomaly is likely to be caused by a rock formation that is rich in ferrous or ferric minerals, which have usually high-density values that would lead a gravity effect to be expected. Estimating this effect, we calculated a maximum gravity anomaly of $\sim$10 mGal for a density contrast of 300 kg/m3 between anomaly body (Fig. 5.4b) and host rock at a flight elevation of 3500 m. It is possible that such a small gravity anomaly could have been missed owing to the experimental and processing constraints of our airborne gravimeter system, because a) the cross point error of the gravity data is specified at 4.3 $\pm$ 5.2 mGal (Riedel et al., 2012), and b) a 90 s low pass filter is applied to the

data, corresponding to a spatial resolution of ∼7 km. Unfortunately, the perpendicular lines measured at a lower flight altitude of 1960 m were too short for obtaining useable aerogravity data.

Golynsky and Aleshkova (2000) described the magnetic anomaly pattern of the Grunehogna craton based on a compilation on Russian data and reported two large magnetic anomalies. They interpreted the anomalies as expressions of Jurassic olivine-gabbro intrusions similar to that of Vestfjella, where a strong magnetic high (Fig. 5.5, 'c') with values of ∼1900 nT is observed at a terrain clearance of ∼1000 m (Golynsky et al., 2000). Riedel et al. (2013) adopted this interpretation for the Giæver Magnetic Anomaly. Jurassic intrusive bodies are also assumed to cause the magnetic highs along the Jutulstraumen-Pencksøkket graben at Sistefjell (Fig. 5.5, 'd') by Golynsky and Aleshkova (2000) , at Straumsnuntane (Fig. 5.5, 'e') by Ferraccioli et al. (2005a), and for the Fimbulisen several kilometers offshore (Fig. 5.5, 'f') by Riedel et al. (2013). We prefer to interpret the Giæver Magnetic Anomaly as an expression of a Paleoproterozoic banded iron formation, based on the following arguments. First, outcrop geology at the Førstefjell nunatak suggests that the Giæver Magnetic Anomaly is located well within the Grunehogna craton and not in a zone of Jurassic break-up (Krynauw, 1989). Second, the theoretical magnetic anomaly amplitude at bedrock surface is similar to that of the Ruker magnetic anomaly. The calculated value of magnetic susceptibility ($>193 \times 10^{-3}$ SI) more closely matches those measured for samples of the Ruker banded iron formation (McLean et al., 2008) than the olivine-gabbro at Vestfjella, which are in a range of 1-100 $\times 10^{-3}$ SI (Vuori and Luttinen, 2003; value range corrected after Luttinen, pers. comm.). And third, the WDMAM magnetic anomaly pattern (Korhonen et al., 2007) over the Mhlapitsi fold belt in South Africa (Fig. 5.5, 'b') can be associated with the deformed and duplicated Paleoproterozoic banded iron stones of the Penge formation (Beukes, 1983 and references therein; Watkeys, pers. comm.) and its magnetic anomaly pattern shows similarities to the Giæver Magnetic Anomaly in amplitude range, wavelength and strike direction in our Gondwana reconstruction.

5.7 Conclusions

We have presented a compilation of magnetic data over Giæverryggen in western Dronning Maud Land and studied the Giæver Magnetic Anomaly in more detail. The main

conclusions are:

- The recently acquired magnetic data in 2012/13 constrain the extent of the Giæver Magnetic Anomaly and revealed a secondary anomaly 48 km farther NNW.
- The calculated minimum magnetic susceptibility is 193 $\times$ 10^{-3} SI and the theoretical magnetic anomaly value at top of bedrock is about +4000 to +4200 nT.
- A cylindrical shape of the anomaly source body is likely and the midpoint depth has been estimated to be ∼3 km b.s.l.
- A simple 2.75-D forward model reproduces the anomaly quite well, using a strong magnetic susceptibility value of 300 $\times$ 10-$^{-3}$ SI, and assuming no phase effects due to remanent magnetization.
- No pronounced gravity expression is observed across the Giæver Magnetic Anomaly at a flight altitude of 3500 m, though modeling predicts a maximum anomaly of ∼10 mGal at this altitude for a density contrast of 300 kg/m^3 between the anomaly body and the host rock.
- We prefer to interpret the Giæver Magnetic Anomaly as an expression of a Paleoproterozoic banded iron formation within the Archaean Grunehogna craton, comparable to those of the Mhlapitsi fold belt south of Polokwane in South Africa and at the Ruker Mountains west of Prydz Bay in East Antarctica.

5.8 Acknowledgments

We thank the flight and science crews of AWI-Polar aircraft for data acquisition, the visited research station in Dronning Maud Land for logistic support, M. K. Watkeys for inspiring and supporting discussion about the Mhlapitsi fold belt, and G. Eagles for improvements of the English language.

Chapter 6

New detailed aeromagnetic and geological data of eastern Dronning Maud Land: Implications for refining the tectonic and structural framework of Sør Rondane, East Antarctica

Matthias Mieth, Joachim Jacobs, Antonia Ruppel, Detlef Damaske, Andreas Läufer, and Wilfried Jokat

6.1 Abstract

The Sør Rondane Mountains (SRM) in eastern Dronning Maud Land (DML) are located in an area, where two apparent Pan-African (650-520 Ma) orogenic mobile belts appear to intersect, the East African-Antarctic Orogen and the Kuunga Orogen. Hence, a better understanding of the tectonic structure of the Sør Rondane region is an important key for unravelling the complex geodynamic evolution of the eastern DML and adjacent regions of East Antarctica during the Late Neoproterozoic/Early Palaeozoic amalgamation of Gondwana. The SRM were recently (2011-2012) aerogeophysically investigated with a 5

km flight line spacing, covering a total area of ∼140˙000 km^2. The aeromagnetic data are correlated with ground-based magnetic susceptibility measurements and geological field data and allow to project tectonic terranes and individual structures into ice-covered areas. Magnetic anomalies and basement foliation trends are collinear in areas dominated by simple shear deformation, whereas an area of large-scale refolding correlates with a subdued small-scale broken magnetic anomaly pattern. The latter area can be regarded as a distinct tectonic domain, the central Sør Rondane corridor. It magnetically separates the SRM into an eastern, a central, and a western portion. This subdivision is presumably related to late Pan-African extensional tectonics and suggests that such a tectonic regime may play a larger role than previously assumed. Voluminous late Pan-African granitoids, which are mainly undeformed, correlate with positive magnetic anomalies between +30 and +80 nT, while a strong magnetic high (+680 nT) near the granitic intrusion at Dufekfjellet is caused by a highly magnetised enigmatic body. The recently discovered prominent magnetic anomaly province of southeastern DML continues into the southern part of the Sør Rondane region, where only a few outcrops are exposed. Findings at these westernmost nunataks of the SRM indicate that the subdued magnetic anomaly pattern of this southeastern DML province is most likely caused by the predominance of metasedimentary rocks of yet unknown age.

KEY WORDS: Aeromagnetics, Magnetic susceptibility, Gondwana assembly, Tectonics, Sør Rondane Mountains, Dronning Maud Land

6.2 Introduction

East Antarctica underwent a complex tectonic evolution since the Archaean, especially during the Pan-African (∼650-520 Ma) assembly of Gondwana (e.g. Boger, 2011 and references therein). Our study area, the Sør Rondane region, is located within two apparently overlapping Pan-African mobile belts (e.g. Satish-Kumar et al., 2013), namely, the East African-Antarctic Orogen (Jacobs et al., 1998, 2003; Jacobs and Thomas, 2004) and the Kuunga Orogen (Boger, 2011; Meert, 2003) as illustrated in Fig. 6.1a. The former is thought to have formed a more or less continuous orogen extending from the Arabian Peninsula to the western DML, while the latter is thought to have formed an orogen extending from Australia through western India, the Prydz Bay region, and eastern DML into Mozambique and beyond. DML is, as most of Antarctica, widely

covered with a thick ice sheet, and only a few outcrops provide scattered insights into the subglacial tectonic framework. Aerogeophysical investigations have allowed several large-scale crustal domains to be distinguished in DML (Golynsky and Aleshkova, 2000; Mieth and Jokat, 2014; Riedel et al., 2012, 2013), while airborne data of higher resolution ($\leq$ 5 km flight line spacing) could be correlated with geological findings on a smaller scale (Damaske et al., 2005; Golynsky and Jacobs, 2001; Ferraccioli et al., 2005a,b). During the "Soviet Antarctic Expedition 36" in 1990, the Sør Rondane region was aerogeophysically investigated the first time with a flight line spacing of 20 km at an altitude of 4000 to 4500 m (Golynsky et al., 1996). However, the sparse flight line spacing and the high altitude above ground did not allow any geologically detailed interpretation of the aeromagnetic data. Therefore, the region was investigated in more detail during three geological-geophysical expeditions in the framework of the collaborative research programme "Geodynamic Evolution of East Antarctica" (GEA) of the German Federal Institute of Geosciences and Natural Resources (BGR) and the Alfred-Wegener-Institut Helmholtz-Zentrum für Polar- und Meeresforschung (AWI).
Here, we report on the newly acquired aeromagnetic data in the Sør Rondane region. Together with new ground-based susceptibility measurements and structural information, we use these data to extrapolate outcropping terrane boundaries and discontinuities into ice-covered areas to constrain the overall size of the mapped geological structures. This is a first step towards a better constraining of the geodynamic evolution of the SRM during the amalgamation of Gondwana in the Late Proterozoic and Early Palaeozoic.

6.3 Geological overview of Sør Rondane

The broad geological framework of the Sør Rondane Mountains (SRM) was first established by Belgian researchers, who published the first geological map of the mountain range (Van Autenboer, 1969; Van Autenboer and Loy, 1972; Picciotto et al., 1964). This early work recognised two fundamentally different basement complexes, the Nils Larsenfjellet Group, a major (meta)-granitoid body in the SW part of the SRM, and the Teltet-Vengen Group (undifferentiated metamorphic rocks), occupying the remaining major part of the mountain range. This early work was followed by extensive geological studies of the Japanese Antarctic Programme until today (e.g. Shiraishi et al., 2008; Satish-Kumar et al., 2013 and references therein). The Japanese teams published detailed geological

maps of most of the mountain range and conducted detailed petrological, geochemical, and geochronological studies of the SRM (e.g. Asami et al., 1992, 1996, 1997, 2005; Osanai et al., 1992, 2013; Owada et al., 2013; Satish-Kumar et al., 2008, 2013; Shiraishi and Kagami, 1992; Shiraishi et al., 1991, 1994, 2008). Osanai et al. (1996) and Shiraishi et al. (2008) subdivided the SRM into the distinct SW-terrane and the NE-terrane, separated by the so-called Sør Rondane Suture (Fig. 6.1c; SRS). This subdivision was based on contrasting geochemical composition and metamorphic grades on either side of the Sør Rondane Suture. Whilst the NE-terrane is dominated by granulite facies rocks, the SW-terrane consists mainly of greenschist to amphibolite facies assemblages. In the granulite facies rocks of the NE-terrane, metamorphic U-Pb zircon ages of ∼640-600 Ma were interpreted to represent collision tectonics, whilst slightly younger ages of ∼570 Ma in both terranes were interpreted to represent retrograde metamorphism, orogenic collapse, and exhumation in both terranes postdating the collision (Shiraishi et al., 2008). In the western SRM, the structural grain, including the Sør Rondane Suture, trend roughly E-W, while it swings into a SE direction in its eastern portion (Fig. 6.1).

Different granulite facies rocks with contrasting PTt-loops within the NE-terrane were

Figure 6.1 ***(facing page)*****: Overview of study area. (a) Sketch of part of Gondwana (∼500 Ma), showing the study area to be located close to the intersection of two Pan-African (650-520 Ma) mobile belts, abbreviations: B – BLM (Coats Land block), G – Grunehogna, N – Napier, R – Ruker. (b) Survey area with grounding line (thick black), ice shelf edge (grey), outcrops (thin black), and magnetic flight lines (blue). Measurement lines are 5 km separated in the onshore region, and 10 km over the ice shelf and beyond. Tie lines were flown every 30 km. Base stations for flight operation were Princess Elisabeth station (PE) and a temporary camp at Crown Bay. (c) Geological overview map of the SRM after Shiraishi et al. (2008) and Osanai et al. (2013). The SW-terrane is separated from the NE-terrane by the Main Tectonic Boundary (MTB). The SW-terrane is composed of a TTG subterrane (∼995 Ma and 940-920 Ma) and a range of metamorphic rocks from greenschist to granulite facies, close to the MTB. The northern contact of the TTG subterrane is a major dextral shear zone, the Main Shear Zone (MSZ). The NE-terrane is predominated by granulite facies rocks, which were metamorphosed at ∼640-600 Ma, similar to granulites within the SW-terrane, however with contrasting PTt-loops. Whilst metamorphic zircon ages of ∼640 – 600 Ma are thought to indicate collision between the SW- and NE-terranes, metamorphic zircon ages of ∼570 Ma are interpreted to indicate extensional exhumation and orogenic collapse following collision. The Sør Rondane Suture (SRS) is no longer considered an important boundary. Major volumes of late tectonic A-type granitoids and mafic dykes, dated at ∼560 – 520 Ma, occur in the SW-terrane.**

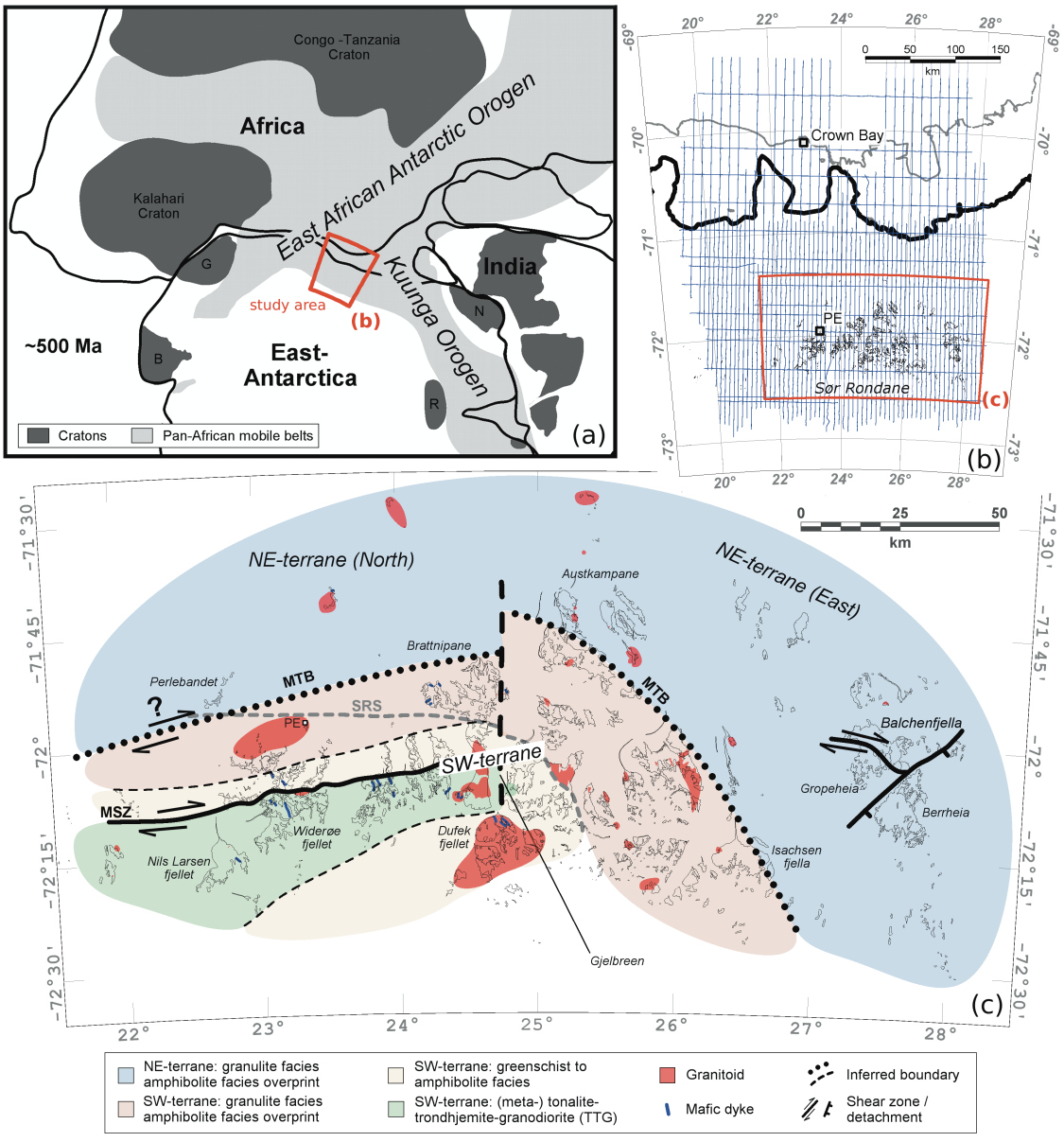
Congo -Tanzania Craton
Africa
Kalahari Craton
East African Antarctic Orogen
Kuunga Orogen
India
study area
(b)
~500 Ma
East-Antarctica
G
B
N
R
Cratons
Pan-African mobile belts
(a)
Crown Bay
PE
Sør Rondane
(c)
(b)
0 50 100 150
km
NE-terrane (North)
NE-terrane (East)
Austkampane
Brattnipane
Perlebandet
MTB
SRS
PEo
SW-terrane
MSZ
Widerøe fjellet
Dufek fjellet
Nils Larsen fjellet
Balchenfjella
Gropeheia
Berrheia
Isachsen fjella
Gjelbreen
0 25 50
km
(c)
NE-terrane: granulite facies amphibolite facies overprint
SW-terrane: granulite facies amphibolite facies overprint
SW-terrane: greenschist to amphibolite facies
SW-terrane: (meta-) tonalite-trondhjemite-granodiorite (TTG)
Granitoid
Mafic dyke
Inferred boundary
Shear zone / detachment

recently described close to the Sør Rondane Suture (Adachi et al., 2013; Baba et al., 2013; Osanai et al., 2013). Based on these different granulite facies rocks, the spatial extent of, and the boundary between, the SW- and NE-terranes were redefined. The boundary between the SW-terrane and the NE-terrane is called the Main Tectonic Boundary (MTB) by e.g. Osanai et al. (2013). The MTB is described as a high-strain zone with at present unknown kinematics. It separates granulites to the SW, which are characterised by a counter-clockwise PTt-path, and granulite facies rocks to the NE, which are characterised by a clockwise PTt-path, both dated at ∼640-600 Ma (Osanai et al., 2013). The latter authors interpret the MTB as a suture with the NE-terrane thrust on top of the SW-terrane, which caused metamorphic zircon growth between ∼640-600 Ma. Furthermore, they suggest that the Sør Rondane Suture has no great tectonic significance and it is no longer interpreted as a suture.

The SW-terrane after Osanai et al. (2013) consists of rocks with a wide range of metamorphic grades. Metamorphism increases towards the contact with the NE-terrane, where granulite facies is reached at Brattnipane (Baba et al., 2013). Generally, the SW-terrane is composed of two major rock units, a southern trondhjemite-tonalite-granodiorite (TTG) suite, metamorphosed under greenschist to amphibolite facies conditions (the Nils Larsenfjellet Group of Van Autenboer, 1969) and a northern greenschist to granulite facies metamorphic complex, predominated of a variety of metasedimentary and metaigneous rocks (Fig 1c). These are separated from each other by the several hundred metre wide dextral Main Shear Zone (Fig. 6.1c; MSZ), first described by Kojima and Shiraishi (1986). To the south of the TTG subterrane, small exposures of metasupracrustal rocks crop out, similar to those north of the MSZ, hence, a southern boundary of the TTG subterrane is inferred (Fig. 6.1c).

The TTG suite is subdivided into geochemically, petrologically, and geochronologically distinct domains with zircon crystallisation ages of ∼995 Ma and 940-920 Ma (Ikeda and Shiraishi, 1998; Kamei et al., 2013; Shiraishi et al., 2008; Takahashi et al., 1990). Whilst the earlier magmatism appears more tholeiitic in composition, the later formed more calc-alkaline adakites (Kamei et al., 2013). The two groups differ not only in their ages but also in the regional distribution. The western portion of the TTG subterrane is dominated by rocks with more tholeiitic affinity, whilst the eastern part is dominated by rocks with a tendency to calc-alkaline composition (Kamei et al., 2013). This plutonic complex is interpreted to have formed along a juvenile oceanic arc. A U-Pb titanite age

of ∼516 Ma (Shiraishi et al., 2008) together with Rb-Sr and K-Ar mineral ages of ∼510-460 Ma (Picciotto et al., 1964) indicate substantial Cambrian tectono-thermal overprint, although there appear also apparently undeformed portions of this igneous complex at the meso-scale. The TTG subterrane is laterally discontinuous.

To the north, the TTG subterrane is bounded by the ENE-trending MSZ. The MSZ is a steeply south-dipping, dextral mylonite zone with mostly subhorizontal and often shallowly easterly inclined stretching lineations (Ruppel, 2012). The MSZ separates the TTG subterrane from a variegated sequence of greenschist to granulite facies rocks. The area to the north of the MSZ is characterised by subordinate greenschist facies schists and a highly migmatitic sequence of volcano-sedimentary rocks. Metasedimentary rocks include quartzo-feldspathic gneisses interlayered with marbles. The metavolcanic rocks include grey homogenous gneisses, as well as finely banded plagioclase-hornblende gneisses, interpreted as metatuffites. Geochemically, these rocks have island arc to continental margin affinities (Shiraishi et al., 2008). This sequence is intruded by numerous small granitoids that were intensely transposed together with the metasupracrustal rocks. Both, isoclinal as well as open refolding occurs and two distinct foliations are recognised. Granulite facies rocks close to the MTB (Brattnipane) have metamorphic U-Pb zircon ages of ∼640-600 Ma and are characterised by counterclockwise PTt-paths (Adachi et al., 2013; Baba et al., 2013; Osanai et al., 2013).

The granulite facies NE-terrane is dominated by metasupracrustal rocks that were deposited on a juvenile Late Mesoproterozoic basement. Mafic rocks are also recorded, and an oceanic affinity is documented (Shiraishi et al., 2008). Based on the age of detrital zircons, it is thought that sedimentary protoliths were deposited at least in part after 750 Ma (Shiraishi et al., 2008) and Neoproterozoic deposition ages are independently confirmed by a strontium isotope study on metacarbonate rocks (Otsuji et al., 2013). In contrast to the SW-terrane, granulites of the NE-terrane document a clockwise PTt-path at ∼640-600 Ma (Shiraishi et al., 2008; Adachi et al., 2013; Osanai et al., 2013).

The contrasting PTt-paths on either side of the MTB are explained in a model, where the NE-terrane was thrust over the SW-terrane; granulite facies zircon growth at ∼640-600 Ma is thought to date the collision (e.g. Shiraishi et al., 2008; Osanai et al., 2013). This infers that the MTB is a suture; note the difference to the Sør Rondane Suture (Shiraishi et al., 2008), of which some authors now believe that it is not a significant tectonic boundary within the SRM (e.g. Osanai et al., 2013).

Across the entire SRM, a number of metamorphic U-Pb zircon ages between ~570-530 Ma are recorded (Adachi et al., 2013; Grantham et al., 2013; Osanai et al., 2013; Picciotto et al., 1964; Pasteels and Michot, 1970; Shiraishi et al., 2008). These ages are interpreted to represent a post-collision hydration event that affected many of the granulite facies rocks and is thought to be associated with extensional tectonics, following the main collision at ~640-600 Ma (Shiraishi et al., 2008). In the NE-terrane, the NE-trending and extensional Balchen detachment (fault / shear zone) is interpreted to have evolved during this late-tectonic extension (Ishikawa et al., 2013). The Balchen detachment juxtaposes mafic and ultramafic rocks of the Gropeheia unit next to gneisses of the Berrheia unit. Also late-tectonically, the SRM are intruded by in part large volumes of granitoids and a number of mafic dykes. The main volumes of melts occur in the SW-terrane. Late-tectonic granitoids include syenites and bt-granites, dated at ~620 Ma (group I), 570-560 Ma (group II), and 530-520 Ma (group III) (Li et al., 2006; Shiraishi et al., 2008). The largest granite, the Dufek granite, provided the oldest U-Pb zircon age of ~620 Ma. The late-tectonic Vengen granite, dated at ~560 Ma (U-Pb zircon) intrudes the MSZ, but is still deformed, which implies that the MSZ was active after ~560 Ma (Shiraishi et al., 2008). The mafic dykes are mainly lamprophyres and high-K dolerites and they are thought to have derived from a metasomatised mantle source (Owada et al., 2013). A major inferred N-S trending fault dissects the SRM and separates the predominantly E-W trending western portion from the mainly NW-SE trending eastern part of the mountain range (e.g. Osanai et al., 2013). The fault follows the Gjelbreen (Fig. 6.1c; along 24.7°E), and is probably collinear with a number of apparent lineaments, now occupied by major ice streams.

6.4 Data acquisition and processing

Airborne geophysical data of the GEA campaign have been acquired during three consecutive austral summer seasons in January / February 2011, January 2012, and November / December 2012 using the AWI Basler BT-67 aircraft Polar-5 in 2011 and Polar-6 in 2012. The target area over the SRM between 72.5°S / 20°E and 71°S / 28°E was surveyed from the Belgian Princess Elisabeth station as well as from a temporary base at Crown Bay. The survey area was extended northward across the ice shelf to 69.5°S during the third flight campaign, covering a total area of ~140˙000 km^2. The measurement lines

were flown in N-S orientation, with a spacing of 5 km in the main target area and 10 km in the northern extension. The E-W oriented tie lines were flown every 30 km. The length of all flights sums up to 37˙000 km. Data were acquired at a constant barometric flight altitude ensuring a minimum distance to the surface of 500 m. Four Novatel global navigation satellite system (GNSS) receivers recorded the position of the aircraft with a sample rate of 50 Hz for scientific purposes. Two receivers were installed on the cabin roof and one on each aircraft wing. The GNSS positions were post-processed with Waypoint GPS software using the method of precise-point-positioning, which ensured the accuracy to be independent of distance to a GNSS base station. The magnetic data were acquired using Scintrex Cs-2 Caesium magnetometers in 2011 and Cs-3 sensors in 2012 mounted in nose and tail booms of the aircraft. In both aircraft, a Billingsley TFM 100 fluxgate magnetometer was operated and used for magnetic compensation. Magnetic base station for recording the diurnal variations of the Earth magnetic field were deployed near the airfields of Novolazarevskaya, Princess Elisabeth, and during the second field season at Crown Bay. Magnetic data processing was carried out using Geosoft Oasis montaj software. The processing flow included de-spiking, core-field and diurnal variation corrections, upward continuation to 4600 m, and full levelling. The automatic full levelling reduced the cross-point error to 0.1 ± 0.8 nT, without introducing artificial anomalies. However, more than 80% of the lines were flown at an altitude of 3200 to 3600 m, and many small wavelength anomalies became subdued due to the upward continuation. Therefore, the levelling process was repeated without applying an upward continuation beforehand. First, static shifts were applied to all lines flown significantly higher or deeper than 3400 m, followed by a careful low pass filtered tensioned spline levelling, resulting in a cross-point error of 4.7 ± 5.7 nT. Thus, the higher frequencies of the recorded data were maintained, in particular in the region of the outcropping mountain range. Comparison to the upward continued full-levelled data ensured that no artificial anomalies had been introduced and that a similar levelling quality was reached. The final data were gridded with a grid cell size of 1.25 km (Fig. 6.2a). Grid-based reduction-to-the-pole were performed with mean inclination of -62.8° and mean declination of -38.2° and, subsequently, the positive tilt derivative was calculated in order to enhance and to analyse the orientation of positive magnetic anomalies (Fig. 6.2b).

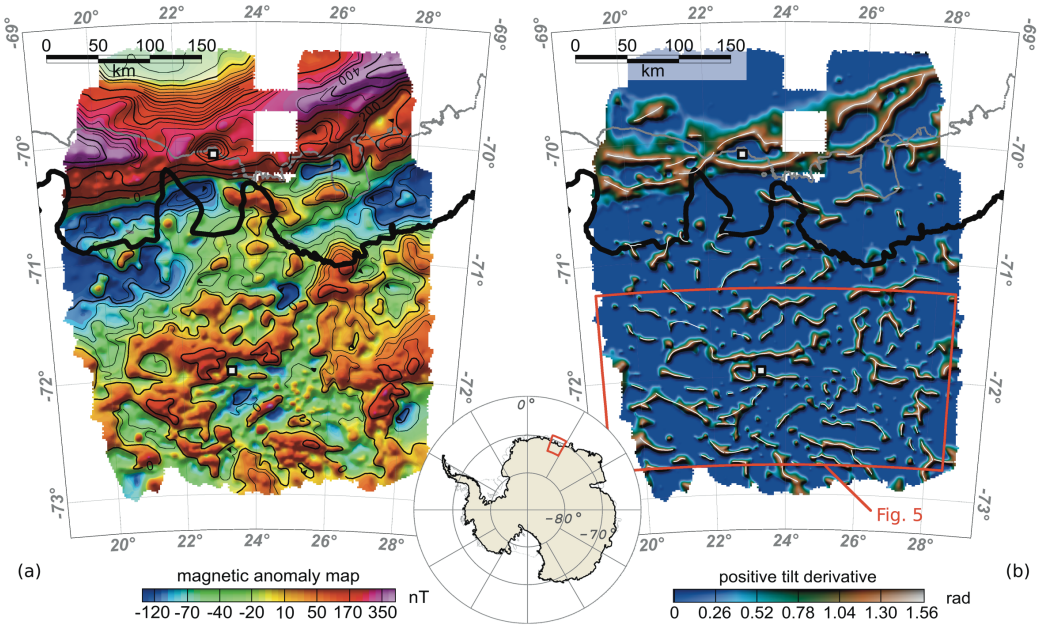

Figure 6.2: Magnetic data. Grounding line (thick black), ice shelf edge (grey) and location of base stations (squares) are shown for orientation. (a) Magnetic anomaly map with contour lines every 20 / 100 nT. The anomaly pattern can be described as moderate with values between -220 and +350 nT, except of the offshore region and one strong anomaly (+680 nT) near Dufekfjellet (72.25°S / 24.41°E). (b) Positive tilt derivative, which indicates the strike of positive magnetic anomalies and support confining different magnetic domains. White lines are picked along the maxima.

6.5 Results

6.5.1 Airborne magnetics

The gridded data are reduced-to-the-pole for interpretation (Fig. 6.3), as we assume that induced magnetisation is predominant for most continental rock formations. The continuation of the anomaly pattern beyond the survey area is shown in the inset of Fig. 6.3, where the dataset of this study is merged with the AWI magnetic data compilation of DML (Mieth and Jokat, 2014) in the west and with the ADMAP dataset (Golynsky, 2007) of lower spatial resolution in the east.

The magnetic anomaly pattern of the Sør Rondane region is characterised by moderate amplitudes ranging between -220 to +350 nT, except of the coastal region and one circular magnetic high within the mountain range. We identified seven magnetic domains ('I-VII') and nine boundaries / lineaments ('1-9'), which are described in the following.

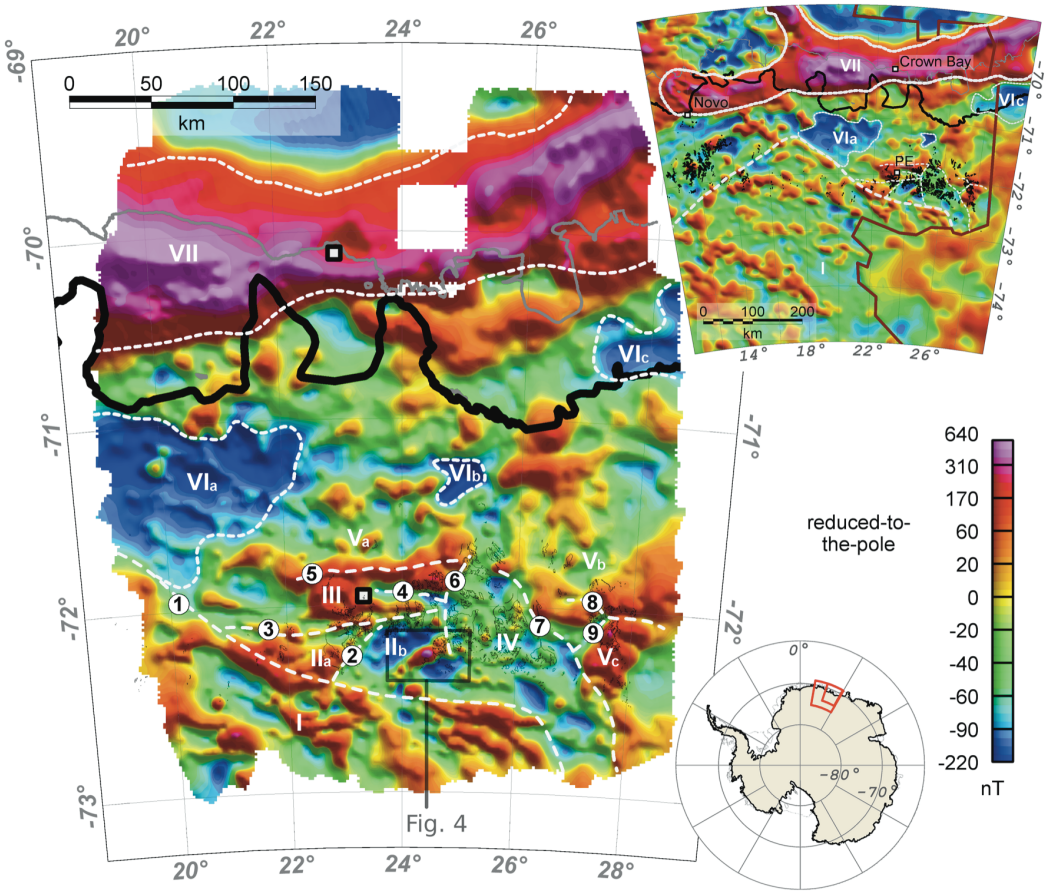

Figure 6.3: Magnetic anomaly data reduced-to-the-pole with inclination / declination of -62.8° / -38.2°. Grounding line (thick black), ice shelf edge (grey), and location of base stations (squares) are shown for orientation, white dashed lines are showing boundaries ('1-9') of magnetic domains ('I-VII'). The inset (top right) shows the continuation of the anomaly pattern beyond the survey area, based on a compilation of magnetic data from this study, from the AWI-DML compilation in the west (Mieth and Jokat, 2014) and from ADMAP data (Golynsky, 2007) east of the brownish line.
Boundary '3' corresponds to the Main Shear Zone, lineament '4' to the Sør Rondane Suture, and lineament '9' to the Balchen detachment, while boundary '5' and '7' correspond to the Main Tectonic Boundary, and boundary '6' represents the Gjelbreen lineament. Domain 'I' corresponds to the SE-DML province, domain 'II', 'III', and 'IV' to the SW-terrane, domain 'V' to the NE-terrane, domain 'VI' to the transition zone, and domain 'VII' to the much larger Antarctic Continental Margin Magnetic Anomaly (Golynsky et al., 1996). Domain 'II' coincides with the TTG subterrane and domain 'Vc' with the Berrheia unit. The subdued and small-scale broken anomaly pattern of domain 'IV', the cenral Sør Rondane corridor, is conspicuous and separates magnetically the SRM into an eastern and a western portion.

Domain 'I' comprises small amplitudes of ±50 nT and highs of +150 to +250 nT. Most of the highs are elongated anomalies of 4 to 8 km width and 30 to 50 km length, striking WNW-ESE. Boundary '1' marks a change in strike and wavelength of the anomalies. It separates domain 'I' from domain 'II' and 'IV' and is located south of the outcropping SRM.

Anomalies of 10 to 20 km length strike NE-SW in domain 'II'. Along boundary '2', this domain is divided into subdomain 'IIa', which is characterised by positive amplitudes up to +170 nT, and subdomain IIb, which shows mainly negative amplitudes down to -160 nT. Within the latter, a remarkably magnetic high (+680 nT) was detected near the granitic intrusion at Dufekfjellet. Domain 'II' is confined to the north by boundary (3), which is characterised by a chain of small circular positive anomalies of +20 to +70 nT. Besides the weak magnetic signature, it marks a change of orientation and elongation of magnetic anomalies in domain 'III'. Here, anomalies reach values of +100 to +260 nT, they strike E-W, and have an elongation of 30 to 80 km. An elongated magnetic low (-110 nT) is located within this domain, with a width of 5 to 10 km and a length of 50 km. This low is labelled as lineament '4', whereas the northern boundary ('5') of domain 'III' is marked by a 100 km long and 4 km wide high of +80 to +200 nT.

To the east, the magnetic pattern of domain 'IV' differs clearly in amplitude range and wavelengths from all other magnetic domains. The amplitudes vary between -100 and +50 nT and the anomaly pattern can be described as small-scale, broken, and with a diffuse orientation. The extent of domain 'IV' is well defined by the boundaries to the west ('6') and to the east ('7'), whilst its northern extent is not clearly confined and southwards it might continue beyond our study area.

Domain 'V' is characterised by longer wavelength anomalies of small amplitudes in subdomain 'Va' (±50 nT), moderate amplitudes in subdomain 'Vb' (-100 to +200 nT), and shorter wavelength and relatively high amplitudes in subdomain 'Vc' (up to +350 nT). A 70 km long winding and 5 km narrow band of ±0 to +50 nT separates domain 'Vc' from 'Vb', labelled as boundary '8'. Whereas lineament '9' marks a 10 km wide channel of magnetic low amplitudes down to -100 nT. Domains 'VIa-c' are distinct magnetic lows, with amplitudes between -140 and -220 nT. A circular shaped positive anomaly of +15 nT and some NW-SE striking anomalies of higher amplitudes (-80 nT) are detected within domain 'VIa'. These anomalies are 3-5 km wide and ∼40 km long, striking NW-SE. Very high magnetic amplitudes are measured over the ice shelf edge with values of

up to +630 nT (domain 'VII'). This anomaly feature consists of two narrow ridges of high amplitudes with a variable spacing to each other of up to 40 km.

6.5.2 Magnetic susceptibility measurements

Magnetic susceptibility readings were carried out in the western part of the SRM using a Kappameter KT-6. Measurements were collected at 231 sites during the GEA campaign, consisting of 12 single readings for each site, taken within an area of up to 10 m^2. The highest and lowest values were considered as outliers, thus 10 single measurements contributed to a mean value for each site. These mean values were grouped and averaged for each terrane and lithology. The results are presented in Tab. 6.1, including data from the westernmost SRM (SE-DML province) and from granitic intrusions. Relatively high values have been measured for grey gneisses, granulites, and amphibolites, while metasedimentary rocks show very low values in all terranes. Readings at granitoids show a wide range of magnetic susceptibilities, with a tendency to higher values for the older intrusions (group I and II).

Region	**Lithology (No. of sites)**	**Mean** (10-3 SI)	**Range** (10-3 SI)
NE-terrane			
Perlebandet	Grey gneiss (8)	26	8.3-95
	Qtz-Fsp gneiss, granulite (8)	12	0.1-57
	Augen gneiss (4)	1.2	0.2-25
	Metasedimentary rocks (5)	0.2	0.1-0.2
SW-terrane			
TTG-subterrane	Pyroxenite (1)	110	
	Mafic dyke (1)	19	
	Amphibolite, Enclave/ultramafic (6)	11	0.5-64
	Granite gneiss (8)	6.9	0.4-16
	(Meta)-granodiorite/tonalite (21)	3.0	0.1-11
	Myl. granodiorite/tonalite (7)	2.3	0.1-4.7
	(Meta)-gabbro (2)	0.5	0.4-0.6
Other (north of MSZ)	Grey (mig.) gneiss, metavolcanic? (22)	14	0.1-55
	Augen gneiss, orthogneiss, Qtz-Fsp gneiss, gneissic granite, migmatitic melt (24)	9	0-32
	Schist, meta-chert (5)	2.8	0.1-7.8
	Meta-sedimentary rocks (18)	0.1	0-0.9
SE-DML province			
	Gneiss, not classified (5)	0.3	0-0.3
	Metasedimentary rocks (8)	0.2	0-0.6
	Granitic gneiss (10)	0.1	0-0.3

Granitoids			
Group I	Dufek, gneissic enclave* (1)	21	
(∼620 Ma)	Dufek granite* (5)	7.6	5.4-12
Group II	Vengen granite (7)	20	8.6-44
(570-560 Ma)	Tertene granite (2)	8.8	6.6-11
	Lågkollane granite (1)	8.4	
Group III	Bamseungen granite (1)	5.1	
(530-520 Ma)	Utsteinen granite (4)	0.6	0.1-1.7
	Pingvinane granite (3)	0.1	0.1-0.2
Age unknown	Lunckeryggen granite (1)	9.8	
	Mefjell granite (1)	0.2	

* Measurements were carried out on rock samples instead of field exposures

Table 6.1: Summary of magnetic susceptibility readings in the western part of the SRM. Mean values of each location were grouped for lithology and tectonic terrane in Sør Rondane and subsequently averaged. Relatively high values have been measured for grey gneisses, granulites, and amphibolites, while metasedimentary rocks show very low values in all terranes. Readings at granitoids show a wide range of magnetic susceptibilities, with a tendency to higher values for the older intrusions (group I and II).

6.5.3 Magnetic high near Dufekfjellet intrusion

The strong localised magnetic high (+680 nT) near Dufekfjellet is by far the highest magnetic anomaly observed in the entire Sør Rondane region. Fig. 6.4a shows that this anomaly is located near, but not at an outcrop. Rocks of the labelled nunataks in Fig. 6.4 are all granites. Mean magnetic susceptibilities measured on rock samples of Dufekfjellet range between 4.5 and 12 $\cdot 10^{-}3$ SI (Tab. 6.1). Attempts to model the observed strong anomaly with a large and thick granitic intrusion of similar magnetic susceptibility failed. The 2.75-D model displayed in Fig. 6.4b rather demonstrates that a highly magnetised rock formation must be the source of the anomaly. The only constraints for the model, beside the magnetic anomaly data, are the outcropping granite at Rogerstoppane (Fig. 6.4, R) and the bedrock elevation that was calculated from ice thickness radar measurements. Therefore, the degree of freedom in the modelling is rather high. We set the remanent magnetisation to zero and kept the magnetic susceptibility of the source body with 150 $\cdot 10^{-}3$ SI as low as possible. Note that a higher susceptibility value would directly lead to a smaller extent of the source body. The horizontal extension perpendicular to the profile is 8 km for the source body and 12 km for the granite. The vertical extent

of the modelled source body is in good agreement with the result of a located 3D-grid based Euler deconvolution, which estimated a midpoint depth of ∼800 m below sea level for a sphere-shaped source. Near Roggerstoppane, the discrepancy between observed and calculated aeromagnetic values indicates an even lower magnetisation of the granite as the used 5 ·10⁻3 SI and / or a much small extent. However, this discrepancy is related to the simplicity of the model as well and, therefore, it is not investigated further.

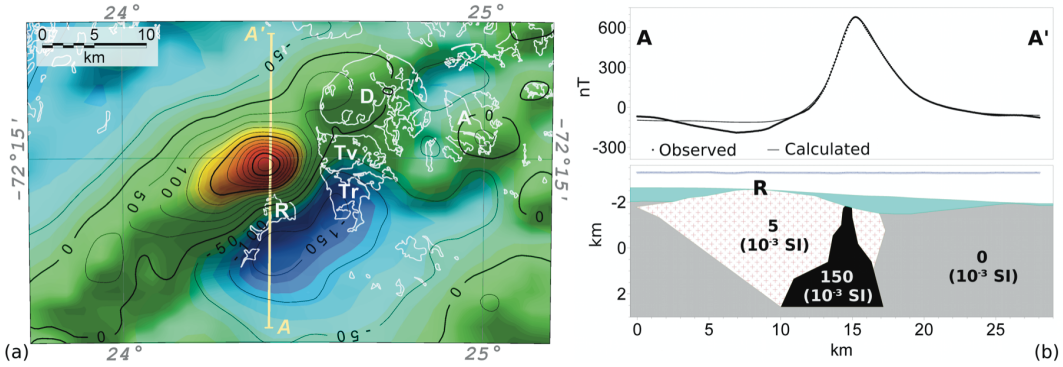

Figure 6.4: Strong magnetic high near Dufekfjellet. (a) Magnetic anomaly map with contour lines every 50 / 250 nT and outcrops in white. (b) 2.75-D model along a flight line profile from A to A' and the observed (dotted black line) and calculated magnetic anomaly (black line) at flight elevation (blue line). Displayed magnetic susceptibilities are homogeneous for each unit. Cyan represents the ice sheet (non-magnetic), red plus sign pattern the outcropping granite, black the highly magnetised source body, and grey the host rock. The granite body has an extension of 12 km perpendicular to the profile and the source body an extension of 8 km. No remanent magnetisation was assumed and a DC shift of -60 nT is applied to the calculated anomaly values. Abbreviation of nunataks: A – Arden, D – Dufekfjellet, Tr – Trerindane, Tv – Tvihøgda, R – Rogerstoppane. The simplistic model demonstrates that even a large granitic intrusion itself cannot cause the observed strong magnetic high. A highly magnetised rock formation must be hidden under the ice (and possibly under a thin overlaying rock layer). Near Roggerstoppane, the discrepancy between observed and calculated values indicates a lower magnetisation of the granite and / or a much smaller extent as shown, but this discrepancy is related to the simplicity of the model as well. The magnetic susceptibility of the source body was chosen to be as low as possible. Note that a higher value would directly lead to a smaller extent of the body.

In addition, in order to estimate thicknesses of granitoids, we calculated the magnetic values of outcropping granitic intrusions modelled with a horizontal size of 12 x 12 km and varying thicknesses at an altitude of 800 m above the surface. The resulting maximum anomaly values are given in Tab. 6.2 for a constant magnetic susceptibility of 10·10⁻3 SI for the intrusion body.

Thickness	Max. anomaly
1 km	32 nT
2 km	52 nT
3 km	70 nT
4 km	86 nT
5 km	99 nT
8 km	124 nT

Table 6.2: Aeromagnetic response to 2.75-D models of a granitic intrusion into a non-magnetic host rock. The intrusion body reaches the surface and has a dimension of 12 x 12 km, a varying thickness, and a magnetic susceptibility of 10 $\cdot 10^{-}3$ SI. Distance to the top of the anomaly is 800 m, which was the usual mean distance to the rock surface over the mountain range during flights of the GEA campaign.

6.6 Interpretations and discussion

6.6.1 Magnetic domains and tectonic terranes

The magnetic pattern over the SRM broadly supports the separation into a NE-terrane and a SW-terrane separated by the MTB, and most magnetic anomalies are co-linear with the general structural trend of the region (Osanai et al., 2013; Toyoshima et al., 2013). The new magnetic data reveal that both terranes can be roughly subdivided into western and eastern portions (Fig. 6.5), separated by the N-S trending, curvilinear Gjelbreen lineament, which coincides with the magnetic boundary '6' (Fig. 6.3).

The eastern part of the NE-terrane is characterised by moderate to high magnetic anomalies, striking either NE-SW or E-W, and is divided into two magnetic subdomains 'Vb' and 'Vc'. The latter matches with the geological Berrheia unit (quatzo-feldspathic gneisses), located SE of the Gropheia unit (mafic and ultramafic rocks). The quartzo-feldspathic gneisses of the Berrheia unit are characterised by low magnetic values (Ishikawa et al., 2013). However, we have measured the highest magnetic values (up to +350 nT) in the Balchenfjella area over Berrheia. This unit, close to the SE-inclined Balchen detachment, must be rather thin and is probably underlain by the mafic- and ultramafic Gropeheia unit, which would explain the magnetic high. The NE-trending Balchen detachment coincides with a narrow distinct magnetic low (Fig. 6.3, lineament '9'). In contrast to the geological interpretation of Ishikawa et al. (2013), this magnetic lineament is truncated by the magnetic boundary '8', which coincides in its NW-part

with a dextral shear zone (Ishikawa et al., 2013) and continues to the SE into an ice covered area (Fig. 6.5). Hence, we infer that either the NE continuation of the Balchen detachment is magnetically masked or that the dextral shear zone was reactivated during the tectonic extensional phase and only domain 'Vc' was displaced to the SE.

In the western part of the NE-terrane, the magnetic anomalies mainly trend ENE-WSW and the amplitude level is lower than in its eastern part. In general, the magnetic pattern tends to become lower frequency towards the coast, which reflects the increasing distance to the top of the bedrock due to the constant barometric flight altitude. Three prominent magnetic lows are mapped in this transition zone between the mountain range and the coast. They are similar to the large magnetic low found between the central DML mountain range and the Riiser-Larsen Sea (Damaske et al., 2005; Riedel et al., 2013). The meaning of these magnetic lows is thus far unresolved, as no outcrops constrain their origins. Another prominent magnetic low in the Grubergebirge (71.3°S / 13.5°E), central DML, is correlated with a large anorthosite complex with a crystallization age of ∼600 Ma (Damaske et al., 2005; Jacobs et al., 1998). In contrast to the enigmatic magnetic lows, the interpretation of the magnetic high zone along the coastal region (domain 'VII') is well constrained by seismic reflection data. This feature is part of the Antarctic Continental Margin Magnetic Anomaly, which extends from Enderby Land to central Dronning Maud Land (Golynsky et al., 1996). It is interpreted to reflect basaltic intrusions during Gondwana break-up (Leitchenkov et al., 2008). The higher resolution of the GEA aeromagnetic data reveals two ridges of magnetic highs along most parts of the continental margin. They probably indicate two distinct phases of basaltic intrusions during the Jurassic Gondwana break-up.

The magnetic expression of the boundary between the NE- and the SW-terrane (MTB) is different in its eastern and western part. In the east, the MTB is very well constrained between the high amplitude domain of the NE-terrane and the magnetically small amplitude domain ('IV') of the eastern portion of the SW-terrane. Here, the NE-trending anomalies of the NE-terrane appear clearly truncated by the MTB, which is refined in its location (Fig. 6.5). In the west, the MTB is collinear with an E-W trending, 100 km long, linear magnetic high (boundary '5'). It is unclear, if this major anomaly is part of either the NE-terrane or the SW-terrane, or if it reflects the MTB itself. If this anomaly reflects the MTB, then the boundary of the NE- and SW-terranes would be to the north of Perlebandet (Fig. 6.5) and not to the south of it (e.g. Osanai et al., 2013).

Therefore, it remains to be tested, whether the granulite facies rocks of Perlebandet document a clockwise or counter-clockwise PTt-path and subsequently belong to either the NE- or SW-terrane. Field observations during the GEA campaign at the southern outcrop of Perlebandet revealed a high strain zone with subhorizontal stretching lineations but uncertain sense of shear. The vicinity of the western portion of the MTB is clearly characterised by substantial transcurrent shearing with parallel anomalies on either side. This parallelism might be the reason why the precise location of the MTB is difficult to describe based on our magnetic data.

The complex magnetic anomaly pattern of the SW-terrane reflects the geological complexity of this region. The TTG subterrane coincides with the magnetic domain 'II' (Fig. 6.3). It is characterised by SW-NE trending magnetic anomalies, matching the foliation strike (Fig. 6.5). The magnetic TTG domain can be subdivided into a positive amplitude subdomain ('IIa') and a negative amplitude subdomain ('IIb'). The older, ∼995 Ma and more tholeiitic, western portion of the TTG subterrane (Kamei et al., 2013) might be associated with subdomain 'IIa', which is in good agreement with the magnetic susceptibility measurements in this area (0.5-110 $\cdot 10^{-}3$ SI). On the other hand, the younger (940-920 Ma; Kamei et al., 2013), more calc-alkaline eastern part might correlate with

Figure 6.5 ***(facing page)*****: Interpretation of aeromagnetic data over Sør Rondane Mountains. (a) Magnetic anomaly map reduced-to-the-pole with inclination / declination of -62.8° / -38.2°. (b) Positive tilt derivative. (c) Combination of geological findings and interpretation of aeromagnetic data. The magnetic boundaries confirm, redefine, and reveal new tectonic lineaments and fault systems. Previously defined tectonic boundaries in grey (Osanai et al., 2013) are redefined by our interpretation in black. Form-line contour of foliations are based on Toyoshima et al. (2013). Abbreviations: central SR-corridor – central Sør Rondane Suture, MTB - Main Tectonic Boundary, MSZ – Main Shear Zone, SRS – Sør Rondane Suture. Strike of foliation and mineral stretching lineation in the westernmost nunataks of the study area are mainly collinear with the strike of elongated positive anomalies within the prominent magnetic SE-DML province. A ductilely undeformed granitoid was found at Tertene and coincides with an observed elongated magnetic high near the NE boundary of the SE-DML province. In contrast to previous interpretations, Perlebandet is magnetically interpreted to be part of the SW-terrane, which is supported by the occurrence of high magnetic grey gneisses at these nunataks and farther south. The MTB is magnetically not constrained within the central Sør Rondane corridor. Apparently, this corridor continues in the magnetic anomaly map farther north and separates magnetically the NE-terrane. Some granitoids could be associated with magnetic anomalies, others are either to small in extent or have magnetic susceptibilities similar to that of the host rock.**

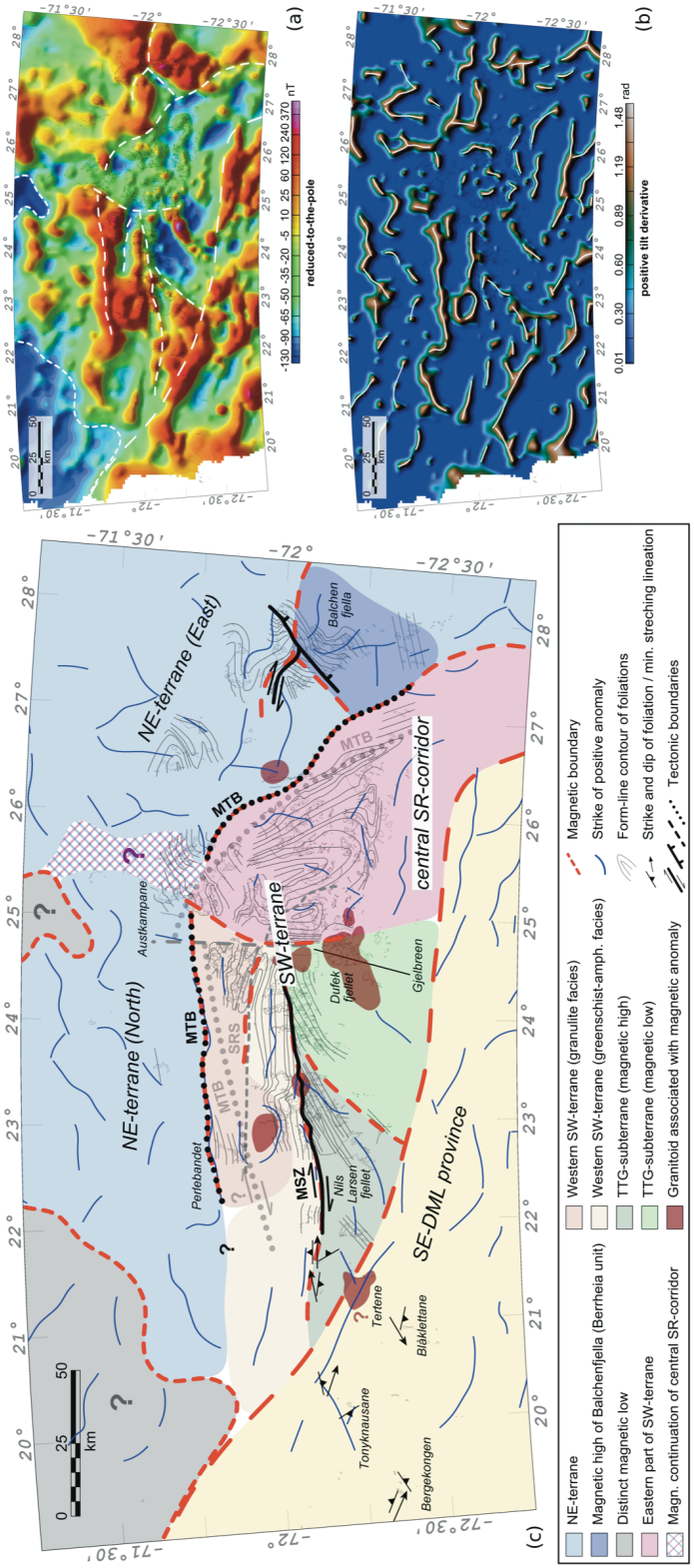
(a)
reduced-to-the-pole
nT
(b)
positive tilt derivative
rad
(c)
NE-terrane (East)
NE-terrane (North)
SW-terrane
central SR-corridor
SE-DML province
MTB
MSZ
SRS
Balchen fjella
Austkampane
Perlebandet
Dufek fjellet
Gjelbreen
Nils Larsen fjellet
Terfene
Blåklettane
Tonyknausane
Bergekongen
Magnetic boundary
Strike of positive anomaly
Form-line contour of foliations
Strike and dip of foliation / min. streching lineation
Tectonic boundaries
NE-terrane
Magnetic high of Balchenfjella (Berrheia unit)
Distinct magnetic low
Eastern part of SW-terrane
Magn. continuation of central SR-corridor
Western SW-terrane (granulite facies)
Western SW-terrane (greenschist-amph. facies)
TTG-subterrane (magnetic high)
TTG-subterrane (magnetic low)
Granitoid associated with magnetic anomaly

subdomain 'IIb'. During our fieldwork, one location was visited within the subdomain 'IIb' at Verheyefjellet 72.2°S / 23.7°E), revealing corresponding low magnetic susceptibility values $< 0.8 \cdot 10^{-}3$ SI. In the north, the TTG subterrane is confined by the dextral, steeply south-dipping Main Shear Zone MSZ), which coincides with the magnetic boundary '3'. The curvilinear magnetic anomalies of the TTG subterrane apparently swing into the east-trending MSZ, probably as a result of major dextral shear strain within the MSZ. The geologically inferred southern boundary of the TTG subterrane has not been identified by our data set. Hence, we assume that the TTG subterrane continues farther south to boundary '1'. The maximum E-W extension of the TTG subterrane is 130 km.
To the north of the MSZ, grey gneisses with high magnetic susceptibilities up to $55 \cdot 10^{-}3$ SI) are found and most likely cause the elongated magnetic high in the south of domain 'III'. This domain includes the greenschist to granulite facies units of the western SW-terrane, where magnetic anomalies as well as the E-W-trending foliation appear collinear Fig. 6.5). The narrow magnetic low lineament '4') within domain 'III' coincides partly with what was previously considered the Sør Rondane Suture (Shiraishi et al., 2008). Extent, wavelength and amplitude of this narrow magnetic low are conspicuously similar to the narrow low along the Balchen detachment zone within the NE-terrane (lineament '9'). Although the Sør Rondane Suture is not considered to be an important tectonic boundary by some authors (e.g. Osanai et al., 2013), it still has a significant magnetic expression. Higher amplitude anomalies in the northern part of domain 'III' can be correlated with high-grade metamorphic rocks of the SW-terrane.
East of the Gjelbreen lineament (Fig. 6.3; boundary '6'), the magnetic pattern changes abruptly to a diffuse and small amplitude pattern, without a dominant strike direction. Here, the tectonic structures appear complex and large-scale refolding is documented (Toyoshima et al., 2013). It is probably because of the large-scale refolding that no continuous, elongated magnetic anomalies are developed. There is a hint that this diffuse, small amplitude pattern continues to the north and it is speculative, whether this vague N-S trending belt of subdued anomalies may be related to large-scale extensional tectonics, separating the NE- and SW-terranes in a western and an eastern portion respectively. The magnetic data reveal a southern boundary ('1') of the SW-terrane, which is located south of the mountain range and is accompanied by WNW-ESE striking elongated magnetic highs. We interpret this southwestern-most domain ('I') of the survey area as part of the prominent SE-DML province. Mieth and Jokat (2014) interpret this large mag-

netic province as an orogenic belt of unknown age, but inferred the structures to predate Pan-African ages (∼650-520 Ma). A few nunataks of the southwestern-most SRM are located within the SE-DML province (Fig. 6.5), some of which were visited during the Belgian expeditions in 1959/60 (Van Autenboer et al., 1964), others during our fieldwork. Both expeditions found a none-TTG basement predominated of metasedimentary rocks, including marbles, paragneisses and graphite schists. Typically, magnetic susceptibility data show very low values (∼0.2 $\cdot 10^{-}3$ SI) on a variety of rock samples. Probably, the general subdued magnetic signature of the SE-DML province (except of the elongated highs) is caused by the predominance of metasedimentary rocks. The elongation of the magnetic anomalies in the SE-DML province correlates with the general foliation trend of the outcrops (Fig. 6.5). The age of the foliation is thus far unresolved. Furthermore, ductilely undeformed granitoids are found within this province (Fig. 6.4). These intrusions are similar in age and chemical composition to the late tectonic intrusions (group II and III) of the SW-terrane of the SRM (Kleinhanns et al., 2013).

6.6.2 Granitic intrusions

Granitoids of various sizes crop out all over the mountain range, but mainly in the SW-terrane, whereas associated mafic dykes have been found only west of the Gjelbreen lineament (Fig. 6.1c, along 24.7°E). The mafic dykes are in their extent too small to be identified and properly mapped by the 5 km flight line spacing. Similarly, some granitoid outcrops of small to moderate size (5 to 10 km) are often not well imaged by our data set. Magnetic susceptibility measurements revealed a broad range from 0.1 to 44 $\cdot 10^{-}3$ SI for samples of the granitoids. The group II intrusions (570 to 560 Ma; Li et al, 2006; Shiraishi et al., 2008) show usually higher susceptibilities above 5 $\cdot 10^{-}3$ SI, whilst most of the group III intrusions (530 to 520 Ma; Li et al., 2006; Shiraishi et al., 2008) show values below $1 \cdot 10^{-}3$ SI with some exceptions (Tab. 6.1). Therefore, it is comprehensible that the granitoids cannot be identified in the magnetic anomaly map at the first glance. Larger granitoids can be identified in the magnetic anomaly map in the western portion of the SW-terrane and one in the eastern NE-terrane (Fig. 6.5), which are all characterised by anomalies between +30 and +80 nT. Forward modelling indicates that this anomaly range could be associated with thicknesses of the intrusions of 1 to 4 km (Tab. 6.2).
Two larger granitoids in the eastern part of the SW-terrane (Fig. 6.1; at Mefjell 72.1°S / 25.2°E and at Bergersenfjella 72.1°S / 26.1°E) could not be correlated with a distinct

magnetic anomaly pattern, which is in accordance with the low magnetic susceptibility ($0.2 \cdot 10^{-}3$ SI) measured at Mefjell, though Tainosho et al. (1992) reported values of 2 to $10 \cdot 10^{-}3$ SI for this granite. The granitoid at Pingvinane (SSE of Perlebandet) show low magnetic susceptibilities ($0.1\text{-}0.2 \cdot 10^{-}3$ SI) as well, but it intruded into highly-magnetic granulite facies rocks, correlated with magnetic anomalies of up to +240 nT. Therefore, the granitoid appears as a zone of low amplitudes (+30 nT).

The most outstanding magnetic anomaly is that measured SW of Dufekfjellet. It is by far the highest value (+680 nT) measured in the SRM. The 2.75-D modelling (Fig. 6.4) indicates that a highly magnetised body either within the granite body or at its rim causes the anomaly.

Magnetic anomalies, similar in both spatial extent and anomaly values, in the vicinity of granitic intrusions have been reported from central DML within the Drygalskiberge and the A. v. Humboldt Gebirge at a slightly lower flight altitude of 2845 m (Damaske et al., 2005). Their origin is thus far unresolved. We speculate that ultra-mafic rocks or gabbro bodies are responsible for these anomalies. Contact metamorphism with ore formation can also not be ruled out. Notably, the granite of Dufekfjellet has not only a conspicuous magnetic signature within the SRM, its crystallization age (620 Ma; Li et al., 2006) is also by far the oldest amongst the voluminous Pan-African granitoids. This would infer that the granite of Dufekfjellet intruded during a different tectonic phase and has probably a different magmatic source. A similar age for a Pan-African intrusion in DML is only reported from the anorthosite complex in the Grubergebirge (600 Ma; Jacobs et al., 1998). A hitherto unknown granitoid was recorded at Tertene nunataks during our fieldwork (Fig. 6.5). These 1800 m high nunataks were crossed at a flight altitude of 3150 m, and a local magnetic maximum of +256 nT had been measured over the southern outcrop. This local maximum corresponds to an elongated high along the boundary ('1') of the SE-DML province (Fig. 6.3). Compared with the other magnetic anomalies over granitic intrusions in the SRM, this magnetic anomaly shows much higher amplitudes, while the magnetic susceptibility of the outcropping granite is in the same range than other intrusions in the SRM (Tab. 6.1). Either this granitoid is much larger in extent and thickness, or the outcropping intrusion is rather thin and underlain by higher magnetised rocks. A more detailed geochemical and mineralogical analysis of this granitoid and of another found at Sarkofagen and Urna (72.2°S / 16.8°E) could reveal the differences or similarities to the granitoids of the SRM. Such a study might be crucial for understanding

the meaning of the elongated parallel anomalies of the SE-DML province and, thereby, for constraining its geodynamic evolution.

6.6.3 Open questions

Although the correlation between geological and geophysical data is reasonably good in large parts of the mountain range, there are areas, where detailed geological investigations as well as additional geophysical research would substantially enhance our understanding of the tectonic evolution of the SRM.

The significance of the central Sør Rondane corridor that apparently separates the SRM into an eastern and western part is not sufficiently well understood. This aeromagnetic domain ('IV') has characteristic low magnetic anomalies and coincides with an area of large-scale refolding (Toyoshima et al., 2013). It also coincides at least in parts with the assumed collision zone between the NE- and SW-terrane (e.g. Osanai et al., 2013). The question, however, is, whether the large-scale refolding is really related to compression tectonics during juxtaposition of the two terranes. Since the MTB does not appear to cross the central Sør Rondane corridor, it could well be of extensional nature and then it would be late-tectonic. A more detailed aeromagnetic survey acquired in an E-W direction across this zone should improve our understanding of the central Sør Rondane corridor. The MTB is exposed at Austkampane, however, very little is known about the kinematics along the MTB. Clearly, a better structural characterisation of the MTB, the central Sør Rondane corridor and its boundaries to the east and west is needed. If the central Sør Rondane corridor is of extensional nature, then the finite juxtaposition of the different granulite facies rocks (e.g. Adachi et al., 2013; Baba et al., 2013; Osanai et al., 2013) could be of extensional rather than compressional nature.

In the west, the aeromagnetic data suggest that Perlebandet could be part of the SW- and not the NE-terrane. A detailed PTt-path for Perlebandet is so far not available. It should therefore be tested, whether these granulite facies rocks really follow a clockwise PTt-path, as typical for the NE-terrane, or rather follow an anticlockwise PTt-path as would be typical for the SW-terrane. The geophysical interpretation that Perlebandet is part of the SW-terrane is supported by the occurrence of the same type of highly magnetic grey gneisses, the significance and origin of which is however not known at present. It should also be investigated whether these grey gneisses are absent from the NE-terrane and are typically found in the SW-terrane only. It should be tested, whether

the two magnetically different parts of the TTG subterrane are exclusively a result of the more calc-alkaline and the more tholeiitic parts of the TTG suite. Whereas, the question why only the SW part of the Balchen detachment has a magnetic significant expression will probably remain unresolved due to limited outcrops at its NE continuation.

6.7 Conclusions

The careful correlation of aeromagnetic data together with susceptibility measurements and structural information allowed a reasonably good correlation of geological and geophysical information, despite a 5 km flight line spacing and the varying distance to top of the bedrock, varying from a few hundred metres to some kilometres. Magnetic susceptibility measurements proved important to link aeromagnetic and outcrop information and to trace and map major tectonic terranes and boundaries into ice-covered areas. The three-fold subdivision of the western SRM into a northern, a central, and the TTG subterrane is relatively well imaged by the aeromagnetic data. The eastern portion of the MTB is also well imaged in our new data. However, our results also reveal certain discrepancies to the hitherto tectonic models, and therefore suggest a refinement and modification of the existing models. The main discrepancies can be summarized as follows. (a) Our data suggest the existence of the central Sør Rondane corridor, which separates the SRM into a western, a central and an eastern part, rather than into a NE- and a SW-terrane. Whilst the eastern portion of the MTB is well imaged with the aerogeophysical data, it does not appear to continue through the Sør Rondane corridor. Therefore, the central Sør Rondane corridor might reflect a late Pan –African tectonic structure, possibly related to extensional tectonics, similar to the Balchen detachment to the east.
(b) The TGG subterrane is magnetically divided into two distinct parts, and its southern boundary is farther south as previously assumed. (c) The interpretation of the western portion of the MTB is ambiguous based on the magnetic data. Its magnetic signal differs from that of the eastern portion of the MTB, which might reflect a significant difference of them in their tectonic relevance. (d) The Sør Rondane Suture, which is no longer considered as an important boundary, can clearly be identified and its magnetic signal is very similar to that of the Balchen detatchment (fault / shear zone).
Furthermore, we can conclude that late to post Pan-African tectonic granitoids show

a significant varying magnetic signal, both in their magnetic susceptibility and in the aeromagnetic data. From a size of >10 km, granitoid bodies can be revealed underneath the ice, if their magnetic susceptibilities sufficiently differ from that of the host rocks. The boundary between the SE-DML province and the SRM could be mapped based on the aeromagnetic data, but its tectonic significance is uncertain. Although metasedimentary rocks have been found at a few outcrops within this province, its age and tectonic evolution remains thus far enigmatic.

6.8 Acknowledgments

We thank the flight and science crews of AWI-Polar aircraft for data acquisition and the visited research station in Dronning Maud Land for logistic support. Particularly, we would like to express our thanks to Alain Hubert and his team at the Belgian Princess Elisabeth station for the wonderful time there and support in the field. Many thanks go also to the crew of Sky Heli, Germany, who took the geological party safely to the field and back to the station. Last-not-least, we wish to thank the entire expedition team for cooperative fieldwork and stimulating discussions. J. Jacobs is indebted to BGR for the invitation to participate at GEA I and II and to AWI for providing polar clothing; support from NFR-NARE, and the Meltzer Fund during a research visit at AWI are gratefully acknowledged. This study was partly supported by the Deutsche Forschungsgemeinschaft (Grant LA1080/9 to A. Läufer) in the framework of the priority programme “Antarctic Research with comparative investigations in Arctic ice areas”.

Chapter 7

Compilation of gravity measurements in Dronning Maud Land

7.1 Introduction

Airborne gravity readings were taken together with magnetic and ice-penetrating radar measurements for most aerogeophysical survey flights of the Alfred-Wegener-Institut Helmholtz-Zentrum für Polar- und Meeresforschung (AWI) in Dronning Maud Land (DML). A major challenge within the scope of this thesis was the proper processing of the aerogravity data, including post-processing of satellite positioning. All aerogravity data acquired by AWI in DML from 2007 to 2013 (Fig. 7.1, red lines) were processed and combined with previously acquired and processed data (Fig. 7.1, blue lines; Riedel et al., 2012). The merged free-air gravity data set has been subjected to a common leveling procedure, resulting in a free-air gravity map of DML. However, by December 2013, the ice-thickness data of the research area are not completely processed by the radar group of AWI. Consequently, a detailed geological discussion of the gravity data in conjunction with the subglacial topography is not possible within this thesis. Nevertheless, the gravity dataset is presented here. A Bouguer anomaly is calculated from it using bedrock topography and ice-thickness information from BEDMAP-2 (Fretwell et al., 2013), allowing some important preliminary interpretations and conclusions based on the geological constraints given in chapters 4.3, 5.3, and 6.3.

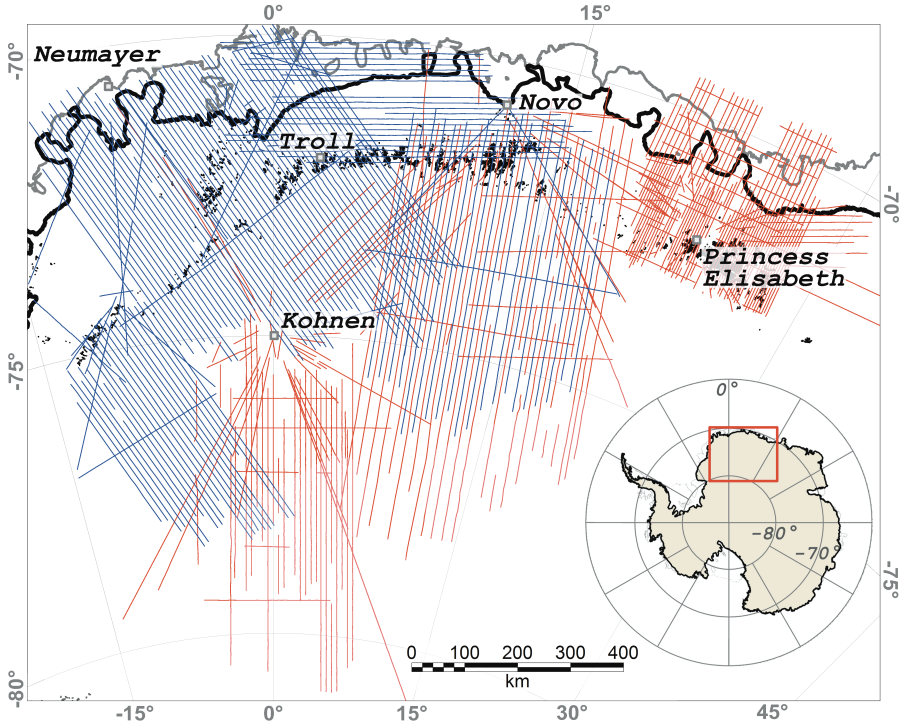

Figure 7.1: Flight lines of useable gravity readings in DML. Red lines: new data, blue lines: previously published data (Riedel et al., 2012). Thick black line marks the grounding line, thick gray line marks the ice shelf edge, squares indicate locations of some research stations, thin black lines and dots represent outcropping rocks. Inset displays the area outline (red box).

7.2 Data processing and acquisition

Useable gravity readings with the ZLS modified LaCoste&Romberg air/sea gravimeter (s56) can only be obtained from sections of straight flights at a constant barometric flight level. AWI obtained more than 120˙000 line kilometers of aerogravity data onshore DML in the period 2001 to 2013. An area of over 1.1 million km^2 was covered with an average line spacing of 10 km (Fig. 7.1). The region at Sør Rondane around Princess Elisabeth station was surveyed at 5 km flight line spacing as part of the Geodynamic Evolution of East Antarctica (GEA) campaign (see chapter 6). The gravimeter was mounted on a gimbal-stabilized platform near the centers of gravity in the AWI aircraft *Polar 2*, *Polar 4* (both Dornier DO-228), *Polar 5*, and *Polar 6* (both Basler BT-67). Base readings were taken before and after each flight with the air/sea gravimeter in the parked aircraft and simultaneously with a LaCoste & Romberg portable land gravimeter on the surface

directly below the aircraft. Readings with the portable land gravimeter were also taken frequently at absolute gravity points research stations Princess Elisabeth (O. Francis, pers. comm.) and Novolazarevskaya (J. Mäkinen, pers. comm.), and the International Gravity Standard Network (IGSN-71) points in Cape Town, in order to tie the relative airborne gravity readings to absolute values.

Data processing comprised positioning post-processing as described in chapter 2.1, Eötvös corrections and corrections for latitude, height, vertical aircraft acceleration and tilt, as well as low pass filtering with a 90 s length (see chapter 2.3). Leveling, gridding, and Gaussian regional filtering with 15 km filter length were carried out using Geosoft Oasis Montaj software. Cross-point errors were reduced from 15.5 ± 14.8 mGal to 5.8 ± 5.7 mGal by applying a careful leveling procedure based on the random line leveling technique described in chapter 2.2.3. The leveling procedure clearly reduced the visual anomaly artefacts along flight lines (Fig. 7.2).

The same Gaussian regional filter as for the free-air gravity was applied to the bedrock topography and ice thickness of BEDMAP-2 data before calculating a preliminary Bouguer anomaly to avoid introducing artificial high frequency signals. Terrain and curvature (Bullard B) corrections have not been calculated owing to the absence of suitable input parameters from ice-penetrating radar data, which are yet to be fully processed. Because of this, it is only appropriate to analyze regional lithospheric aspects here.

7.3 Results

The free-air gravity field (Fig. 7.2b) primarily reflects topographic effects. The mountain ranges of DML (up to 3000 m above sea level) cause strong anomalies of +100 to +170 mGal, while the Jutulstraumen graben, which reaches depths of -1600 m, results in negative anomalies of –20 to -90 mGal. The region at the continental margin departs prominently from this general correlation. Here, free-air gravity values range between +80 and +150 mGal along the entire coast, forming a prominent and almost continuous anomaly in spite of bedrock elevations that are consistently in the range of 100 to 500 m below sea level.

Low pass filtering of the airborne-derived free-air anomaly field with a 150 km filter length provides a resulting field with strong similarity to the satellite-derived free-air anomaly field of the GOCO03s model (Fig. 7.3). The GOCO03s model is derived from

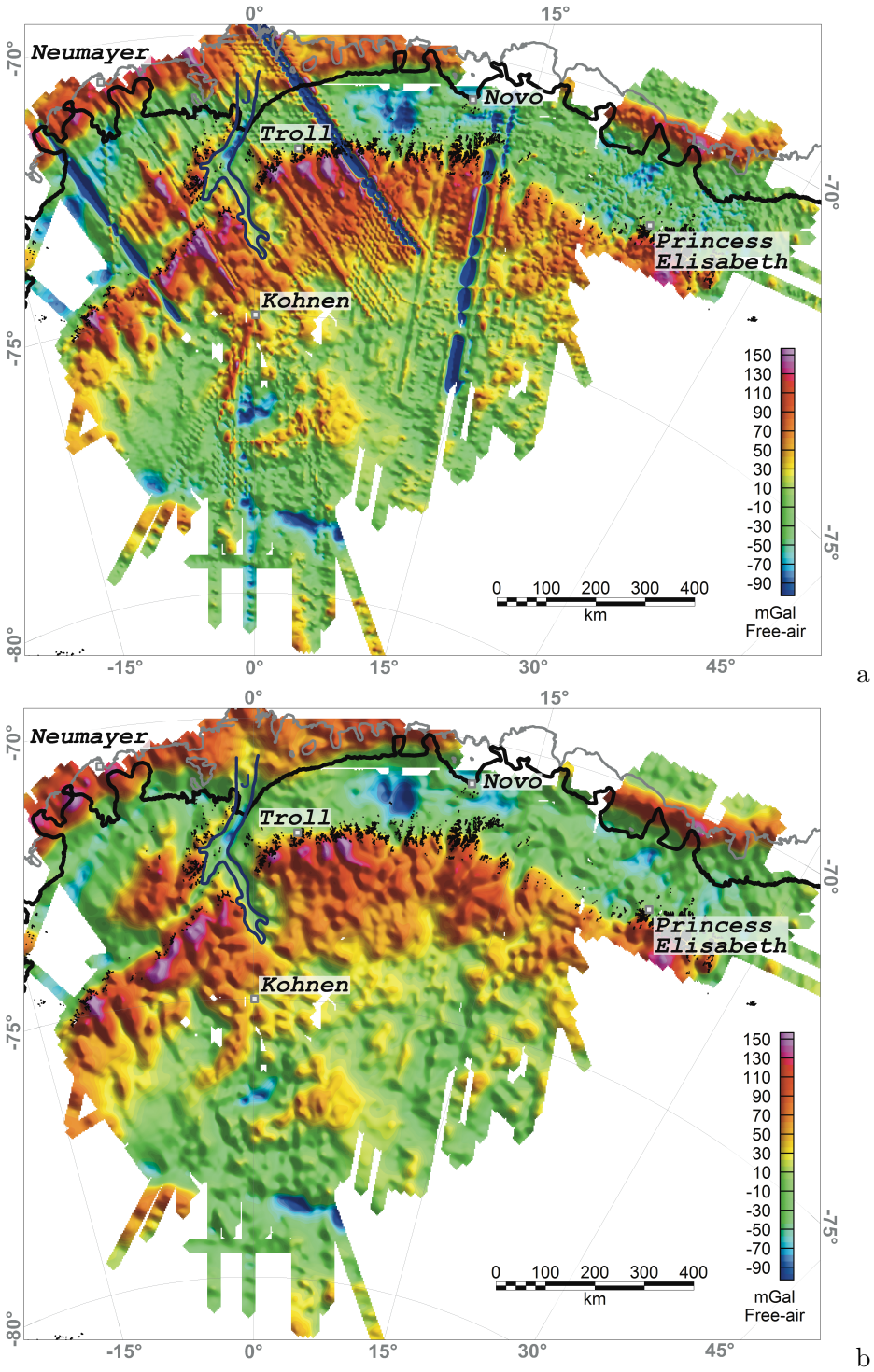

Figure 7.2: Free-air gravity of DML: (a) processed data before leveling, (b) processed data after gentle leveling and regional Gaussian low pass filtering with 15 km filter length. Outline of the area is given in Fig. 7.1-inset. Abbreviation: J – Jutulstraumen graben.

a combination of long period satellite observations by the Gravity Recovery And Climate Experiment (GRACE; 7.5 years), Gravity field and steady-state Ocean Circulation Explorer (GOCE; 1.5 years), CHAllenging Minisatellite Payload (CHAMP; 8 years) and Satellite Laser Ranging (SLR; 5 years) from five satellites (Mayer-Guerr et al., 2012). It is an advancement of the GOCO01s (Pail et al., 2010) and GOCO02s (Goiginger et al., 2011) models, which are based on complementary data series. The correlation coefficient is 0.92 between the airborne and satellite free-air anomaly fields and a mean difference of 11.5 mGal is observed by a standard deviation of 12.0 mGal.

A Bouguer anomaly was calculated based on the ice-thickness and bedrock information of BEDMAP-2 (Fretwell et al., 2013) in order to account for topographic effects in the free-air gravity. BEDMAP-2 data coverage is very sparse in the south, which can be seen by the exceptionally smooth surface. These areas are marked by the white transparent overlay in Figs. 7.4 and 7.5. As well as anomalies associated with named features such as the Grunehogna Craton and Jutulstraumen graben, the Bouguer map reveals four major regional anomalies (Fig. 7.4c, 'I-IV'), which are analyzed and discussed here.

Area 'I' is situated in eastern DML, to the south of the Wohlthatmassiv and Sør Rondane Mountains. It covers an area of 240˙000 km^2, and is characterized by negative amplitudes between -200 and –120 mGal that decrease eastwards.

Area 'II' is separated from area 'I', lying more than 100 km WSW of it, and forms a nearly circular anomaly with a radius of ∼50 km. The anomaly is one of pronounced negative Bouguer values in the range of -195 to -140 mGal.

Area 'III' is much larger, irregularly shaped, and situated at the SW edge of the DML Bouguer anomaly map. It is dominated by higher anomaly values of -70 to +80 mGal.

Area 'IV' is a distinct area of negative Bouguer anomalies in the range –190 to –120 mGal, and is confined to the Sør Rondane Mountains. A lack of data between areas 'I' and 'IV' leaves open the possibility that the two anomalies might be contiguous. Similar lows (-190 to –150 mGal) are evident east of ∼6°E, within the eastern portion of the central DML mountain range at the Mühlig-Hoffmann Gebirge, Wohlthatmassiv, and between the Wohlthatmassiv and Sør Rondane Mountains. West of ∼6°E, in contrast, Bouguer anomalies occupy a higher range between –150 and -70 mGal.

The Archaean Grunehogna craton (Fig.7.4c, 'G') is characterized by moderate Bouguer anomaly values of -110 to +80 mGal, the Jutulstraumen graben (Fig. 7.4c, 'J') with values between -40 to +120 mGal, and the highest Bouguer anomaly values (+90 to +200

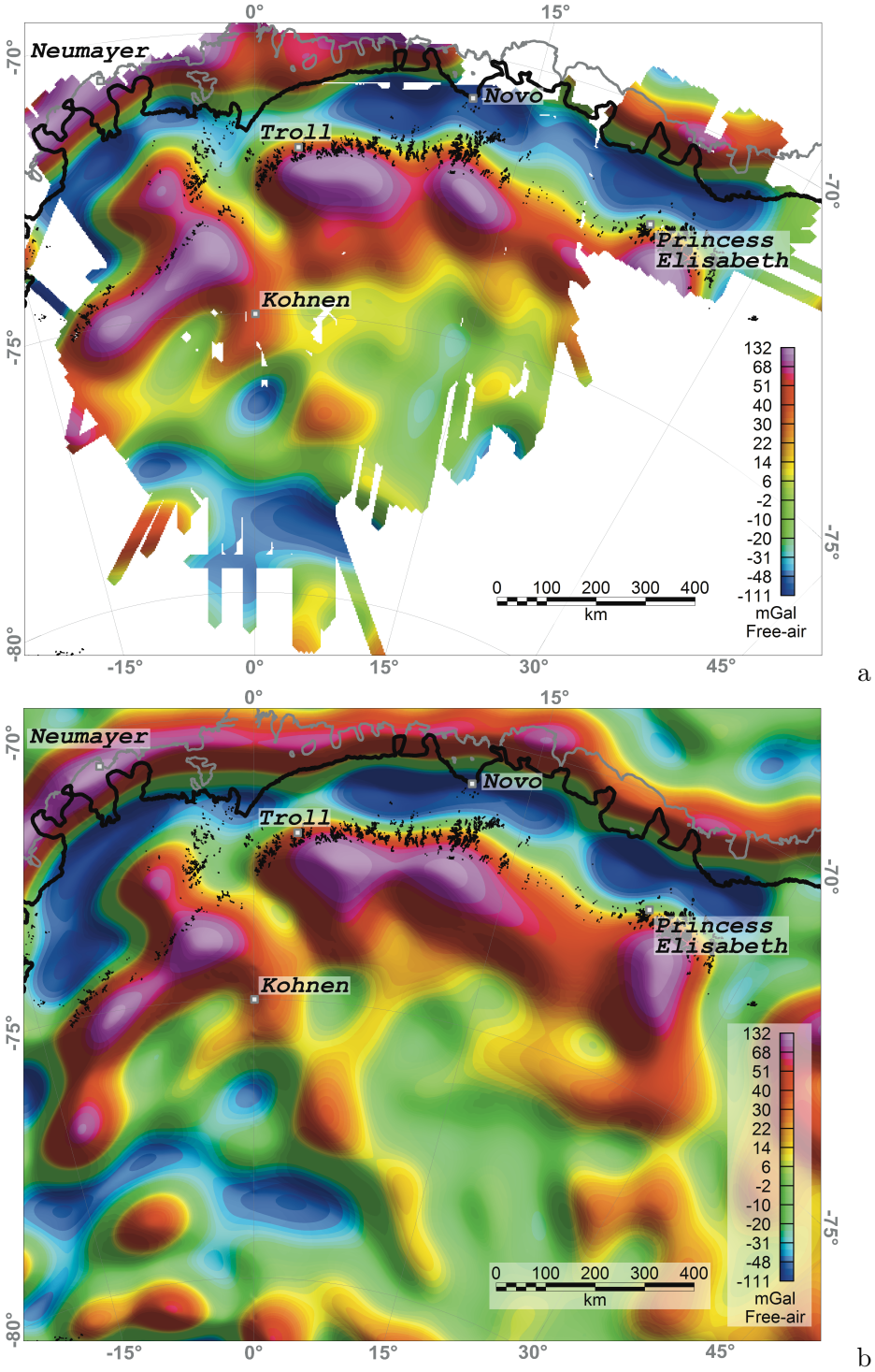

Figure 7.3: Comparison of free-air and satellite gravity in DML: (a)low pass filtered free-air gravity with 150 km filter length, DC-shift of -11.5 mGal applied, (b) satellite gravity of GOCO-03s model (Mayer-Guerr et al., 2012). Outline of the area is given in Fig. 7.1-inset.

mGal) are to be found along the continental margin just north of DML coast.
There is no discrete free-air or Bouguer gravity anomaly to correlate with the Forster Magnetic Anomaly south of the central DML mountains (Fig. 7.4c, 'F'). Here, instead, the Bouguer anomaly increases from ENE to WSW in the range -140 to -60 mGal.

Over large regions, isostatic compensation leads to thicker crust below regions of higher elevation and vice versa. This is the reason for the negative correlation between topography and Bouguer anomaly that can be observed world wide (Long and Kaufmann, 2013). To demonstrate this correlation in DML, the topographic effects of the lower-density ice and water layers must be accounted for. For this, the thicknesses of water and ice are converted to rock equivalent layers of identical masses assuming densities of 2670 kg/m^3 for upper crustal rocks, 1025 kg/m^3 for water, and 915 kg/m^3 for ice. These layers are then added to the bedrock elevation, with negative sign for layers below sea level. The resulting product is known as rock equivalent topography (RET; Fig. 7.5a). The correlation of RET with the Bouguer anomaly at each grid point is shown in Fig. 7.5b. The correlation is, as expected, an inverse one with an overall slope of -0.0625 mGal/m$_{RET}$, and secondary facets of -0.3 mGal/m$_{RET}$ over ±700 m$_{RET}$ and -0.016 mGal/m$_{RET}$ between 90 and 140 mGal and RET of -1500 to -400 m$_{RET}$.
The Bouguer anomaly is corrected by the main correlation function (-0.0625 mGal/m$_{RET}$) as shown in (Fig. 7.5c) in order to recognize and map areas where the Bouguer anomaly deviates from the main correlation with RET. Six prominent areas of such a deviation are identified (Fig. 7.5c, 'a-f'). Areas 'a', 'b', and 'd' are negative, with the lowest values for the nearly circular area 'b' (–125 mGal$_{trend\ corr}$). Areas 'c' and 'e' show moderate positive values (+30 to +80 mGal$_{trend\ corr}$), and area 'f' is recognizable as an intense high (+150 to +200 mGal$_{trend\ corr}$).

7.4 Interpretations and discussion

The free-air gravity anomaly is the processed result of direct airborne measurements and should be examined thoroughly before interpretation of any subsequently calculated product. However, due to its strong correlation with topography, a calculation of the Bouguer anomaly is mandatory for a sound geological interpretation. Positive Bouguer anomalies correspond to rocks of density above average, while negative anomalies correspond to density below the average. Thus, Bouguer anomalies reflect variations in

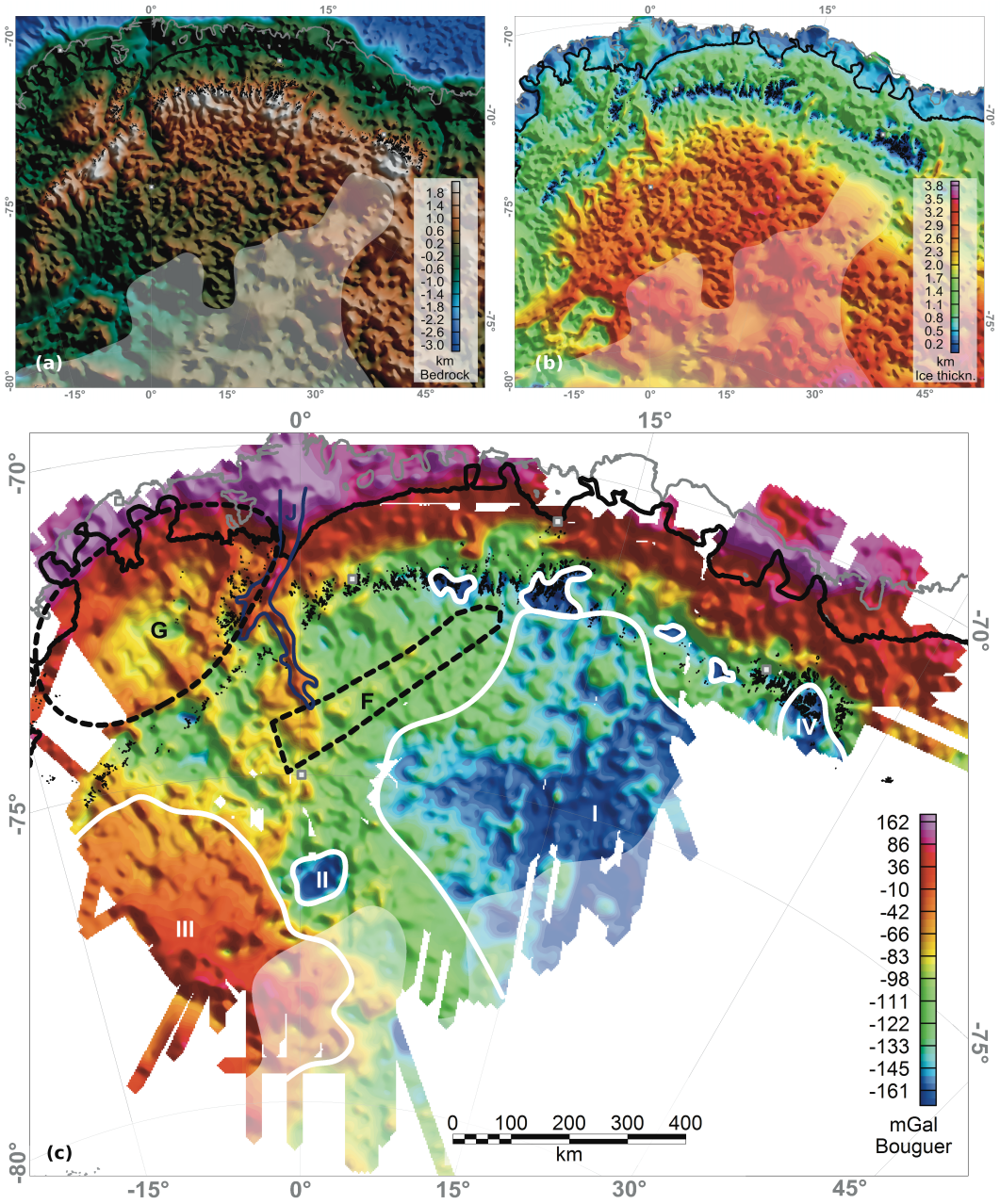

Figure 7.4: Bouguer anomaly of DML: (a) bedrock topography, (b) ice thickness, (c) calculated Bouguer anomaly without terrain correction. Outline of the area is given in Fig. 7.1-inset. Bedrock topography and ice thickness maps are derived from BEDMAP2 datasets (Fretwell et al., 2013), with regional Gaussian low pass filter of 15 km filter length applied, whereas areas of insufficient data coverage is marked by a semi-transparent white layer. Abbreviations: G - Grunehogna craton, F - Forster Magnetic Anomaly (Riedel et al., 2013; Mieth and Jokat, 2014), J – Jutulstraumen graben, 'I-IV' - here analyzed and discussed anomaly areas.

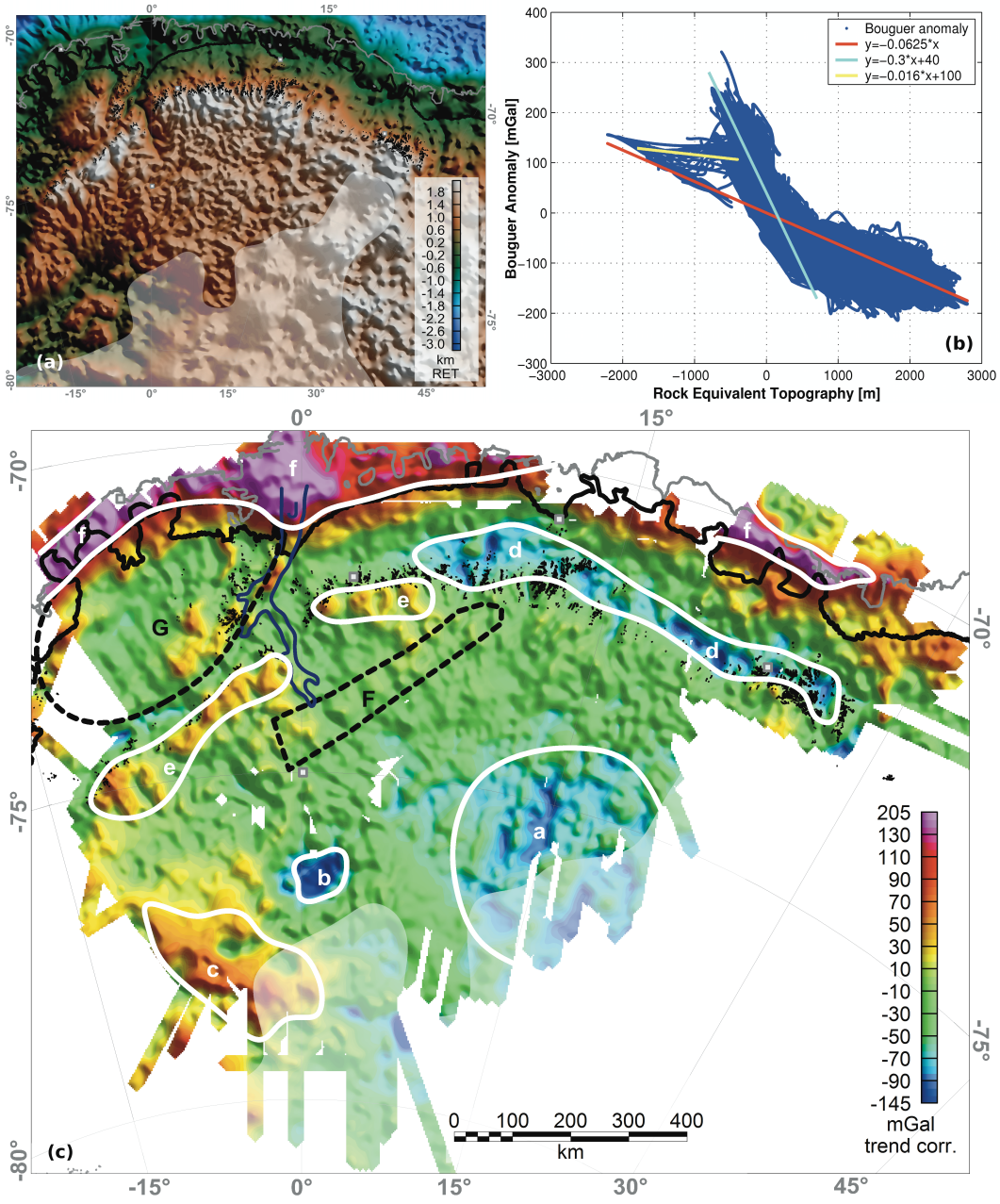

Figure 7.5: Trend corrected Bouguer anomaly of DML: (a) rock equivalent topography (RET), ice (density of 915 kg/m^3) and water (density of 1025 kg/m^3) layers are converted into a rock density (2670 kg/m^3) equivalent-mass layer and added to the bedrock topography, with negative sign for layers below sea level, (b) Bouguer anomaly vs. RET, with trend estimations, (c) Bouguer anomaly corrected by the main correlation trend of Bouguer anomaly and RET (-0.0625 mGal/m$_{RET}$). Outline of the area is given in Fig. 7.1-inset. Abbreviations: G - Grunehogna craton, F - Forster Magnetic Anomaly (Riedel et al., 2013; Mieth and Jokat, 2014), J – Jutulstraumen graben, 'a-f': anomalies with respect to the main correlation of Bouguer anomaly and RET, as discussed in the text.

isostatically-compensated crustal thickness. Large negative anomalies correspond to the presence of low-density roots of thick continental crust displacing the denser rocks of the upper mantle, as the density of continental crust is much lower than the density of the displaced upper mantle.

A subdivision into coastal, southwestern, and southeastern regions can be made by the first glance at the Bouguer anomaly field (Fig.7.4c). The southeastern region (area 'I') coincides with the prominent magnetic southeastern DML province (Mieth and Jokat, 2014), reinforcing its interpretation as a distinct tectonic terrane. Riedel et al. (2012) calculated that the low Bouguer anomaly indicates that this terrane exists in a relatively thick crust of approximately 40 to 50 km. The negative trend-corrected Bouguer anomaly in Fig.7.5c ('a') supports a similar interpretation, but may alternatively be related to the presence of thick sediment layers or an even thicker flexurally-supported crust. The location of the free-air and Bouguer anomaly signatures of the southeastern DML province at the survey's edge, like its magnetic anomaly pattern (see Fig. 4.4, in chapter 4), permit the interpretation that the southeastern DML province represents the NW part of a much larger tectonic terrane, possibly a large mobile belt of yet unknown age (Mieth and Jokat, 2014).

Area 'II' forms the most conspicuous Bouguer anomaly in southern DML (Fig.7.5c, 'II'). The strongly negative values are similar to those of the eastern part of the southeastern DML province (area 'I'), but are disconnected from it by ∼100 km. The free-air anomaly of this region shows a clear negative anomaly, which is also present in satellite gravity compilations. Despite the gravity low, the BEDMAP-2 bedrock topography does not reveal a physiographic basin, and this is the reason for the feature's appearance as negative Bouguer and trend-corrected Bouguer anomalies (Fig.7.5c, 'b'). The simplest explanation for this prominent anomaly would be the usage of incorrect bedrock topography data. A bedrock topography error of ∼700m would explain the anomaly in area 'II'. This possibility should be tested as soon as results of the ice-penetrating radar measurements are available.

If, on the other hand, the topography is accurate and the Bouguer anomaly is therefore real, it can be interpreted as the signature of a small but ∼4.5 km deep sediment-filled basin, by an assumed average density of 2400 kg/m^3 for sediments. As outlined above, basins that are formed by crustal thinning tend to exhibit regional positive Bouguer anomalies. In addition, they tend to be elongated features because they form in regional

stress fields related to plate boundary forces. The circular form of this apparent DML basin and its strong negative Bouguer anomaly suggest instead an upper crustal feature formed by processes other than crustal strain. Both the area and the Bouguer anomaly are too large to represent a sediment-filled crater of a typical volcano or breccia pipe. Only a very large meteorite impact would be reasonable to assume. Notably, a large circular positive magnetic anomaly is observed near the northwestern edge of area 'II' (see Fig. 4.5, anomaly 'C1') and strong magnetic anomalies can be a feature of impact structures, where they indicate the presence of impact suevites – rocks formed by shock melting (Elbra et al., 2009).

The gravity anomalies of southeastern DML differ from those of southwestern DML, where Bouguer anomalies are considerably higher (Fig.7.4c, 'III'), indicating substantially thinner crust. Riedel et al. (2012) calculated a crustal thickness between 37 and 39 km for the northern part of anomaly area 'III' and an even thinner crust can be assumed for its southern part. The trend-corrected Bouguer anomaly (Fig.7.5c, 'c') indicates a greater crustal density in the southwestern part of area 'III'. This very obvious difference between the gravity anomalies of southwestern and southeastern DML mirrors the conclusions based on the regional aeromagnetic observations (see chapter 4). Magnetic anomalies in southwestern DML are much larger in extent and amplitude than those of southeastern DML. Based on the magnetic and gravity result, it can be assumed that layers of sediments, which typically have a lower density and weak magnetization, are thinner or absent between the ice and the crystalline basement in southwestern DML.

The prominent Bouguer anomaly low in the Sør Rondane Mountains of eastern DML (Fig.7.4c, 'IV') might be continuous with the Bouguer anomaly low of southeastern DML (anomaly area 'I'). However, area 'IV' coincides exactly with the magnetic central Sør Rondane corridor that does not form part of the magnetic southeastern DML province (Fig. 6.3 ('IV') and Fig. 6.5). From outcrop studies, the corridor is known to be characterized by large-scale refolding and complex tectonic structures (Toyoshima et al., 2013). The Bouguer anomaly low suggests the central Sør Rondane corridor is formed over a thick crust with sharp eastern and western boundaries at the Main Tectonic Boundary (Osanai et al., 2013) and Gjelbreen lineament (Fig. 6.5). Other distinct Bouguer anomaly lows of similar extent and amplitude are to be found in the eastern portion of the DML mountain ranges at the Mühlig-Hofmann Gebirge, Wohlthatmassiv, and between the Wohlthatmassiv and the Sør Rondane Mountains. Riedel et al. (2012)

concluded that a mountain root must be present underneath the Wohlthatmassiv but that the crust is not in isostatic equilibrium there, consistent with GPS registered topographic uplift. Based on the trend-corrected Bouguer anomaly, it can be seen that the crust of the entire eastern portion of the DML mountain range is either thicker than average or of lower than usual density (Fig.7.5c, 'd'). The consequence of the former would be an ongoing uplift of the entire eastern portion. Further west, however, the western portion of the DML mountain range shows positive trend-corrected Bouguer anomalies (Fig.7.5c, 'e') that indicate thinner crust or greater than average crustal densities. Thus, it can be concluded that there is a difference in the tectonic structures of the eastern and western portions of the DML mountains, effective across a boundary at ∼6°E, east of the Jokulkyrkja Mountain in the Mühlig-Hofmann Gebirge. Such a tectonic difference remains to be identified in surface geological investigations of the region (J. Jacobs, pers. comm.).

The strong positive free-air and Bouguer anomalies along the continental margin mark the transition zone between continental and oceanic crust. This region shows a noticeably different trend between Bouguer anomaly and RET (-0.3 mGal/m$_{RET}$) and reaches therefore the highest trend corrected Bouguer anomaly values (Fig.7.5c, 'f'). The interpreted continent-ocean transition zone is also characterized by magnetic highs (Figs. 4.3 and 6.3 ('VII'), in chapters 4 and 6). Both remarkable aerogeophysical anomalies are interpreted as the signatures of strongly-magnetized and dense mafic rocks, which intruded into the transition zone during Gondwana rifting in Jurassic times (Golynsky et al., 1996; Leitchenkov et al., 2008; Mieth and Jokat, 2014; Riedel et al., 2012, 2013). The very shallow Bouguer/RET correlation slope of -0.016 mGal/m$_{RET}$ pertains for areas north of the continental margin gravity high, where the Bouguer anomaly range between +90 and +140 mGal and the RET between -1500 and -400 m$_{RET}$. Given its location, these anomaly areas most likely represent the onset of oceanic crust.

Chapter 8

Conclusions

Systematic airborne geophysical surveys conducted by the Alfred-Wegener-Institut Helmholtz-Zentrum für Polar- und Meeresforschung (AWI) over the last decades have covered a significant part of Dronning Maud Land (DML) in East Antarctica. This thesis describes how more than 60˙000 line kilometers of new aerogeophysical data were acquired, processed, combined with previously published data, and interpreted as the signals of tectonic structures, terranes, and their boundaries. Several new structures are discovered in this subset of new data and provide constraints, which will contribute to unravel the geodynamic evolution of East Antarctica. One of the most important findings of this work is the southeastern DML province - an aerogeophysically-prominent and distinct region. The province's magnetic and gravity signatures differ clearly from those of central, western, and southwestern DML. Consequently, the southeastern DML province is interpreted to represent a distinct tectonic terrane. This province is characterized by a subdued magnetic anomaly field with elongated and parallel positive anomalies, which are truncated in the northwest by the Forster Magnetic Anomaly, flanked by the complex magnetic anomaly pattern of the Sør Rondane Mountains in the northeast, and is presumed to continue eastwards. Pronounced negative Bouguer anomaly values indicate continental crust of up to 50 km thickness in this region (Riedel et al., 2012) in contrast to the thinner crust according to considerably higher Bouguer anomaly values in western and southwestern DML. A few nunataks crop out within the northern portion of the southeastern DML province between the Wohlthatmassiv and the Sør Rondane Mountains. Recently (in 2011 and 2012) collected rock samples from these nunataks and nearby moraines show a predominance of metasedimentary rocks whose age is yet to be

determined. Furthermore, undeformed post- or late-tectonic granitoids have been found within the northern portion of the southeastern DML province. These findings supplement the hypotheses that East Antarctica is rather composed of a mosaic of Archaean cratonic nucleii encircled by Proterozoic to Palaeozoic mobile belts (Boger, 2011) than mainly of a single stable craton. Furthermore, the hypotheses of a continuous suture zone connecting the Shackleton Range south of Coats Land in the west to the Lützow Holm Bay region in the east (Moyes et al., 1993; Shiraishi et al., 1994; Grunow et al., 1996; Shackleton, 1996; Jacobs et al., 1998; Boger and Miller, 2004; Kleinschmidt and Boger, 2009) has to be revised, as the aerogeophysical data provide no evidence of for such a scenario.

Another prominent crustal element in the study area is the BLM craton (named after the nunataks Bertrab, Littlewood, and Moltke) in Coats Land west of DML and northeast of the Shackleton range (Studinger and Miller, 1999; Golynsky and Aleshkova, 2000; Kleinschmidt, 2002; Kleinschmidt and Boger, 2009; Loewy et al., 2011). In this thesis, the eastern and southern boundary of the BLM craton is completely mapped. The compiled data indicate that its magnetic anomaly pattern is unique in DML and even compared to the formerly-adjacent parts of southern Africa. This result will be very helpful to identify a conjugate piercing point of the BLM craton in a yet-to-be-identified conjugate province, for reconstruction of the supercontinent Rodinia (1100–800 Ma) or an older supercontinent.

Although the much younger history of Gondwana break-up in Jurassic times is constrained significantly better, it is not completely understood yet. The locations of continental blocks bearing the Falkland Islands and Maurice Ewing Bank are controversial topics in recent Gondwana reconstruction models (König and Jokat, 2006; Leinweber and Jokat, 2012). These blocks are assumed to have been located somewhere between southern Africa and western DML during the lifetime of the supercontinent Gondwana (∼650-200 Ma). Their locations might be better constrained by tracing a presumed continuation of the South African Beattie Magnetic Anomaly (Corner, 1989) across them into western DML. Two magnetic highs northeast of the BLM craton have been identified as such a supposable continuation of the Beattie Magnetic Anomaly.

Another prominent magnetic high in DML that has been correlated with a magnetic anomaly feature in southern Africa is the Giæver Magnetic Anomaly at the Giæverryggen in western DML. This strong magnetic anomaly, located within the Archaean

Grunehogna craton, was investigated and analyzed in more detail within the scope of this thesis. The results revealed similarities to the magnetic anomaly pattern of the Mhlapitsi fold belt near Polokwane (former Pietersburg) in South Africa, where a folded layer of banded iron formation at an unusually-high structural level causes a strong magnetic anomaly (Beukes, 1983 and references therein; M. Watkeys, pers. comm.). Such an interpretation as source body appears more plausible, given its location within the Archaean craton and the high value for the estimated minimum magnetic susceptibility, rather than as Jurassic mafic intrusions as previously assumed (Golynsky and Aleshkova, 2000; Riedel et al., 2013). However, the bedrock surface is covered by approximately one kilometer of ice and, thus, direct geological sampling is not possible. Land-based geophysical investigations are needed in order to verify the new interpretation of a folded near-surface banded iron formation as the source of the Giæver Magnetic Anomaly.

The airborne geophysical program of the Geodynamic Evolution of East Antarctica (GEA) campaign was successfully completed over three consecutive austral summer seasons between January 2011 and December 2012. The analysis of the aeromagnetic anomaly data, ground-based magnetic susceptibility measurements, and structural information from the outcropping rocks provides a reasonably good correlation of geological and geophysical information. Magnetic susceptibility measurements at outcropping rock sites proved important to link aeromagnetic and geological data in order to trace and map major tectonic terranes and boundaries into ice-covered areas. The aeromagnetic data broadly supports the three-fold subdivision of the western Sør Rondane Mountains, and facilitated mapping of the eastern portion of the Main Tectonic Boundary. The results also suggest refinements to existing tectonic models (Shiraishi et al., 2008; Grantham et al., 2013; Ishikawa et al., 2013; Osanai et al., 2013). Of greatest importance and interest for future investigation is the detection of the central Sør Rondane corridor as a distinct aerogeophysical domain. Airborne gravity data show that the Sør Rondane corridor is characterized by a prominent Bouguer anomaly low, which indicates a thick crust and underlines the significance of the eastern Main Tectonic Boundary and Gjelbreen fault as important structural boundaries.

Detailed analysis of the prominent magnetic high near Dufekfjellet in the Sør Rondane Mountains and magnetic susceptibility measurements at the granitoid outcrop in its vicinity showed that the high must be caused by a strongly magnetized source body either within or at the rim of the granitoid, as all investigated granites show much lower

values of magnetic susceptibility in the Sør Rondane region as it would be necessary for a rock formation to cause this strong magnetic anomaly. This finding is in agreement with that of Damaske et al. (2005) for magnetic highs observed near granitic intrusions in the central DML mountain range. Furthermore, the aeromagnetic data of the GEA campaign revealed that the magnetic anomaly pattern of the southeastern DML province continues eastwards into the southern Sør Rondane region and allow to presume that its subdued magnetic anomaly pattern is caused by a predominance of metasedimentary rocks.

The western boundary of the southeastern DML province lies southeast of Kohnen station. Both the magnetic and gravity anomaly patterns change here. The subdued magnetic anomaly field with elongated short wavelength anomalies is replaced by stronger long-wavelength magnetic anomalies, and the gravity data indicate a decrease in crustal thickness from east to west. Approximately 200 km south of Kohnen station, a conspicuous Bouguer anomaly low and nearby magnetic high are detected, but their origin remains enigmatic. The Bouguer anomaly low is, compared with its rock equivalent topography, outstanding in DML. A thorough (re-)evaluation of the ice-penetrating radar data will reveal whether this prominent feature is an artifact of inaccurate bedrock-depth data, or the signal of a more significant geological structure.

Both the Kohnen lineament southwest of Kohnen station and the Forster Magnetic Anomaly between Kohnen station and the Wohlthatmassiv are aeromagnetic anomaly features only. Corresponding aerogravity anomalies could not be detected, although both anomalies are interpreted to represent important tectonic structures of the Pan-African amalgamation of Gondwana (650-520 Ma). This indicates that both structures are not linked with any significant change in crustal thickness, supporting the theory of a post- to late-tectonic delamination of the orogenic root. In this thesis, the Forster Magnetic Anomaly is interpreted to represent the suture zone of the collision between southern Africa and the southeastern DML province, while the Kohnen linement is interpreted to represent a main shear zone caused by escape tectonics similar to the Heimefront shear zone. However, these interpretations cannot be directly verified as both anomaly features the Forster Magnetic Anomaly and the Kohnen lineament are completely covered by ice and require further detailed geophysical investigations.

The gravity data indicate that the continental crust is thinner in the southwest than beneath the southeastern DML province, central and western DML, and the Grunehogna

craton. Consequently, it can be suggested here that a distinct geophysical southwestern DML province exists beside the southeastern DML province. This southwestern DML province is characterized by moderate negative to positive Bouguer anomaly values and several long wavelength magnetic highs, suggesting a shallow crystalline basement and only a thin or no sediment cover.

This synopsis of the main results, interpretations, and conclusion documents how all main objectives of this thesis (see chapter 1.3) were addressed and that several scientific questions were answered. Furthermore, as a result of this work many new and interesting questions can now be posed about the newly-identified tectonic structures, boundaries, and terranes and their formation in the general context of the geodynamic evolution of DML; such as: Where is the eastern boundary of the southeastern DML province located, what is the age of the rocks that forms its prominent magnetic anomaly pattern, and of what nature is the boundary to the Sør Rondane Mountains? What tectonic kinematics have been involved in the formation of the central Sør Rondane corridor? What is most likely the highly magnetized source of the magnetic high near Dufekfjellet and similar highs near granitoids in central DML? What is the reason for the observed gravity differences east and west of ∼6°E in central DML? Is the Giæver Magnetic Anomaly accompanied by a localized gravity anomaly and can the hypotheses of banded iron formation as source be confirmed? What is causing the magnetic highs south of Kohnen and what structures do we find farther south? Does the Kohnen lineament represents the eastern boundary of the East African-Antarctic Orogen in southern DML?

The fundamental aerogeophysical surveying and mapping of crustal structure of East Antarctica in general and DML in particular is, however, not complete with this thesis. Some suggestions for future investigations are given in the next chapter. The compilation of the AWI magnetic data set in DML (chapter 4) has been submitted to the Antarctic Digital Magnetic Anomaly Project 2 (ADMAP-2) working group, in order to contribute to a larger, more informative, and more complete picture of the magnetic anomaly field of Antarctica, and to invite researchers world wide to analyze the data themselves, possibly combine them with their own datasets, and to study and broaden the fundamental knowledge of the tectonic structures of the lithosphere and their geodynamic evolution.

Chapter 9

Outlook

The nature of science includes that by addressing and answering scientific questions new questions inevitably arise and demand further investigation. This study is no exception, especially with its character of fundamental geophysical surveying and mapping of potential field signals of the almost-completely ice-covered bedrock of the Antarctic interior. This outlook gives some suggestions for future research and enterprises with the potential to further extend the findings and to test the interpretations and conclusions of this study.

9.1 Detailed analysis of the aerogravity data

The preliminary analysis of airborne gravity data given in chapter 7 is very basic and focused on regional aspects. A profound study of the processed and compiled aerogravity data of DML is to be carried out in the near future and will reveal important information about the thickness, structure, composition, and segmentation of the crust in DML. For this purpose, the complete Bouguer anomaly must be modeled as soon as the complementary ice-penetrating radar data have been thoroughly evaluated in the study area. Crustal thickness can then be estimated from gravity inversion, guided by independent spot or line measurements of crustal thickness that have been made using receiver function studies and deep seismic sounding experiments (see Riedel et al., 2012 and references therein).

Furthermore, in a number of areas small-scale gravity anomalies should be investigated in detail and correlated with aeromagnetic anomaly features and ground-based geological

findings. Following the results and findings of this thesis, special foci should be put on the Sør Rondane region (in particular the central Sør Rondane corridor, the Main Shear Zone and the Main Tectonic Boundary), the Forster Magnetic Anomaly in central DML, the Kohnen lineament in southern DML, the conspicuous gravity low 200 km south of Kohnen, and the contrast of crustal fabric between the eastern and western portions of the central DML mountain range along ∼6°E. In addition, the gravity data will potentially provide valuable information about the crustal structure and geodynamic evolution of southwestern DML.

9.2 Eastward continuation of the southeastern Dronning Maud Land province

One of the most interesting scientific questions for future aerogeophysical investigation in DML is the assumed eastward continuation of the southeastern DML province and identification of its eastern boundary. For this purpose, two suitable and feasible flight line patterns are calculated for future campaigns starting from the Belgian Antarctic summer research station Princess Elisabeth (Fig. 9.1, blue and red lines). The calculated

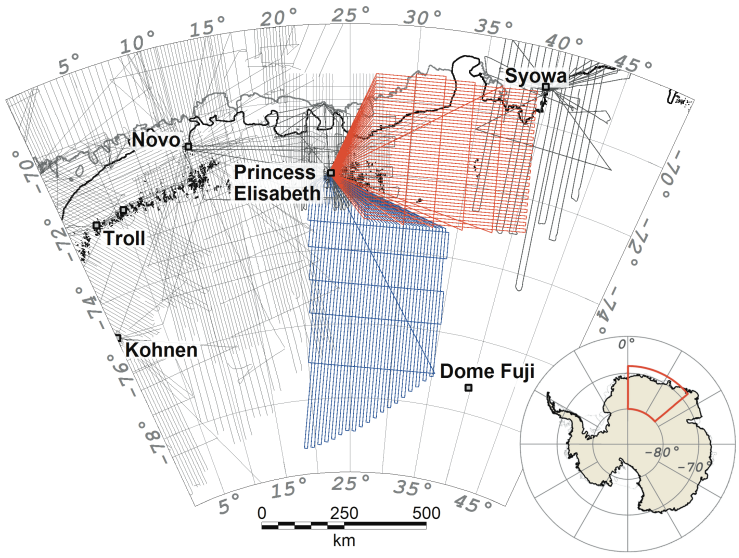

Figure 9.1: Planned airborne geophysical surveys of eastern Dronning Maud Land in upcoming field seasons: thin red lines - flight lines of an E-W oriented survey, thin blue lines - flight lines of an N-S oriented survey, thin gray line - completed aerogeophysical measurement flights, thick black line - grounding line, thick gray line - ice shelf edge. Inset displays the map outline (red polygon).

distance for each flight matches the flight range of *Polar 5* or *Polar 6* when configured for geophysical surveying. The red survey will investigate the coastal range and outcropping mountains between Princess Elisabeth and Syowa stations using an E-W oriented flight pattern at a flight line spacing of 10 km and tie line spacing of 90 km. These 25 flights will return up to 34˙600 line kilometers of new data and survey a total area of 240˙000 km^2. This survey will require approximately 72˙000 liters of fuel. The blue survey will investigate the region south of the Sør Rondane Mountains as far south as possible in a N-S pattern with a flight line spacing of 10 km and tie line spacing of ∼100 km. The blue survey will cover a total area of 260˙000 km^2 in 22 flights with a total distance of 36˙600 km, requiring approximately 78˙000 liters of fuel. In Fig. 9.1 it can been seen that the N-S flights in the east are shorter than the N-S flights in the west, owing to the long transit segments from Princess Elisabeth station. A fuel depot and a temporary base camp would be required somewhere half way between the Japanese all-year station Syowa and their summer station at Dome Fuji (Fig. 9.1) for surveying the region between 35°E and 50°E and south of 73°S.

9.3 Detailed airborne magnetic survey in central Dronning Maud Land

Analysis of the aeromagnetic data of the GEA campaign in the Sør Rondane region has shown that magnetic anomalies can be correlated with surface geology reasonably well for a survey design with a flight line spacing of 5 km. This combination permits tracing and mapping of important tectonic structures, boundaries, and terranes in ice-covered areas. With similar goals in mind, it is suggested here to carry out an infill survey over the western portion of the central DML mountain range (Fig. 9.2a, thick white polygon) in order to reduce the flight line spacing of the region's existing aerogeophysical data (Fig. 9.2a, thin black lines) from 10 to 5 km. The resulting data set would be well suited to be combined with the magnetic data of the 1995/96 GeoMaud expedition over the eastern portion of the central DML mountain range, which were acquired with a towed bird below a helicopter in a flight line spacing of 4.4 km at a barometric flight altitude of 2845 m (Damaske et al., 2005).

This infill survey should extend as far south as to entirely cover the Forster Magnetic Anomaly, which this thesis has revealed to reflect a major tectonic structure, possibly the

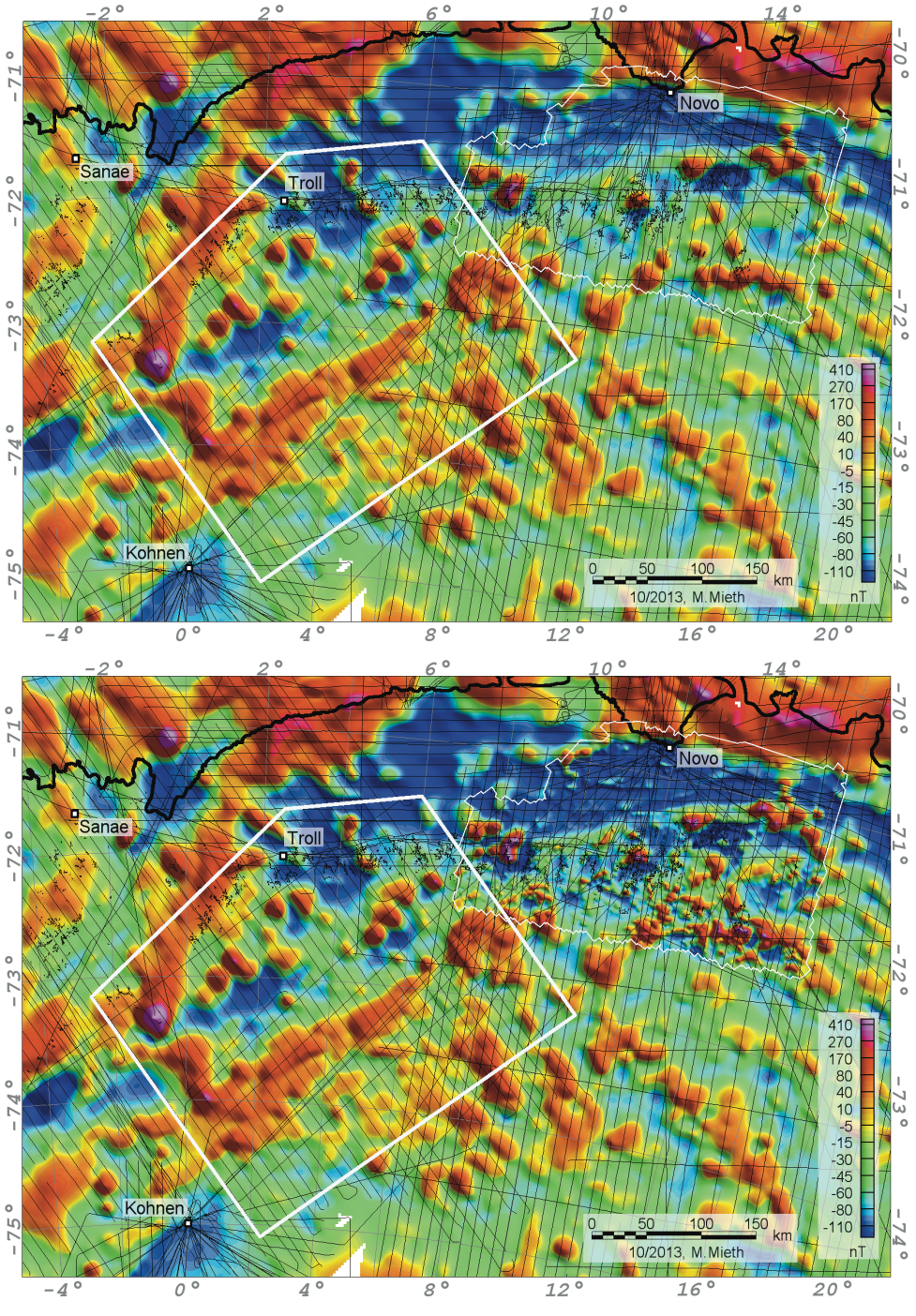

Figure 9.2: Suggested area of interest for detailed magnetic study in western central DML: (a) suggested area of interest (thick white polygon) plotted on compilation map of AWI magnetic dataset of DML (Mieth and Jokat, 2014), (b) adjusted GeoMaud magnetic dataset within thin white polygon (Damaske et al., 2005) superimposed on map (a).

suture zone between the Maud belt in central DML and the southeastern DML province. Furthermore, such an investigation might reveal more details about the observed gravity differences between the eastern and western portions of the central DML mountain range as highlighted in chapter 7.
The flight activity should be carried out from the Norwegian all-year research station Troll. It would require approximately 28˙000 liters of fuel for 8 flights, during which a flight distance of 13˙000 km would be covered in total. The prospective improvement to the magnetic anomaly pattern can be seen in the comparison of Fig. 9.2a and Fig. 9.2b. The latter shows the adjusted magnetic anomaly data of the GeoMaud expedition (shifted by +55 nT in order to match the AWI magnetic data compilation of DML) superimposed within the thin white polygon at the eastern portion of the central DML mountain range.

9.4 Land-based gravity survey across the Giæver Magnetic Anomaly

The favored interpretation for the source of the localized magnetic high at the Giæverryggen is an unusually shallow folded layer of banded iron formation (see chapter 5). However, only maximum depth and minimum magnetic susceptibility could be unambiguously calculated from the magnetic measurements at two different flight levels. The aerogravity data have not revealed an indication of an accompanying gravitational anomaly, which might be due to the coarse (∼7 km) spatial resolution of aerogravity data acquired by the ZLS modified LaCoste&Romberg air/sea gravimeter system at a acquisition speed of 75 m/s. However, a land-based survey across the completely ice-covered area of the Giæver Magnetic Anomaly might detect an accompanying localized gravity anomaly. AWI's ground-based EKSEIS campaign aims to reach this region early 2014. This campaign will traverse from Neumayer-III along the Ekström ice shelf, to the Giæverryggen, and back along the Halvfarryggen to Neumayer-III, collecting seismic reflection data with a towed snow streamer and seismic vibrator as source. The target of the measurements is the ice itself, but reflections from subglacial rock layers will be recorded as well and might reveal at least the top of the Giæver Magnetic Anomaly source. Planned locations for accompanying land-based gravity readings are displayed in Fig. 9.3 consisting of a dense local survey (short yellow lines) and longer lines coinciding with the seismic sounding

profiles (long yellow lines). As part of EKSEIS campaign it is also planned that magnetic data will be recorded constantly along the seismic sounding profiles, and if possible along with the local gravity survey. A magnetic anomaly value of ∼2400 nT is estimated for the maximum of the Giæver Magnetic Anomaly at ice surface elevation (∼1030 m a.s.l.) based on the calculation for a spherical source body (see Fig. 2.11b). The recorded deviation from this value will provide information about the real source geometry and its depth. With the combination of land-based seismic, gravity, and magnetic data it will presumably be possible to distinguish between the hypotheses of an Archaean banded iron formation source and a Jurassic intrusive source.

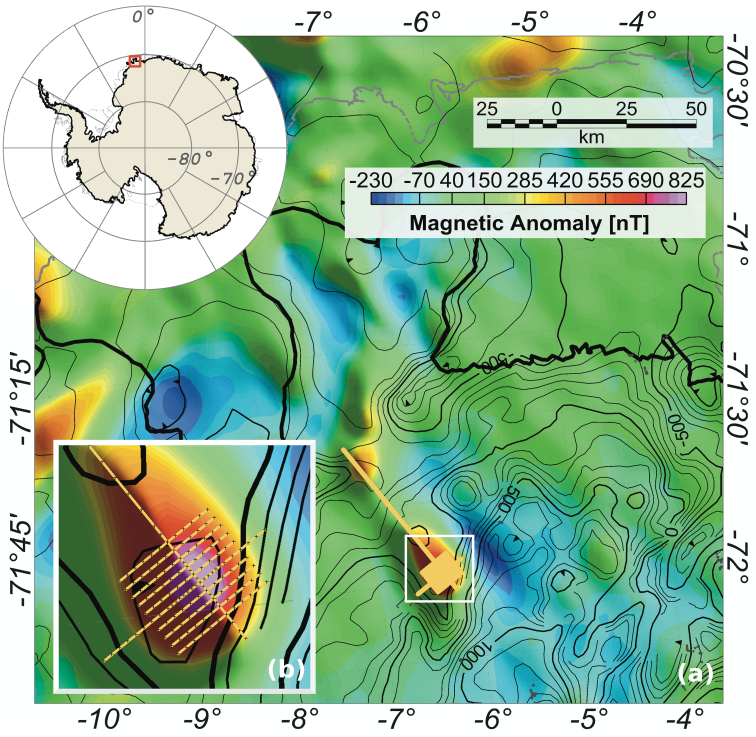

Figure 9.3: Planned land based gravity profiles (yellow lines) at Giæverryggen in western Dronning Maud Land: (a) Magnetic anomaly map reduced-to-the-pole (see chapter 5) overlain by contour lines of bedrock topography (Fig. 5.1c). Inset shows outline (red box) of map (a). White box indicates zoom area (b).

Bibliography

Adachi, T., Osanai, Y., Hokada, T., Nakano, N., Baba, S., and Toyoshima, T., 2013. Timing of metamorphism in the central Sør Rondane Mountains, eastern Dronning Maud Land, East Antarctica: constrains from SHRIMP zircon dating and EPMA monazite dating, *Precambrian Research*, **234**, 136–160. http://dx.doi.org/10.1016/j.precamres.2012.11.011.

Arndt, J., Schenke, H., Jakobsson, M. andNitsche, F., Buys, G., Goleby, B., Rebesco, M., Bohoyo, F., Hong, J., Black, J., Greku, R., Udintsev, G., Barrios, F., Reynoso-Peralta, W., Morishita, T., and Wigley, R., 2013. The International Bathymetric Chart of the Southern Ocean (IBCSO) Version 1.0 - A new bathymetric compilation covering circum-Antarctic waters, *Geophysical Research Letters*, **40**, 3111–3117. http://dx.doi.org/10.1002/grl.50413.

Asami, M., Osanai, Y., Shiraishi, K., and Makimoto, H., 1992. Metamorphic evolution of the Sør Rondane Mountains, East Antarctica, *In: Yoshida, Y., Kaminuma, K., Shiraishi, K. (Eds.), Recent Progress in Antarctic Earth Science, TERRAPUB, Tokyo*, p. 7–15. http://www.terrapub.co.jp/e-library/aes/pdf/RP0007.PDF.

Asami, M., Suzuki, K., and Adachi, M., 1996. Monazite ages by the chemical Th–U–total Pb isochron method for pelitic gneisses from the eastern Sør Rondane Mountains, East Antarctica, *Proceedings of the NIPR Symposium on Antarctic Geosciences*, **9**, 49–64.

Asami, M., Suzuki, K., and Adachi, M., 1997. Th, U and Pb data and CHIME dating of monazites from metamorphic rocks of the Rayner, Lützow-Holm, Yamato-Belgica and Sør Rondane Complexes, East Antarctica, *Proceedings of the NIPR Symposium on Antarctic Geosciences*, **10**, 130–152.

Asami, M., Suzuki, K., and Grew, E., 2005. Monazite and Zircon Dating by the

Chemical Th–U–Total Pb Isochron Method (CHIME) from Alasheyev Bight to the Sør Rondane Mountains, East Antarctica: A Reconnaissance Study of the Mozambique Suture in Eastern Queen Maud Land, *Journal of Geology*, **113**, 59–82. http://dx.doi.org/10.1086/425969.

Baba, S., Osanai, Y., Nakano, N., Owada, M., Hokada, T., Horie, K., Adachi, T., and Toyoshima, T., 2013. Counterclockwise P–T path and isobaric cooling of metapelites from Brattnipene, Sør Rondane Mountains, East Antarctica: Implications for a tectonothermal event at the proto-Gondwana margin, *Precambrian Research*, **234**, 210–228. http://dx.doi.org/10.1016/j.precamres.2012.10.002.

Beukes, N., 1983. Paleoenvironmental setting of iron-formations in the depositional basin of the Transversal Supergroup, South Africa, *In: Iron-Formation: Facts and Problems, edited by Trendall, A. F., Morris, R. C. Developments in Precambrian Geology*, **6**, 131–209.

Boebel, T., 2000. Flugzeuggestützte Topographie- und Schweremessungen: Messsystem und Anwendung auf die Region Framstrasse, Spitzbergen und Nordostgrönland, *Berichte zur Polar- und Meeresforschung, Universität Bremen, Bremen*, **366**. http://epic.awi.de/26546/1/BerPolarforsch2000366.pdf.

Boger, S., 2011. Antarctica - before and after Gondwana, *Gondwana Research*, **19 (2)**, 335–371. http://dx.doi.org/10.1016/j.gr.2010.09.003.

Boger, S. and Miller, J., 2004. Terminal suturing of Gondwana and the onset of the Ross–Delamerian Orogeny: the cause and effect of an Early Cambrian reconfiguration of plate motions, *Earth and Planetary Science Letters*, **219**, 35–48. http://dx.doi.org/10.1016/S0012-821X(03)00692-7.

Boger, S., Carson, C., Wilson, C., and Fanning, C., 2000. Neoproterozoic deformation in the Radok Lake region of the northern Prince Charles Mountains, East Antarctica: evidence for a single protracted orogenic event, *Precambrian Research*, **104**, 1–24. http://dx.doi.org/10.1016/S0301-9268(00)00079-6.

Choy, S. L., 2009. An investigation into the accuracy of single frequency PPP, *Doctoral Thesis, School of Mathematical and Geospatial Sciences, RMIT University, Melbourne, Australia*. http://researchbank.rmit.edu.au/view/rmit:6635.

Clarkson, P., Tessensohn, F., Thomson, J., et al., 1995. Geological map of the Shackleton Range, Antarctica, *Cambridge, British Antarctic Survey, GEOMAP series, sheet 4*, pp. 57–60.

Corner, B., 1989. The Beattie anomaly and its significance for crustal evolution within the Gondwana framework, *Extended Abstracts, South African Geophysical Association, First Technical Meeting*, pp. 15–17.

Damaske, D. and McLean, M. A., 2005. An aerogeophysical survey south of the Prince Charles Mountains, East Antarctica, *Terra Antarctica*, **12**, 87– 98.

Damaske, D., Marcinkowski, V., and Möller, H. D., 2005. Aeromagnetic Survey in Central Dronning Maud Land, East Antarctica, during the 1995/1996 GeoMaud Expedition: Layout, Execution, and Data Processing, *Bundesanstalt für Geowissenschaften und Rohstoffe, Geologisches Jahrbuch*, **97 (B)**, 53–83.

Elbra, T., Kontny, A., and Pesonen, L., 2009. Rock-magnetic properties of the ICDP-USGS Eyreville core, Chesapeake Bay impact structure, Virginia USA, *Geological Society of America Special Papers*, **458**, 119–135. http://dx.doi.org/10.1130/2009.2458(06).

Farr, T., Rosen, P., Caro, E., Crippen, R., Duren, R., Hensley, S., Kobrick, M., Paller, M., Rodriguez, E., Roth, L., Seal, D., Shaffer, S., Shimada, J., Umland, J., Werner, M., Oskin, M., Burbank, D., and Alsdorf, D., 2007. The Shuttle Radar Topography Mission, *Reviews of Geophysics*, **45**, RG2004. http://dx.doi.org/10.1029/2005RG000183.

Fedi, M. and Florio, G., 2001. Detection of potential fields source boundaries by enhanced horizontal derivative method, *Geophysical Prospecting*, **49**, 40–58. http://dx.doi.org/10.1046/j.1365-2478.2001.00235.x.

Ferraccioli, F., Gambetta, M., and Bozzo, E., 1998. Microlevelling procedures applied to regional aeromagnetic data: an example from the Transantarctic Mountains (Antarctica)., *Geophysical Prospecting*, **46 (2)**, 177–196. http://dx.doi.org/10.1046/j.1365-2478.1998.00080.x.

Ferraccioli, F., Jones, P. C., Curtis, M. L., Leat, P. T., and Riley, T. R., 2005a. Tectonic and magmatic patterns in the Jutulstraumen rift(?) region, East Antarctica, as

imaged by high-resolution aeromagnetic data, *Earth Planets and Space*, **57**, 767–780. http://svr4.terrapub.co.jp/journals/EPS/pdf/2005/5708/57080767.pdf.

Ferraccioli, F., Jones, P. C., Curtis, M. L., and Leat, P. T., 2005b. Subglacial imprints of early Gondwana break-up as identified from high resolution aerogeophysical data over western Dronning Maud Land, East Antarctica, *Terra Nova*, **17 (6)**, 573–579. http://dx.doi.org/10.1111/j.1365-3121.2005.00651.x.

Ferraccioli, F., Finn, C. A., Jordan, T. A., Bell, R. E., Anderson, L. M., and Damaske, D., 2011. East Antarctic rifting triggers uplift of the Gamburtsev Mountains, *Nature*, **479**, 388–392. http://dx.doi.org/10.1038/nature10566.

Fretwell, P., Pritchard, H. D., Vaughan, D. G., Bamber, J. L., Barrand, N. E., Bell, R., Bianchi, C., Bingham, R. G., Blankenship, D. D., Casassa, G., Catania, G., Callens, D., Conway, H., Cook, A. J., Corr, H. F. J., Damaske, D., Damm, V., Ferraccioli, F., Forsberg, R., Fujita, S., Gim, Y., Gogineni, P., Griggs, J. A., Hindmarsh, R. C. A., Holmlund, P., Holt, J. W., Jacobel, R. W., Jenkins, A., Jokat, W., Jordan, T., King, E. C., Kohler, J., Krabill, W., Riger-Kusk, M., Langley, K. A., Leitchenkov, G., Leuschen, C., Luyendyk, B. P., Matsuoka, K., Mouginot, J., Nitsche, F. O., Nogi, Y., Nost, O. A., Popov, S. V., Rignot, E., Rippin, D. M., Rivera, A., Roberts, J., Ross, N., Siegert, M. J., Smith, A. M., Steinhage, D., Studinger, M., Sun, B., Tinto, B. K., Welch, B. C., Wilson, D., Young, D. A., Xiangbin, C., and Zirizzotti, A., 2013. Bedmap2: improved ice bed, surface and thickness datasets for Antarctica, *The Cryosphere*, **7**, 375–393. http://dx.doi.org/10.5194/tc-7-375-2013.

Gao, Y. and Chen, K., 2004. Performance analysis of Precise Point Positioning using Rea-Time orbit and clock products, *Journal of Global Positioning Systems*, **3 (1-2)**, 95–100. http://www.gnss.com.au/JoGPS/v3n12/v3n12p14.pdf.

Giæver, J., 1954. The white desert. The official account of the Norwegian-British-Swedish Antarctic Expedition, *Chatto and Windus, London*.

Goiginger, H., Rieser, D., Mayer-Guerr, T., Pail, R., Fecher, T., Gruber, T., Albertella, A., Maier, A., Höck, E., Krauss, S., Hausleitner, W., Baur, O., Jäggi, A., Meyer, U., Brockmann, J., Schuh, W.-D., Krasbutter, I., and Kusche, J., 2011. The combined satellite-only global gravity field model GOCO02S, *Euro-*

pean Geosciences Union General Assembly 2011, Wien, 04.04.2011, presentation. http://www.goco.eu/data/egu2011-10571-goco02s.pdf.

Golynsky, A., Masalov, V., and Jokat, W., 2000. Magnetic Anomaly Map of the Weddell Sea Region: a New Compilation of the Russian Data, *Polarforschung*, **67 (3)**, 125–132. http://epic.awi.de/28405/1/Polarforsch1997_3_4.pdf.

Golynsky, A. V., 2007. Magnetic anomalies in East Antarctica and surrounding regions: a window on major tectonic provinces and their boundaries, *In Proceedings of the 10th ISAES, edited by Cooper, A. K., and Raymond, C. R., et al.: USGS Open-File Report 2007-1047, Short Research Paper 006*. http://dx.doi.org/10.3133/of2007-1047.srp006.

Golynsky, A. V. and Aleshkova, N. D., 2000. Regional magnetic anomalies of the Weddell Sea Region and their geological significance, *Polarforschung*, **67**, 101–117. http://epic.awi.de/28403/1/Polarforsch1997_3_2.pdf.

Golynsky, A. V. and Jacobs, J., 2001. Grenville-age versus Pan-African magnetic anomaly imprints in western Dronning Maud Land, East Antarctica, *Journal of Geology*, **109 (1)**, 136–142. http://dx.doi.org/10.1086/317964.

Golynsky, A. V., Masolov, V. N., Nogi, Y., Shibuya, K., Tarlowsky, C., and Wellman, P., 1996. Magnetic anomalies of Precambrian terranes of the East Antarctic Shield coastal region (20°E–50°E), *Proceedings of the National Institute of Polar Research Symposium on Antarctic Geosciences*, **9**, 24– 39. http://www.researchgate.net/publication/233884090_Magnetic_anomalies_of_Precambrian_terranes_of_the_East_Antarctic_Shield_coastal_region_(20E-50E)/file/d912f50c8ab5978409.pdf.

Golynsky, A. V., Alyavdin, S. V., Masolov, V. N., Tscherinov, A. S., and Volnukhin, V. S., 2002. The composite magnetic anomaly map of the East Antarctic, *Tectonophysics*, **347 (1–3)**, 109–120. http://dx.doi.org/10.1016/S0040-1951(01)00240-2.

Golynsky, A. V., Masolov, V. N., Volnukhin, V. S., and Golynsky, D. A., 2006. Crustal Provinces of the Prince Charles Mountains Region and Surrounding Areas in the Light of Aeromagnetic Data, *In: Antarctica: Contributions to Global Earth Sciences (IX ISAES Proceedings), edited by Fütterer, D. et al., Springer*, p. 83– 94. http://dx.doi.org/10.1007/3-540-32934-X_10.

Golynsky, A. V., Blankenship, D., Chiappini, M., Damaske, D., Ferraccioli, F., Finn, C., Golynsky, D., Goncharov, A., Ishihara, T., Ivanov, S., Jokat, W., Kim, H. R., König, M., Masolov, V., Nogi, Y., Sand, M., Studinger, M., von Frese, R., and the ADMAP Working Group, 2007. New magnetic anomaly map of East Antarctica and surrounding regions, *In Proceedings of the 10th ISAES, edited by Cooper, A.K., and Raymond, C. R., et al.: USGS Open-File Report 2007-1047, Short Research Paper 005*. http://dx.doi.org/10.3133/of2007.srp050.

Gose, W. A., Helper, M. A., Conelly, J. N., Hutson, F. E., and Dalziel, I. W. D., 1997. Paleomagnetic data and U-Pb isotopic age determinations from Coats Land, Antarctica: Implications for late Proterozoic plate reconstructions, *Journal of Geophysical Research*, **102 (B4)**, 7887–7902. http://dx.doi.org/10.1029/96JB03595.

Grantham, G., Macey, P., Horie, K., Kawakami, T., Ishikawa, M., Satish-Kumar, M., Tsuchiya, N., Graser, P., and Azevedo, S., 2013. Comparison of the metamorphic history of the Monapo Complex, northern Mozambique and Balchenfjella and Austhameren areas, Sør Rondane, Antarctica: Implications for the Kuunga Orogeny and the amalgamation of N and S. Gondwana, *Precambrian Research*, **234**, 85–135. http://dx.doi.org/10.1016/j.precamres.2012.11.012.

Grantham, G. H. and Hunter, D. R., 1991. The timing and nature of faulting and jointing adjacent to the Pencksokket, western Dronning Maud Land, Antarctica, *In: Thomson, M.R.A., Crame, J.A., Thomsan, J.A., (eds), Geological Evolution of Antarctica*, pp. 47–51.

Grosch, E. G., Bisnath, A., Frimmel, H. E., and Board, W. S., 2007. Geochemestry and tectonic setting of mafic rocks in western Dronning Maud Land, East Antarctica: implications for the geodynamic evolution of the Proterozoic Maud Belt, *Geological Society London*, **164**, 465–475. http://dx.doi.org/10.1144/0016-76492005-152.

Grunow, A., Hanson, R., and Wilson, T., 1996. Were aspects of Pan-African deformation linked to Iapetus opening?, *Geology*, **24**, 1063–1066. http://dx.doi.org/10.1130/0091-7613(1996)024<1063:WAOPAD>2.3.CO;2.

Halpern, M., 1970. Rubidium-strontium date of possible three billion years for a granite rock from Antarctica, *Science*, **169**, 977–978. http://dx.doi.org/10.1126/science.169.3949.977.

Hanson, R. E., Martin, M. W., Bowring, S. A., and Munyanyiwa, H., 1998. U-Pb zircon age for the Umkondo dolerites, eastern Zimbabwe: 1.1 Ga large igneous province in southern Africa – East Antarctica and possible Rodinia correlations, *Geology*, **26**, 1143–1146. http://dx.doi.org/10.1130/0091-7613(1998)026<1143:UPZAFT>2.3.CO;2.

Hanson, R. E., Crowley, J. L., Bowring, S. A., Ramezani, J., Gose, W. A., Dalziel, I. W. D., Pancake, J. A., Seidel, E. K., Blenkinsop, T. G., and Mukwakwami, J., 2004. Coeval large-scale magmatism in the Kalahari and Laurentian cratons during Rodinia assembly, *Science*, **304**, 1126–1129. http://dx.doi.org/10.1126/science.1096329.

Harris, C., 1995. Petrogenesis of the Sistfjell syenite complex, Dronning Maud Land: generation of low δ18 O magmas by crustal contamination of rift zone magmas, *Geological Society of South Africa Centennial Geocongress, Extended Abstracts*, **1**, 240–243.

Harris, C., Marsh, J. S., Duncan, A. R., and Erlank, A. J., 1990. The petrogenesis of Kirwan basalts of Dronning Maud Land, Antarctica, *Petrology*, **31**, 341–369. http://dx.doi.org/10.1093/petrology/31.2.341.

Harris, C., Johnstone, W., and Phillips, D., 2002. Petrogenesis of the Mesozoic Sistefjell syenite intrusion, Dronning Maud Land, Antarctica and surrounding low-δ18 O lavas, *South African Journal of Geology*, **105**, 205–226. http://dx.doi.org/10.2113/1050205.

Helferich, S., Läufer, A., Henjes-Kunst, F., and Kleinschmidt, G., 2004. Pan-African events in southern Kirwanveggen (western Dronning Maud Land, Antarctica) – evidence from structural geology and geochronology, *Zeitschrift der deutschen geologischen Gesellschaft*, **154**, 453–468.

Ikeda, Y. and Shiraishi, K., 1998. Petrogenesis of tonalitic rocks from the Sør Rondane Mountains, East Antarctica, *Polar Geoscience*, **11**, 143–153.

International Association of Geomagnetism and Aeronomy, Working Group V-MOD. Participating members: Finlay, C. C., Maus, S., Beggan, C. D., Bondar, T. N., Chambodut, A., Chernova, T. A., Chulliat, A., Golovkov, V. P., Hamilton, B., Hamoudi, M., Holme, R., Hulot, G., Kuang, W., Langlais, B., Lesur, V., Lowes, F. J., Lühr, H., Macmillan, S., Mandea, M., McLean, S., Manoj, C., Menvielle, M., Michaelis, I., Olsen, N., Rauberg, J., Rother, M., Sabaka, T. J., Tangborn, A., Tøffner-Clausen, L.,

Thébault, E., Thomson, A. W. P., Wardinski, I., Wei, Z., and Zvereva, T. I., 2010. International Geomagnetic Reference Field: the eleventh generation, *Geophysical Journal International*, **183**, 1216–1230. http://dx.doi.org/10.1111/j.1365-246X.2010.04804.x.

Ishikawa, M., Kawakami, T., Satish-Kumar, M., Tsuchiya, N., and Grantham, G., 2013. Late Neoproterozoic extensional detachment in eastern Sør Rondane Mountains, East Antarctica: implications for the collapse of the East African Antarctic Orogen, *Precambrian Research*, **234**, 257–278. http://dx.doi.org/10.1016/j.precamres.2013.04.015.

Jacobs, J. and Thomas, R., 2004. Himalayan-type indenter-escape tectonics model for the southern part of the late Neoproterozoic–early Paleozoic East African–Antarctic orogen, *Geology*, **32**, 721–724. http://dx.doi.org/10.1130/G20516.1.

Jacobs, J., Fanning, C., Henjes-Kunst, F., Olesch, M., and Paech, H., 1998. Continuation of the Mozambique belt into East Antarctica: Grenville-age metamorphism and polyphase Pan-African high-grade events in central Dronning Maud Land, *Journal of Geology*, **106**, 385–406. http://dx.doi.org/10.1086/516031.

Jacobs, J., Bauer, W., and Fanning, C., 2003. Late Neoproterozoic/Early Palaeozoic events in central Dronning Maud Land and significance for the southern extension of the East African Orogen into East Antarctica, *Precambrian Research*, **126**, 27–53. http://dx.doi.org/10.1016/S0301-9268(03)00125-6.

Jacobs, J., Damaske, D., Läufer, A., Estrada, S., Jokat, W., Riedel, S., Mieth, M., Ruppel, T., Lucka, A., Ehlburg, M., Clark, C., and Flowerdew, M., 2012. Geodynamic Evolution of East Antarctica, GEA I + II Geological expedition to Sør Rondane and adjacent areas, Eastern Dronning Maud Land, Austral summers 2011/12 and 2011/12, *SCAR Open Science Meeting, Portland (USA), 14 July 2012 - 19 July 2012*.

Jokat, W., Boebel, T., König, M., and Meyer, U., 2003. Timing and geometry of early Gondwana breakup, *Journal of Geophysical Research*, **108 (B9)**, 2428. http://dx.doi.org/10.1029/2002JB001802.

Jones, D., Bates, M., Li, Z., Corner, B., and Hodgkinson, G., 2003. Palaeomagnetic results from the ca. 1130 Ma Borgmassivet intrusions in the Ahlmannryggen region of Dronning Maud Land, Antarctica, and tectonic implications, *Tectonophysics*, **375**, 247–260. http://dx.doi.org/10.1016/S0040-1951(03)00341-X.

Kamei, A., Horieb, K., Owadac, M., Yuharad, M., Nakanoe, N., Osanai, Y., Adachie, T., Haraa, Y., Teraoa, M., Teuchia, S., Shimuraf, T., Tsukadag, K., Hokadab, T., Iwataa, C., Shiraishib, K., Ishizukah, H., and Y., T., 2013. Late Proterozoic juvenile arc metatonalite and adakitic intrusions in the Sør Rondane Mountains, eastern Dronning Maud Land, Antarctica, *Precambrian Research*, **234**, 47–62. http://dx.doi.org/10.1016/j.precamres.2012.09.026.

Kleinhanns, I., Jacobs, J., Engvik, A., Bingen, B., Roland, N., Läufer, A., and Schoenberg, R., 2013. Pan-African granitoid magmatism in central Dronning Maud Land derived from a mantle source, not a lower crustal source: evidence from geochemical and Sr-Nd isotope signatures, *Berichte zur Polar- und Meeresforschung*, **659**, 82–83. http://epic.awi.de/32485/1/BzPM_0569_2013.pdf.

Kleinschmidt, G., 2002. Geology of nunataks of Prinzregent-Luitpold-Land (Coats Land, Antarctica) and their geotectonic importance, *Courier Forschungsinstitut Senckenberg*, **237**, 1–14.

Kleinschmidt, G. and Boger, S. D., 2009. The Bertrab, Littlewood and Moltke Nunataks of Prinz-Regent-Luitpold-Land (Coats Land): enigma of East Antarctic Geology, *Polarforschung*, **78 (3)**, 95–104. http://epic.awi.de/29133/1/Polarforschung_78_3_095-104.pdf.

Kleinschmidt, G., Henjes-Kunst, F., and Tessensohn, F., 2001. Nappe tectonics in the central Shackleton Range, Antarctica, *Zeitschrift der deutschen geologischen Gesellschaft*, **152**, 227–248. http://www.schweizerbart.de/papers/zdgg/detail/152/55329.

Knoper, M., Jackson, C., Harris, P., Ferrar, G., Krynauv, J., Moyes, A., and Harris, C., 1997. Geological maps of the Kirwanveggen, western Dronning Maud Land, East Antarctica, *In: The Antarctic Region: Geological Evolution and Processes, edited by C. A. Ricci, C. A. Terra Antarctica Publication, Siena*, p. 1129–1133.

Kojima, S. and Shiraishi, K., 1986. Note on the geology of the western part of the Sør Rondane Mountains, East Antarctica, *Memoirs of National Institute of Polar Research*, **43**, 116–131. http://ci.nii.ac.jp/naid/110000010154/.

König, M. and Jokat, W., 2006. The Mesozoic breakup of the Weddell Sea, *Journal of Geophysical Research*, **111**, B12102. http://dx.doi.org/10.1029/2005JB004035.

Korhonen, J., Fairhead, J., Hamoudi, M., Hemant, K., Lesur, V., Mandea, M., Maus, S., Purucker, M., Ravat, D., Sazonova, T., and Thébault, E., 2007. Magnetic Anomaly Map of the World, *Map published by Commission for Geological Map of the World, supported by UNESCO, 1st edition. GTK, Helsinki*.

Krynauw, J., 1989. The discovery and significance of sedimentary rocks at Förstefjell, Giaeverryggen, *South African Journal of Antarctic Research*, **19 (1)**, 36–38.

Krynauw, J., D.R., H., and Wilson, A., 1984. A note on the layered intrusions at Annandagstoppane and Juletoppane, western Dronning Maud Land, *South African Journal of Antarctic Research*, **14**, 2–10.

Leinweber, V. T. and Jokat, W., 2012. The Jurassic history of the Africa–Antarctica corridor — new constraints from magnetic data on the conjugate continental margins, *Tectonophysics*, **530**, 87–101. http://dx.doi.org/10.1016/j.tecto.2011.11.008.

Leitchenkov, G., Guseva, J., Gandyukhin, V., Grikurov, G., Kristoffersen, Y., Sand, M., Golynsky, A., and Aleshkova, N., 2008. Crustal structure and tectonic provinces of the Riiser-Larsen Sea area (East Antarctica): results of geophysical studies, *Marine Geophysical Research*, **29 (2)**, 135–158. http://dx.doi.org/10.1007/s11001-008-9051-z.

Leliak, P., 1961. Identification and Evaluation of Magnetic- Field Sources of Magnetic Airborne Detector Equipped Aircraft, *IRE Transactions on Aerospace and Navigational Electronics*, **8**, 95–105. http://dx.doi.org/10.1109/TANE3.1961.4201799.

Li, Z., Du, Z., Yang, S., Chen, H., Song, B., and Liu, D., 2006. First report of zircon SHRIMP U-Pb dating from the Dufek granite in the Sør Rondane Mountains, East Antarctica, *Journal of Zhejiang University Science*, **A**, 315–319. http://dx.doi.org/10.1631/jzus.2006.AS0315.

Lindeque, A., de Wit, M., Ryberg, T., Weber, M., and Chevallier, L., 2011. Deep crustal profile across the southern Karoo Basin and Beattie Magnetic Anomaly, South Africa: Integrated interpretation with tectonic implications, *South African Journal of Geology*, **114 (3-4)**, 265–292. http://dx.doi.org/10.2113/gssajg.114.3-4.265.

Lindner, H. and Scheibe, R., 1978. Die Berechnung von δg - und δT - Anomalien für regelmäßige homogene Störkörper, *Gerlands Beiträge Geophysik*, **87 (1)**, 29–45.

Loewy, S. L., Dalziel, I. W. D., Pisarevsky, S., Connelly, J. N., Tait, J., Hanson, R. E., and Bullen, D., 2011. Coats Land crustal block, East Antarctica: A tectonic tracer for Laurentia?, *Geology*, **39**, 859–862. http://dx.doi.org/10.1130/G32029.1.

Long, L. and Kaufmann, R., 2013. Acquisition and Analysis of Terrestrial Gravity Data, *Cambridge University Press*.

Luttinen, A., Grind, K., Siivola, J., and Räisänen, M., 1994. The mafic igneous rocks of Vestfjella, western Dronning Maud Land, Antarctica, *Antarctic Reports of Finland*, **4**, 12–19.

Luyendyk, A., 1997. Processing of airborne magnetic data, *AGSO Journal of Australian Geology and Geophysics*, **17 (2)**, 31–38.

Marschall, H., Hawkesworth, C., Storey, C., Dhuime, B., Leat, P., Meyer, H., and Tamm-Buckle, S., 2010. The Annandagstoppane Granite, East Antarctica: Evidence for Archaean Intracrustal Recycling in the Kaapvaal-Grunehogna Craton from Zircon O and Hf Isotopes, *Journal of Petrology*, **51 (11)**, 2277–2301. http://dx.doi.org/10.1093/petrology/egq057.

Martin, A. K. and Hartnady, C. J. H., 1986. Plate tectonic development of the South West Indian Ocean: A revised reconstruction of East Antarctica and Africa, *Journal of Geophysical Research*, **91**, 4767–4786. http://dx.doi.org/10.1029/JB091iB05p04767.

Mauring, E.and Beard, L., Kihle, O., and M.A., S., 2002. A comparison of aeromagnetic levelling techniques with an introduction to median levelling, *Geophysical Prospecting*, **50**, 43–54. http://dx.doi.org/10.1046/j.1365-2478.2002.00300.x.

Maus, S., Sazonova, T., Hemant, K., Fairhead, J. D., and Ravat, D., 2007. National Geophysical Data Center candidate for the World Digital Magnetic Anomaly Map, *Geochemistry, Geophysics, Geosystems*, **8**, Q06017. http://dx.doi.org/10.1029/2007GC001643.

Mayer-Guerr, T., Rieser, D., Höck, E., Brockmann, J., Schuh, W.-D., Krasbutter, I., Kusche, J., Maier, A., Krauss, S., Hausleitner, W., Baur, O., Jäggi, A., Meyer, U.,

Prange, L., Pail, R., Fecher, T., and Gruber, T., 2012. The new combined satellite only model GOCO03s, *Symposium on Gravity, Geoid and Height Systems, Venice*. http://www.goco.eu/.

McLean, M., Rawling, T., Betts, P., Phillips, G., and Wilson, C., 2008. Three-dimensional inversion modelling of a Neoproterozoic basin in the southern Prince Charles Mountains, East Antarctica, *Tectonophysics*, **456 (3–4)**, 180–193. http://dx.doi.org/10.1016/j.tecto.2008.04.023.

McLean, M. A., Wilson, C. J. L., Boger, S. D., Betts, P. G., Rawling, T. J., and Damaske, D., 2009. Basement interpretations from airborne magnetic and gravity data over the Lambert Rift region of East Antarctica, *Journal of Geophysical Research*, **114**, B06101. http://dx.doi.org/10.1029/2008JB005650.

Meert, J. G., 2003. A synopsis of events related to the assembly of eastern Gondwana, *Tectonophysics*, **362**, 1–40. http://dx.doi.org/10.1016/S0040-1951(02)00629-7.

Mieth, M. and Jokat, W., 2014. New aeromagnetic view of the geological fabric of southern Dronning Maud Land and Coats Land, East Antarctica, *Gondwana Research*, **25**, 358–367. http://dx.doi.org/10.1016/j.gr.2013.04.003.

Moores, E. M., 1991. Southwest U.S–East Antarctica (SWEAT) connection: A hypothesis, *Geology*, **19**, 425–428. http://dx.doi.org/10.1130/0091-7613(1991)019<0425:SUSEAS>2.3.CO;2.

Moyes, A., Krynauw, J., and Barton, J., 1995. The Age of the Ritscherflya Supergroup and Borgmassivet Intrusions, Dronning Maud Land, Antarctica, *Antarctic Science*, **7 (1)**, 87–97. http://dx.doi.org/10.1017/S0954102095000125.

Moyes, A. B., Barton, J. M., and Groenewald, P. W., 1993. Late Proterozoic to Early Palaeozoic tectonism in Dronning Maud Land, Antarctica: supercontinental fragmentation and amalgamation, *Journal of the Geological Society*, **150**, 833–842. http://dx.doi.org/10.1144/gsjgs.150.5.0833.

Osanai, Y., Shiraishi, K., Takahashi, Y., Ishizuka, H., Tainosho, Y., Tsuchiya, N., Sakiyama, T., and Kodama, S., 1992. Geochemical characteristics of metamorphic rocks from the central Sør Rondane Mountains, East Antarctica, *In: Yoshida, Y.,*

Kaminuma, K., Shiraishi, K. (Eds.), Recent Progress in Antarctic Earth Science. Terra, Tokyo, p. 17–27. http://svr4.terrapub.co.jp/e-library/aes/pdf/RP0017.PDF.

Osanai, Y., Shiraishi, K., Takahashi, Y., Ishizuka, H., Moriwaki, K., Tainosho, Y., Tsuchiya, N., Sakiyama, T., Toyoshima, T., Owada, M., and Kojima, H., 1996. Geological map of Brattnipene, Antarctica, *Antarctic Geological Map Series, Sheet34, Scale 1:50,000. National Institute of Polar Research, Tokyo*.

Osanai, Y., Nogi, Y., Baba, S., Nakano, N., Adachi, T., Hokada, T., Toyoshima, T., Owada, M., Satish-Kumar, M., Kamei, A., and Kitano, I., 2013. Geologic evolution of the Sør Rondane Mountains, East Antarctica: collision tectonics proposed based on metamorphic processes and magnetic anomalies, *Precambrian Research*, **234**, 8–29. http://dx.doi.org/10.1016/j.precamres.2013.05.017.

Otsuji, N., Satish-Kumar, M., Kamei, A., Tsuchiya, N., Kawakami, T., Ishikawa, M., and Grantham, G., 2013. Late-Tonian to early-Cryogenian apparent depositional ages for metacarbonate rocks from the Sør Rondane Mountains, East Antarctica, *Precambrian Research*, **234**, 257–278. http://dx.doi.org/10.1016/j.precamres.2012.10.016.

Owada, M., Kamei, A., Horie, K., Shimura, T., Yuhara, M., Tsukada, K., Osanai, Y., and Baba, S., 2013. Magmatic history and evolution of continental lithosphere of the Sør Rondane Mountains, eastern Dronning Maud Land, East Antarctica, *Precambrian Research*, **234**, 63–84. http://dx.doi.org/10.1016/j.precamres.2013.02.007.

Pail, R., Goiginger, H., Schuh, W.-D., Höck, E., Brockmann, J., Fecher, T., Gruber, T., Mayer-Guerr, T., Kusche, J., Jäggi, A., and Rieser, D., 2010. Combined satellite gravity field model GOCO01S derived from GOCE and GRACE, *Geophysical Research Letters*, **37**, L20314. http://dx.doi.org/10.1029/2010GL044906.

Pasteels, P. and Michot, J., 1970. Uranium-lead radioactive dating and lead isotope study on sphene and K-feldspar in the Sor-Rondane Mountains, Dronning Maud Land, Antarctica, *Eclogae Geologicae Helvetiae*, **53**, 239–254.

Perritt, S. H. and Watkeys, M. K., 2003. Implications of late Pan-African shearing in western Dronning Maud Land, Antarctica, *in Intraplate strike- slip Deformation Belts, edited by Storti, F., Holdsworth, R. E., and Salvini, F.: Geological Society London Special Publications*, **210**, 135–143. http://dx.doi.org/10.1144/GSL.SP.2003.210.01.08.

Picciotto, E., Deutch, S., and Pasteels, P., 1964. Isotopic ages from the Sør Rondane Mountains Dronning Maud Land, *In: Adie, R.J. (Ed.), Antarctic Geology, Proceedings of the first International Symposium on Antarctic Geology, Amsterdam, North-Holland*, p. 570–578.

Powell, C., Jones, D., Pisarevsky, S., and Wingate, M., 2001. Palaeomagnetic constraints on the position of the Kalahari craton in Rodinia, *Precambrian Research*, **110**, 33–46. http://dx.doi.org/10.1016/S0301-9268(01)00179-6.

Reid, A., Allsop, J., Granser, H., Millett, A., and Somerton, I., 1990. Magnetic interpretation in three dimensions using Euler deconvolution., *Geophysics*, **55 (1)**, 80–91. http://dx.doi.org/10.1190/1.1442774.

Riedel, S., 2009. Airborne-based geophysical investigation in Dronning Maud Land, Antarctica, *Doctoral thesis, University of Bremen, Germany*. http://epic.awi.de/20643/1/Rie2009d.pdf.

Riedel, S., Jokat, W., and Steinhage, D., 2012. Mapping tectonic provinces with airborne gravity and radar data in Dronning Maud Land, East Antarctica, *Geophysical Journal International*, **189**, 414–427. http://dx.doi.org/10.1111/j.1365-246X.2012.05363.x.

Riedel, S., Jacobs, J., and Jokat, W., 2013. Aeromagnetics of Dronning Maud Land and geodynamic implications for Rodinia and Gondwana reconstructions, *Tectonophysics*, **585**, 161–171. http://dx.doi.org/10.1016/j.tecto.2012.10.011.

Ruppel, A. S., 2012. Structural Evolution of the Main Shear Zone in Sør Rondane, East Antarctica, *Master Thesis, University of Bremen, Germany*.

Salem, A. and Ravat, D., 2003. A combined analytic signal and Euler method (AN-EUL) for automatic interpretation of magnetic data, *Geophysics*, **68 (6)**, 1952–1961. http://dx.doi.org/10.1190/1.1635049.

Satish-Kumar, M., Hokada, T., Kawakami, T., and Dunkley, D. J., 2008. Geosciences research in East Antarctica (0°E–60°E): present status and future perspectives. From: Satish-Kumar, M., Motoyoshi, Y., Osanai, Y., Hiroi, Y., Shiraishi, K. (eds) Geodynamic Evolution of East Antarctica: A Key to the East–West Gondwana Connection, *Geological Society London, Special Publications*, **308**, 1–20. http://dx.doi.org/10.1144/SP308.1.

Satish-Kumar, M., Hokada, T., Owada, M., Osanai, Y., and Shiraishi, K., 2013. Neoproterozoic orogens amalgamating East Gondwana: Did they cross each other?, *Precambrian Research*, **234**, 1–7. http://dx.doi.org/10.1016/j.precamres.2013.06.010.

Schlüter, J., Estrada, S., Lisker, F., Läufer, A., Kühn, R., Nitzsche, K. N., and Spiegel, C., 2011. First Petrographical Description of Rock Occurrences in the Steingarden Area, Dronning Maud Land, East Antarctica, *Polarforschung*, **80 (3)**, 161–172. http://epic.awi.de/30006/1/35-46.pdf.

Shackleton, R. M., 1996. The final collision zone between East and West Gondwana: where is it?, *Pergamon*, **23**, 271–287. http://dx.doi.org/10.1016/S0899-5362(97)00002-X.

Shepherd, T., Bamber, J. J., and Ferraccioli, F., 2006. Subglacial geology in Coats Land, East Antarctica, revealed by airborne magnetics and radar sounding, *Earth and Planetary Science Letters*, **244 (1–2)**, 323–335. http://dx.doi.org/10.1016/j.epsl.2006.01.068.

Shiraishi, K. and Kagami, H., 1992. Sm-Nd and Rb-Sr ages of metamorphic rocks from the Sør Rondane Mountains, East Antarctica, *In: Yoshida, Y., Kaminuma, K., Shiraishi, K. (Eds.), Recent Progress in Antarctic Earth Science. Terra Scientific Publishing, Tokyo*, p. 29–35. http://www.terrapub.co.jp/e-library/aes/pdf/RP0029.PDF.

Shiraishi, K., Asami, M., Ishizuka, H., Kojima, H., Kojima, S., Osanai, Y., Sakiyama, T., Takahashi, Y., Yamazaki, M., and Yoshikura, S., 1991. Geology and metamorphism of the Sør Rondane Mountains, East Antarctica, *In: Thomson, M.R.A., Crame, J.A., Thomson, J.W. (Eds.), Geological Evolution of Antarctica. Cambridge University Press, Cambridge*, p. 77–82.

Shiraishi, K., Ellis, D. J., Hiroi, Y., Fanning, C. M., Motoyoshi, Y., and Nakai, Y., 1994. Cambrian Orogenic Belt in East Antarctica and Sri Lanka: Implications for Gondwana Assembly, *Journal of Geology*, **102**, 47–65. http://www.jstor.org/stable/30065710.

Shiraishi, K., Dunkley, D., Hokada, T., Fanning, C. M., Kagami, H., and Hamamoto, T., 2008. . Geochronological constraints on the Late Proterozoic to Cambrian crustal evolution of eastern Dronning Maud Land, East Antarctica: a synthesis of SHRIMP U-Pb age and Nd model age data. In: Satish-Kumar, M., Motoyoshi, Y., Osanai, Y.,

Hiroi, Y., Shiraishi, K., (eds). Geodynamic Evolution of East Antarctica: A key to the East-West Gondwana connection, *Geological Society London Special Publications*, **308**, 21–67. http://dx.doi.org/10.1144/SP308.2.

Speranza, F., Minelli, L., Pignatelli, A., and Chiappini, M., 2012. The Ionian Sea: The oldest in situ ocean fragment of the world?, *Journal of Geophysical Research*, **117**, B12101. http://dx.doi.org/10.1029/2012JB009475.

Studinger, M. and Miller, H., 1999. Crustal structure of the Filchner-Ronne Shelf and Coats Land, Antarctica, from gravity and magnetic data; implications for the breakup of Gondwana, *Journal of Geophysical Research*, **104**, 20,379–20,394. http://dx.doi.org/10.1029/1999JB900117.

Tainosho, Y., Takahashi, Y., Arakawa, Y., Osanai, Y., Tsuchiya, N., Sakiyama, T., and Owada, M., 1992. Petrochemical character and Rb-Sr isotopic investigation of the granitic rocks from the Sør Rondane Mountains, East Antarctica, *In: Yoshida, Y., Kaminuma, K., Shiraishi, K. (Eds.), Recent Progress in Antarctic Earth Science. Terra Scientific Publishing, Tokyo*, p. 45–54. http://www.terrapub.co.jp/e-library/aes/pdf/RP0045.PDF.

Takahashi, Y., Arakawa, Y., Sakiyama, T., Osanai, Y., and Makimoto, H., 1990. Rb–Sr and K–Ar whole rock ages of the plutonic bodies from the Sør Rondane Mountains, East Antarctica, *Proceedings of NIPR Symposium on Antarctic Geoscience*, **4**, 1–8. http://ci.nii.ac.jp/naid/110001071662/.

Talarico, F. and Kleinschmidt, G., 2008. The Antarctic continent in Gondwanaland: A tectonic review and potential research targets for future investigations. In: Florindo, F., Siegert, M. (Eds.): Antarctic climate evolution, *Developments in Earth & Environmental Science*, **8**, 257–308. http://dx.doi.org/10.1016/S1571-9197(08)00007-4.

Talarico, F., Kleinschmidt, G., and Henjes-Kunst, F., 1999. An ophiolitic complex in the northern Shackleton Range, Antarctica, *Terra Antarctica*, **6 (3/4)**, 293–315.

Tessensohn, F., Kleinschmidt, G., Talarico, F., Buggisch, W., Brommer, A., Henjes-Kunst, F., Kroner, U., Millar, I. L., and Zeh, A., 1999. Ross-age amalgamation of East and West Gondwana: Evidence from the Shackleton Range, East Antarctica, *Terra Antarctica*, **6 (3/4)**, 317–325.

Thompson, D., 1982. EULDPH—a new technique for making computer-assisted depth estimates from magnetic data, *Geophysics*, **47**, 31–37. http://dx.doi.org/10.1190/1.1441278.

Toyoshima, T., Osanai, Y., Baba, S., Hokada, T., Nakano, N., Adachi, T., Otsubo, M., Ishikawa, M., and Nogi, Y., 2013. Sinistral transpressional and extensional tectonics in Dronning Maud Land, East Antarctica, including the Sør Rondane Mountains, *Precambrian Research*, **234**, 30–46. http://dx.doi.org/10.1016/j.precamres.2013.05.010.

Van Autenboer, T., 1969. Geology of the Sør Rondane Mountains, *In: Craddock, C., et al. (Eds.), Geologic Maps of Antarctica. American Geographical Society, Sheet 8, Pl. VIII (Antarctic Map Folio Series, Folio 12), New York*.

Van Autenboer, T. and Loy, W., 1972. Recent geological investigations in the Sør Rondane Mountains, Belgicafjella and Sverdrupfjella, Dronning Maud Land, *In: Adie, R.J. (Ed.), Antarctic Geology and Geophysics. Universitetsforlagt, Oslo*, p. 563–571.

Van Autenboer, T., Michot, J., and Picciotto, E., 1964. Outline of the geology and petrology of the Sør-Rondane mountains, Dronning Maud Land, *In: Adie, R.J. (Ed.), Antarctic Geology, Proceedings of the first International Symposium on Antarctic Geology, Amsterdam, North-Holland*, pp. 501–514.

Vine, F. and Matthews, D., 1963. Magnetic Anomalies Over Oceanic Ridges, *Nature*, **199**, 947 – 949. http://dx.doi.org/10.1038/199947a0.

Vuori, S. and Luttinen, A., 2003. The Jurassic gabbroic intrusions of Utpostane and Muren: insights into Karoo-related plutonism in Dronning Maud Land, Antarctica, *Antarctic Science*, **15 (2)**, 283–301. http://dx.doi.org/10.1017/S0954102003001287.

Wegener, A., 1912a. Die Entstehung der Kontinente, *Geologischen Rundschau*, **3**, 276–292. http://dx.doi.org/10.1007/BF02202896.

Wegener, A., 1912b. Die Entstehung der Kontinente, *Petermanns Geographische Mitteilungen*, pp. 185–195, 253–256, 305–30.

Wegener, A., 1929. Die Entstehung der Kontinente und Ozeane, *Vieweg Verlag, Braunschweig*, **4. Auflage**.

Wolmarans, L. G. and Kent, L. E., 1982. Geological investigations in western Dronning Maud Land, Antarctica - a synthesis, *South African Journal of Antarctic Research*, **Supplement 2**, 14–53.

Zeh, A., Millar, I. L., and Horstwood, S. A., 2004. Polymetamorphism in the NE Shackleton Range, Antarctica: Constraints from Petrology and U–Pb, Sm–Nd, Rb–Sr TIMS and in situ U–Pb LA-PIMMS dating, *Journal of Petrology*, **45**, 949–973. http://dx.doi.org/10.1093/petrology/egg117.

Zumberge, J. F., Heftin, M. B., Jefferson, D. C., Watkins, M. M., and Webb, F. H., 1997. Precise point positioning for the efficient and robust analysis of GPS data from large networks, *Journal of Geophysical Research*, **102 (B3)**, 5005–5017. http://dx.doi.org/10.1029/96JB03860.

A

Land-based gravity measurements on ice shelves

Measurements with a land gravimeter in manual mode are extremely difficult on ice shelves, due to the movements of the floating ice that cause strong oscillations of the read-out pointer around the reading line. However, AWI upgraded all their LaCoste&Romberg land gravimeters with feedback systems built by L&R Meter (Fig. A.1) in 2011 and 2012. This feedback system has a range of ±150 mGal. Readings can be recorded electronically using a BlueTooth compliant handheld computer running Windows Mobile system software. The L&R Meter feedback software offers the possibility to record continuously with a sample rate of up to 1Hz (Fig. A.1).

a

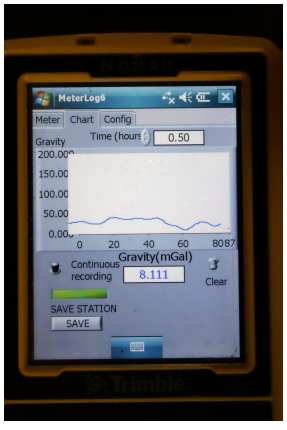

b

Figure A.1: Feedback system of L&R Meter: (a) LaCoste&Romberg land gravimeter with feedback, (b) handheld computer with feedback control and recording software

The feedback software records also electronic level values in the long and cross level directions. This can be used to correct tilt errors. For deriving tilt correction functions, the gravimeter is tilted in several steps in the long level direction while keeping the meter level in the cross direction, and vice versa (Fig. A.2). The measured gravity is at its

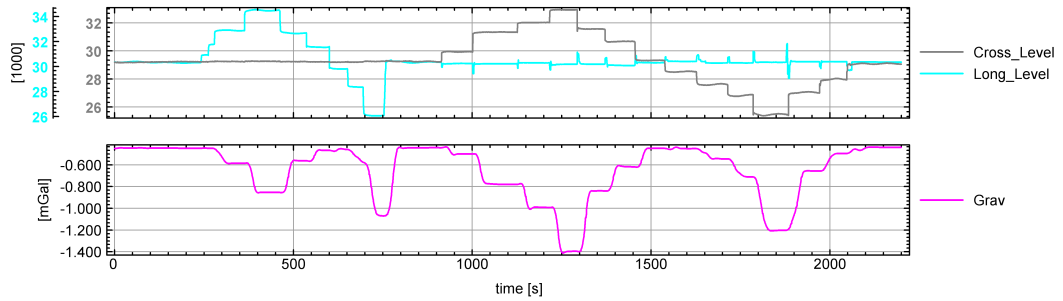

Figure A.2: Tilt measurements of LaCoste&Romberg land gravimeter with feedback system by L&R Meter. Tilt of gravimeter by long- and cross levels (upper figure) and measured feedback gravity with increasing tilt (lower figure).

maximum if the gravimeter is in an upright position and a tilt in any direction leads to a decrease of the measurement value. The decrease follows a parabolic distribution for small deviations from the upright position and correction coefficients can be determined by a least-squares fit (Fig. A.3). Here, we estimated the tilt correction coefficient for

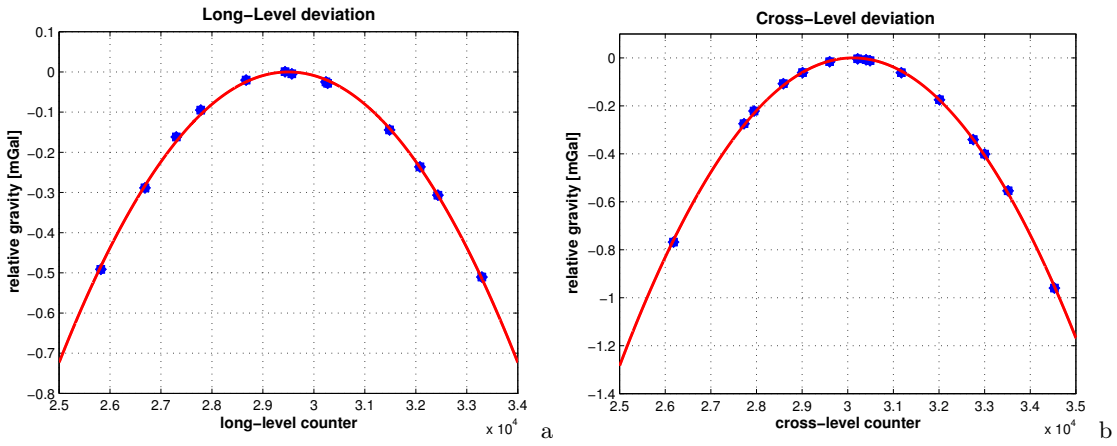

Figure A.3: Derivation of parabolic tilt correction coefficients for LaCoste&Romberg land gravimeter with feedback system by L&R Meter: (a) long level tilt, (b) cross level tilt.

the LaCoste&Romberg G1031, given in Tab. A.1. Note that it is possible to reset the electronic level readouts in the feedback control software. In that case the correlation coefficients need to be adjusted.

$tilt\ correction\ [mGal] = ax^2 + bx + c$		
x	long level	cross level
a	$-3.57153 \cdot 10^{-8}$	$-4.90035 \cdot 10^{-8}$
b	$2.10729 \cdot 10^{-3}$	$2.95198 \cdot 10^{-3}$
c	-31.06985	-44.88875

Table A.1: Parabolic tilt correction coefficients for LaCoste&Romberg gravimeter G1031 with feedback system by L&R Meter.

Long-term feedback gravity measurements with a sample rate of 1 Hz were carried out on the ice shelves at Neumayer-III (∼3 days) and Crown Bay (∼2 days) during the 2011/12 Antarctic summer season. Both measurement experiments were set up in calm conditions inside a container, but the gravimeter in neither could be maintained in an upright position due to the movement of the ice shelf itself. At Neumayer-III the gravimeter was leveled manually after 2 days. The applied tilt correction provided satisfying results with the parabolic coefficients given above (Tab. A.1).

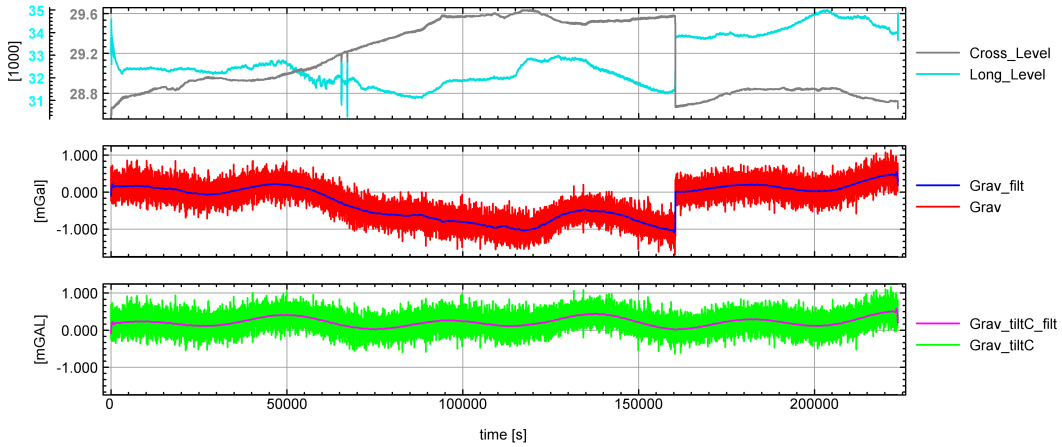

Figure A.4: Continuous gravity measurement on the Ekström ice shelf at Neumayer-III during the 2011/2012 summer season. Tilt of gravimeter is measured by long- and cross levels (upper figure). Measured feedback gravity given in red and is low-pass filtered with 900 s filter length (middle figure). Tilt corrected gravity calculated with parabolic tilt correction function is given in green and is low-pass filtered with 900 s filter length (lower figure).

The continuous gravity measurements show both high- and low-frequency undulations. Tidal movements of ice shelf cause the low frequency oscillation (∼6 hours). A

spectral analysis of the higher frequencies (Fig. A.5) reveals predominant oscillation periods of between 50 and 100 s, while periods shorter than 40 s are surpressed by the feedback system. These high frequency undulations are most probably consequences of the ocean swell.

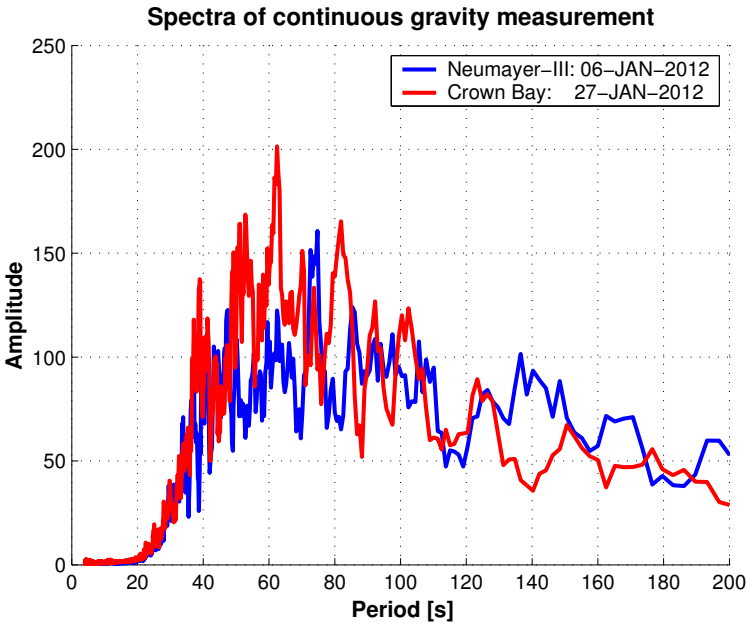

Figure A.5: Amplitude spectra of higher frequencies of continuous gravity measurements on the Ekström and Crown Bay ice shelves during the 2011/2012 summer season. Periods shorter than 40 s are surpressed by the feedback system.

It can be concluded that gravity measurements on floating ice shelf can be carried out with the upgraded LaCoste&Romberg land gravimeter in feedback mode, by taking continuous measurements with a sample rate of 1 Hz for several minutes and averaging the recorded values. Simultaneously, the tidal height changes of the ice shelf should be recorded and the measurement corrected for the tide effect.

B

Aeromagnetic survey around Neumayer-III

A local airborne survey around Neumayer-III station was carried out during the 2011/12 Antarctic summer season, collecting among others aeromagnetic data with a line spacing of 2 km and a tie line spacing of 4 km (Fig. B.1). I acquired and processed the data, but they did not contribute directly to the tectonic interpretation of this study. Nevertheless, the processing details are given here in a compact form (Tab. B.1).

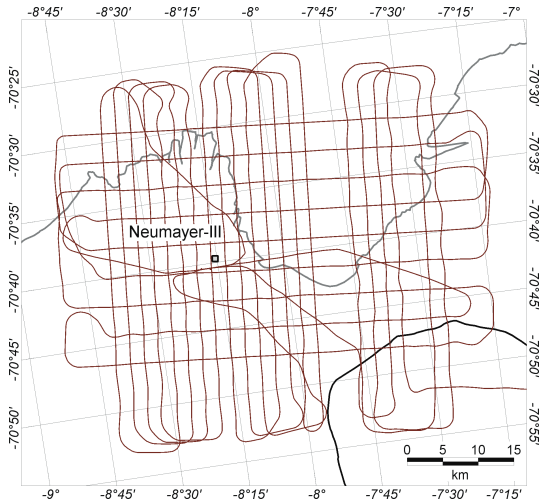

Figure B.1: High-resolution aeromagnetic survey around Neumayer-III station in 2011/12. The black line represents the grounding line, the gray line indicates the edge of the ice shelf, and brown lines are the flight paths.

Data acquisition	
Base:	Neumayer-III
Date:	08 - 09 January 2012
Aircraft:	*Polar 6* (Basler BT-67)
Measurement flights:	3
Sensors	1 Scintrex Cs-2 magnetometer (tail boom)
	1 Billingsley TFM 100 fluxgate (installed near the rear end cabin roof)
Sample rate:	10 Hz
Magnetic base stations	2
Sample rate	0.1 Hz
Locations	near geophysical observatory at Neumayer-III
	near runway at Novo-Airfield

Data processing	
Processor:	M. Mieth
Year:	2012
Software:	Geosoft Oasis montaj
Data sampling rate:	1 Hz
Navigation:	Position of tail boom sensor calculated from GNSS antennas positions
GNSS Post-Processing:	Waypoint GPS software: precise point positioning (PPP) method
Processing sequence A	
Channel:	CRW (compensated tail boom sensor)
IGRF correction:	auto, DATE channel used
Base station processing:	
IGRF correction:	auto, DATE channel used
Quiet level:	average value between 8 am and 4 pm
	160.44 nT (near Neumayer-III)
	-280.04 nT (near Novo-Airfield)
Low-pass filter	1800 s
Edits:	de-spike filtering and additional edits individually for each line
Flight line names:	FL-ANTR12-xxx (xxx := flight number)
Data files:	db_mag_nm3_proc01.gdb (Geosoft)
	db_mag_nm3_proc01.xyz (ASCII)
	db_user_events.gdb (Geosoft)
Processing sequence B	
Line splitting:	straight lines (lines / tie lines)
Line names:	NM3-xxxx-ANTR12 (xxxx := line number)
Data files:	db_mag_nm3_proc02.gdb (Geosoft)
	db_mag_nm3_proc02.xyz (ASCII)

Processing sequence C	
Upward continuation:	900 m
Leveling:	
Step A:	Static shift leveling
Step B:	Low-pass filtered tensioned spline leveling
Gridding:	500 m cell size, minimum curvature
Grid-filtering:	not applied
Line names:	NM3-xxxx-ANTR12 (xxxx := line number)
Data files:	db_mag_nm3_proc03.gdb (Geosoft)
	db_mag_nm3_proc03.xyz (ASCII)

Table B.1: Processing report of local aeromagnetic survey around Neumayer-III station in 2011/12

Magnetic base station data, recorded near the geophysical observatory at Neumayer-III, show a considerable diurnal variation of the geomagnetic field during this survey (Fig. B.2). Both, the standard full leveling method and the random line leveling (description given in chapter 2.2.3) were tested, each resulting in a similar high quality result. For consistency reasons, the random line leveling method was finally applied, the results are displayed in Fig. B.3, and B.4.

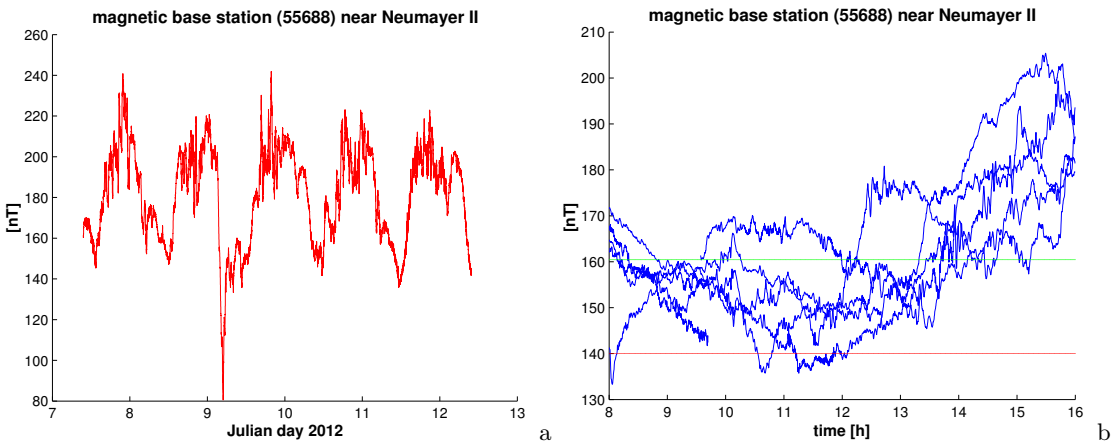

Figure B.2: Magnetic base station data during airborne survey around Neumayer-III in 2011/12: (a) continuous plot, (b) common plot of all days during between 8 am and 4 pm.

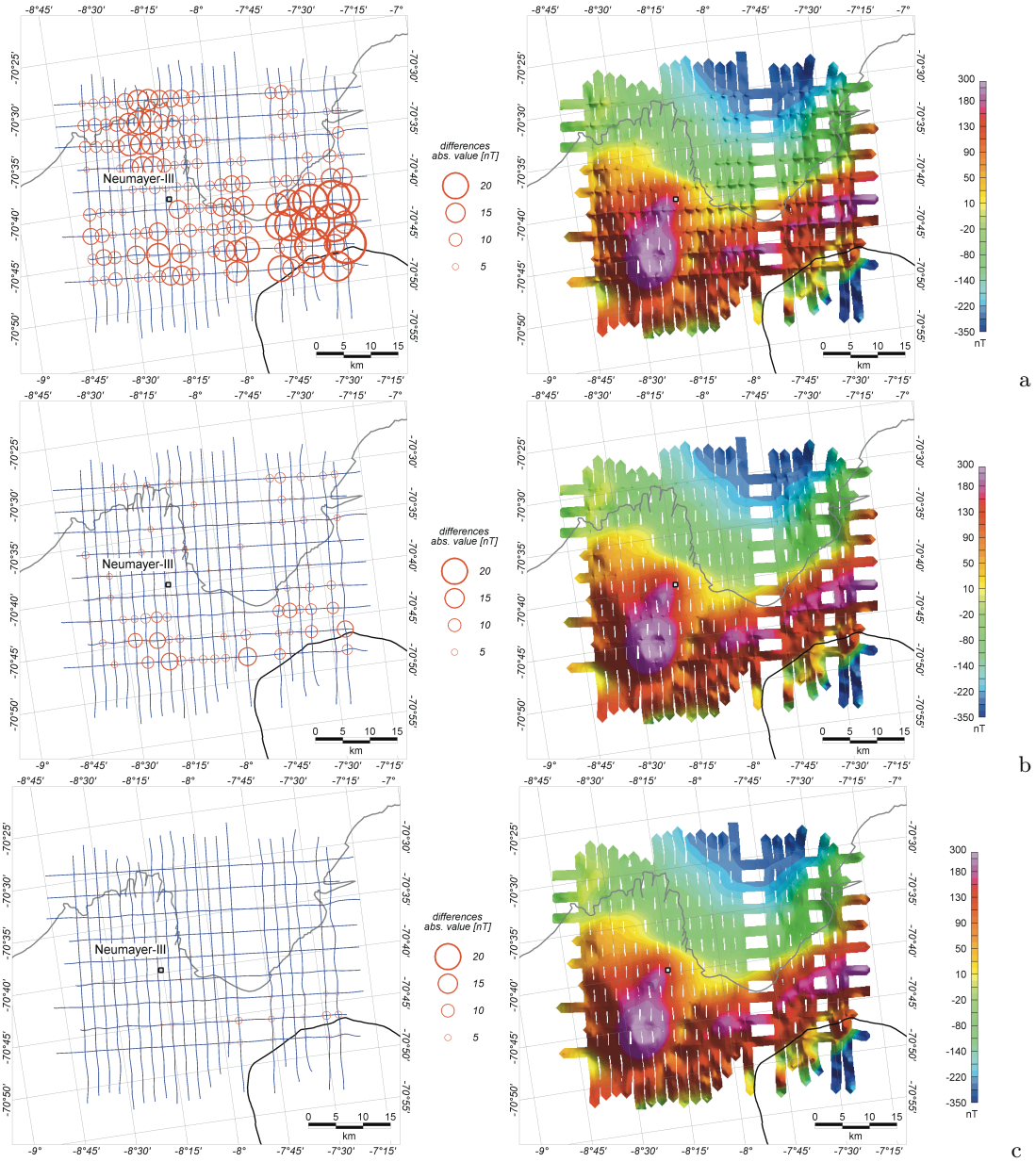

Figure B.3: Cross-point differences between lines and tie lines (left) and gridded magnetic anomaly data (right): (a) before leveling, (b) after static shift leveling, (c) after low-pass filtered tensioned spline leveling.

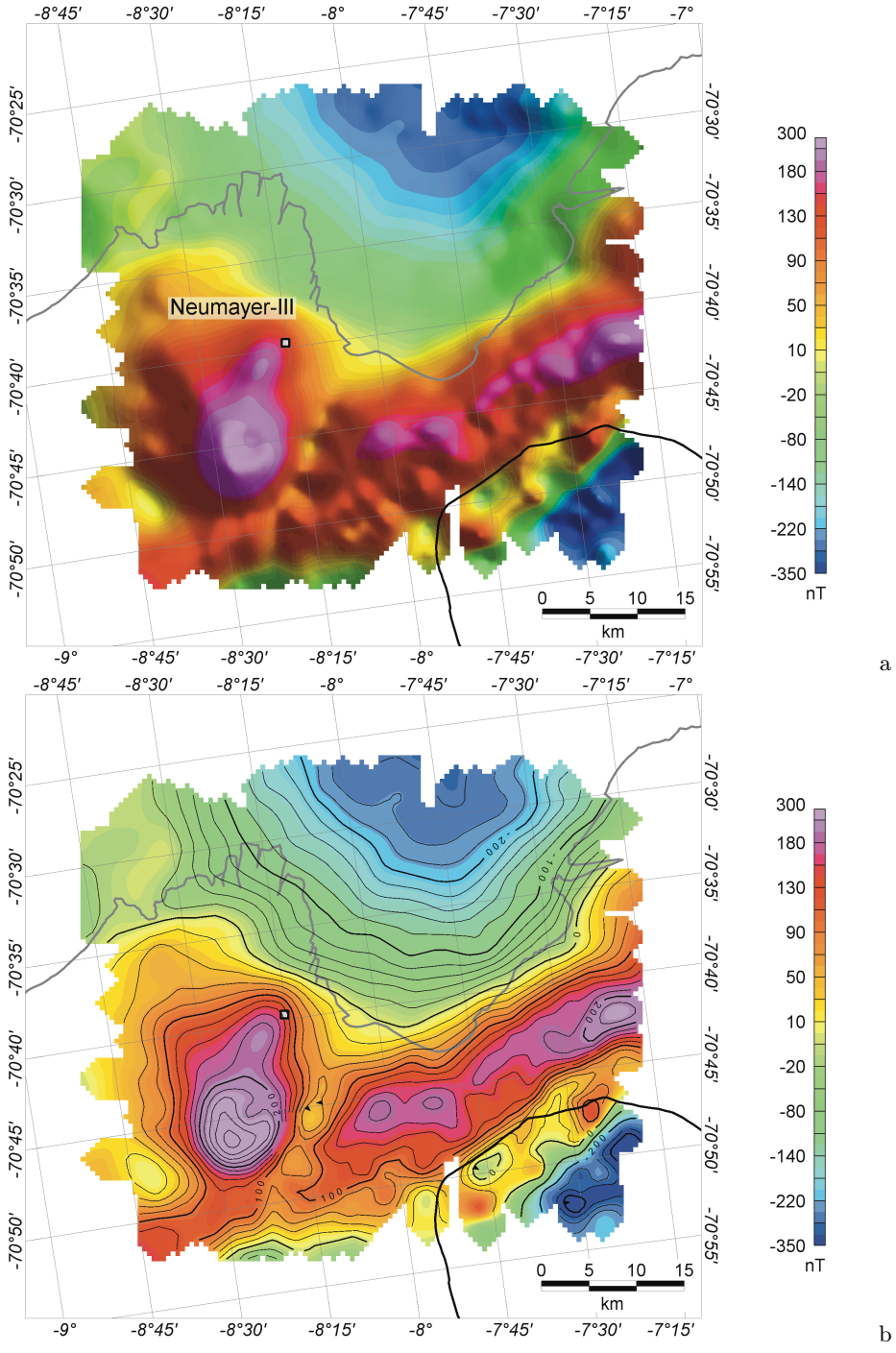

Figure B.4: Results of local aeromagnetic survey around Neumayer-III in 2011/12 summer season. Data are gridded with a grid cell size of 500 m x 500 m: (a) shading applied with 45° inclination and 45° declination, (b) contour line map, with contour line interval of 20/100 nT.

C

Matlab script for calculating the angle between magnetic sensor and inclination of the geomagnetic field

The magnetic total field intensity was measured with Cesium vapor magnetometers (Scintrex Cs-2 and Cs-3). These magnetometers have an inactive (dead) zone along their optical axes (±10°) and at their equatorial planes (±5°). Measurements are erroneous or fail if the angle between the optical axis of magnetometer and the inclination of the geomagnetic field falls into the range of either dead zone. In normal measurement mode this effect results in spikes, which can be edited, but during a compensation box this effect is fatal to surveying, as discussed in chapter 2.2.2. In order to avoid unnecessary and expensive (∼800 USD in 2012) repetition of compensation boxes, the following Matlab script allows to determine the maximum roll and pitch angle, as well as to decide whether to change the vertical orientation of the sensor to a 45° tilt. The sensor orientation will need to be changed if a new survey area is much closer to the magnetic pole or equator than the preceding area. Fig. C.1 shows the visual output of the Matlab script. The -63° inclination value used is typical for southern and eastern DML. The tool shows that the measurement will fail when turning from a southerly to westerly heading with a roll angle of 25° (that is, between the third and fourth legs of a standard compensation box). For DML, the tool shows it would be advisable to turn the aircraft with a roll angle of less than 17° from southerly to westerly heading in order to avoid spikes in the recorded data.

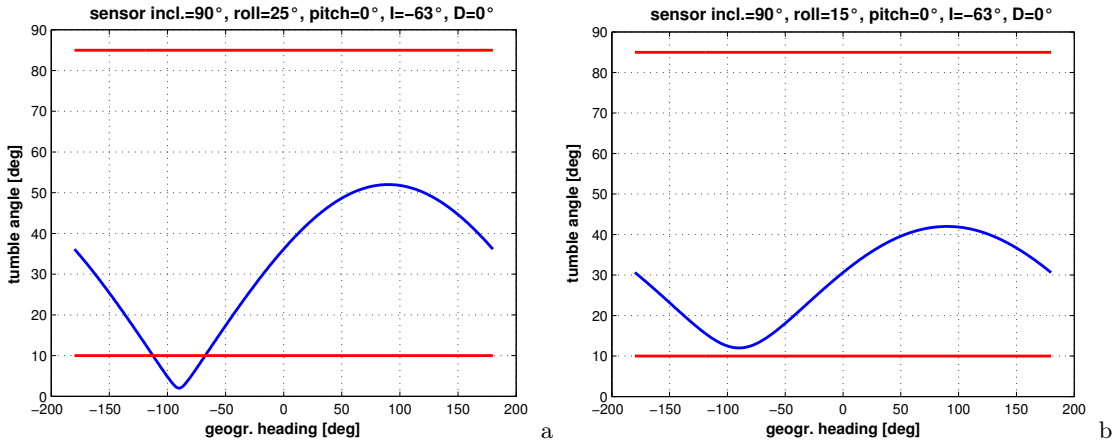

Figure C.1: Calculated angle between magnetic sensor and inclination of the geomagnetic field with Matlab script given below. Sensor orientation is vertical, inclination is set to -63° (present value at Kohnen station), declination is set to be 0° in order to get magnetic heading, roll angle is 25° (a) and 15° (b). Magnetic compensation will fail if the turn maneuver from magnetic south to west is flown with a roll angle exceeding 17°.

```
function A=tumble(g1,roll,pitch,h1,d1)

% A=tumble(g1,roll,pitch,h1,d1)
% author:
%   M.Mieth, October 2012
%
% Input:
%   g1     - angle of sensor orientation (optical axis) to the horizontal plane in degrees
%   roll   - roll angle of aircraft in degrees
%   pitch  - pitch angle of aircraft in degrees
%   h1     - inclination of the geomagnetic field in degrees
%   d1     - declination of the geomagnetic field in degrees
%
% Output:
%   A      - tumble angles depending of geographic heading
%   (angle between optical axis and inclination of the geomagnetic field)

% Set defaults if input variables are not defined
if nargin==0
    g1=90;
    roll=0;
    pitch=0;
    h1=70;
```

```
    d1=0;
elseif nargin==1
    roll=0;
    pitch=0;
    h1=70;
    d1=0;
elseif nargin==2
    pitch=0;
    h1=70;
    d1=0;
elseif nargin==3
    h1=70;
    d1=0;
elseif nargin==4
    d1=0;
end
% set geographic heading variable
hdg=-180:1:180;
% calculate magnetic heading
mhdg=hdg-d1;
% auxillary variable
g2=g1+pitch;
% convert degrees to radians
m=deg2rad(mhdg);
r=deg2rad(roll);
g=deg2rad(g2);
h=deg2rad(h1);

% calculation of tumble angle
sx=sin(g)*sin(r)*cos(m)+cos(g)*sin(m);
sy=-sin(g)*sin(r)*sin(m)+cos(g)*cos(m);
sz=-sin(g)*cos(r);
for ii=1:length(m);
    if sy(ii)==0 && sx(ii)==0
        a(ii)=0;
    elseif sy(ii)==0 && sx(ii)>0
        a(ii)=pi/2;
    elseif sy(ii)==0 && sx(ii)<0
        a(ii)=-pi/2;
    elseif sy(ii)<0
        a(ii)=atan(sx(ii)/sy(ii))+pi;
    elseif sy(ii)>0;
        a(ii)=atan(sx(ii)/sy(ii));
    else
        display('error in calc of azimuth')
        break
    end
```

```
    if sx(ii)==0 && sy(ii)==0 && sz>0
        b(ii)=pi/2;
    elseif sx(ii)==0 && sy(ii)==0 && sz<0
        b(ii)=-pi/2;
    elseif sx(ii)==0 && sy(ii)==0 && sz==0
        display('error: sx==0 & sy==0 & sz==0')
        return
    else
        b(ii)=atan(sz/sqrt(sx(ii)^2+sy(ii)^2));
    end
end
%tumble angle:
q=acos(cos(a).*cos(b)*cos(h)+sin(b)*sin(h));

% graphical display of tumble angle vs. geographic heading
plot(hdg,rad2deg(q))
hold on
n1=0;
n2=0;
if (min(rad2deg(q))>90)
    n1=160;
    n2=10;
end
plot(hdg,10+n1,'r')
plot(hdg,85+n2,'r')
title=['sensor incl.=' num2str(g1) '°, roll=' num2str(roll) '°, pitch=' ...
num2str(pitch) '°, I=' num2str(h1) '°, D=' num2str(d1) ,'°'];
labeling(title, 'geogr. heading [deg]', 'tumble angle [deg]')
hold off
% output variable
A=[hdg;rad2deg(q)];
% display geographic headings where a failure of magnetic sensor is to be expected
A(:,(find(A(2,:)>85)))
A(:,(find(A(2,:)<10)))
```